

Graduate School for Cellular and Biomedical Sciences
University of Bern

Development and application of magnetic resonance spectroscopy methods in studies on insulin resistance and metabolism of human liver and skeletal muscle

PhD Thesis submitted by

Tania Buehler

from Wolhusen LU

Thesis advisor

Prof. Dr. Dr. Chris Boesch
Department of Clinical Research, AMSM
Medical Faculty of the University of Bern

Original document saved on the web server of the University Library of Bern



This work is licensed under a
Creative Commons Attribution-Non-Commercial-No derivative works 2.5 Switzerland licence. To
see the licence go to <http://creativecommons.org/licenses/by-nc-nd/2.5/ch/> or write to Creative
Commons, 171 Second Street, Suite 300, San Francisco, California 94105, USA.

Copyright Notice

This document is licensed under the Creative Commons Attribution-Non-Commercial-No derivative works 2.5 Switzerland. <http://creativecommons.org/licenses/by-nc-nd/2.5/ch/>

You are free:



to copy, distribute, display, and perform the work

Under the following conditions:



Attribution. You must give the original author credit.



Non-Commercial. You may not use this work for commercial purposes.



No derivative works. You may not alter, transform, or build upon this work..

For any reuse or distribution, you must take clear to others the license terms of this work.

Any of these conditions can be waived if you get permission from the copyright holder.

Nothing in this license impairs or restricts the author's moral rights according to Swiss law.

The detailed license agreement can be found at:

<http://creativecommons.org/licenses/by-nc-nd/2.5/ch/legalcode.de>

Accepted by the Medical Faculty, the Faculty of Science and the Vetsuisse Faculty of the University of Bern at the request of the Graduate School for Cellular and Biomedical Sciences

Bern, Dean of the Medical Faculty

Bern, Dean of the Faculty of Science

Bern, Dean of the Vetsuisse Faculty Bern

*Dr beschtä Familie,
wo me sech cha wünsche,
in Liebi und Dankbarkeit gwidmet.*

Contents

Abstract	3
Abbreviations	4
1. Introduction	5
1.1 Theoretical Background	5
1.2 Mitochondria, ³¹ P saturation- and inversion transfer	10
1.3 Volume determination, VISS method.....	12
1.4 Specific aims and hypothesis, importance and relevance, novelty	13
2. Results	15
2.1 ATP synthesis in human liver and skeletal muscle using ³¹ P MRS	15
2.2 Determination of body compartments with VISS	15
2.3 Effect of growth hormone replacement therapy on fat compartments.....	15
2.4 Effect of β-alanine intake on muscle carnosine	15
2.5 Effect of fructose and galactose on liver glycogen synthesis after exercise	16
2.6 Effects of a whey protein on IHCL in obese female.....	16
3. Discussion	19
4. Outlook	21
References	22
Acknowledgements	27
List of Publications	28
Declaration of Originality	31
Original Manuscripts	33

Abstract

The metabolic syndrome describes an exceedingly relevant yet not very well defined disorder that is mainly defined by insulin resistance¹. Insulin resistance is the impaired ability of human cells to use the hormone insulin. The exact mechanisms that lead to insulin resistance are up to today not fully understood^{2,3}. Insulin resistance comes along with obesity and/or aging and represents a serious risk for the individual patient with increased probability to develop type 2 diabetes and cardiovascular disease, including myocardial infarction and stroke^{4,5}. The prevalence of the metabolic syndrome increased during the last few decades and reached epidemic dimensions. It affects up to 40% of the population⁴.

There is a need for suitable methods to investigate the mechanisms that lead to insulin resistance. Magnetic resonance imaging (MRI) and spectroscopy (MRS) are non-invasive methods to investigate patho-physiological mechanisms of the metabolism, which are well suited to characterize the insulin resistant patients and to follow effects of interventions (exercise, diet, surgery)^{6,7}. Phosphorus (³¹P) MRS is widely used to explore human skeletal muscle and/or liver energy metabolism by measuring high-energy phosphates at rest, exercise or recovery⁸.

In the following the focus was set on two different tasks. The first is the development of two ³¹P MRS magnetization transfer methods⁹⁻¹¹ to determine mitochondrial activity¹² in human skeletal muscle and liver tissue. Few years ago it was hypothesized that impaired mitochondrial activity could lead to insulin resistance¹³. Therefore the investigation of mitochondrial activity became an important research task.

Two magnetization transfer sequences, saturation transfer (ST)¹⁴ and inversion transfer (IT)¹⁵ had to be developed first and implemented on a 3 T MR system. With ST and IT one can measure the ATP synthesis, which is a direct measure of mitochondrial activity. The methods were then applied to a cohort of healthy volunteers in skeletal thigh muscle and liver. IT hasn't been applied so far to human skeletal muscle or liver to measure ATP synthesis neither a comparison is done between the two methods. Despite the challenges of volume selection and motion of the organ, it has been shown here that the implementation of ST and IT in the liver was reliable, with reasonable signal-to-noise, and with only little contamination from abdominal wall muscles. Measured ATP synthesis rates with the ST experiment are comparable with previous studies done in human skeletal muscle¹⁶ and/or liver¹⁷. Although it has been shown here that IT overestimates the ATP synthesis rates in both organs and it is the less precise method so far, it has the advantage to measure forward and backward ATP synthesis from which the net ATP synthesis can be calculated. In comparison to the presented ST experiment only the forward ATP synthesis is measurable. IT has also the advantage of being the less complex sequence according to sequence programming. It could be an alternative, if it is not possible to implement a very long saturation pulse on specific scanners as needed for a ST experiment.

The second task was to program a MATLAB® software called versatile, interactive sparse sampling (*VISS*) method for the determination of variable volumes (e.g. visceral adipose tissue (VAT), subcutaneous adipose tissue (SCAT), or single organs). Insulin resistance is connected with obesity¹⁸. Therefore in many studies about insulin resistance fat compartments, e.g. VAT, SCAT, are evaluated^{19,20}. Also intra-hepatocellular lipids (IHCL)²¹ or other metabolites as glycogen²² are often of interest in connection with insulin resistance. The volume of an organ has therefore to be known to calculate the concentration of these metabolites. It has been shown that *VISS* is in contrast to many other available software easily applicable to variable volumes with different characteristics and that it leads to reliable results that are in line with other techniques²³.

Abbreviations

ATP	adenosine triphosphate
γ -ATP	terminal phosphate of ATP
ADP	adenosine diphosphate
BA	β -alanine
^{13}C	carbon nucleus
DICOM	digital imaging and communications in medicine
DIXON	sequence for fat-water imaging, name of inventor of the sequence
FRU	fructose
GAL	galactose
GLU	glucose
^1H	proton nucleus
IDEAL	iterative decomposition of water and fat with echo asymmetry and least squares estimation
IHCL	intra-hepatocellular lipids
IT	inversion transfer
k_{AB}	forward exchange rate constant of ATP synthesis
k_{BA}	backward exchange rate constant of ATP synthesis
NAFLD	non-alcoholic fatty liver disease
NASH	non-alcoholic steatohepatitis
MD	maltodextrin
MRI	magnetic resonance imaging
MRS	magnetic resonance spectroscopy
NMR	nuclear magnetic resonance
^{31}P	phosphorus nucleus
PCr	phosphocreatine
Pi	inorganic phosphate
SCAT	subcutaneous adipose tissue
ST	saturation transfer
T_1	longitudinal relaxation time
T_2	transversal relaxation time
TBM	total body volume
TI	inversion time
TR	repetition time
TSE	turbo spin echo sequence
VAT	visceral adipose tissue
VISS	versatile, interactive sparse sampling method
WBF	whole body volume

1. Introduction

1.1 Theoretical Background

In 1946 two research groups, Purcell, Torrey and Pound²⁴ at MIT, Cambridge and Bloch, Hansen and Packard²⁵ at Stanford independently discovered nuclear magnetic resonance (NMR). Few years later Purcell and Bloch got both the Nobel Prize in physics for their pioneering work according to NMR. NMR spectroscopy is the study of nuclei in a static magnetic field B_0 in combination with electromagnetic radiation in the range of radiofrequencies (usually 10-1000 MHz). Only nuclei with a so called 'spin' are detectable in NMR. These are e.g. ^1H (proton), ^{13}C (carbon), ^{31}P (phosphorus), ^{15}N (nitrogen), ^{17}O (oxygen), ^{19}F (fluor) or ^{129}Xe (Xenon). Absorption and emission of electromagnetic radiation with nuclei can be studied by placing the probe or volunteer in a strong external magnetic field. Because of the so called 'chemical shift' equal nuclei within different locations in a molecule are distinguishable from each another. In combination with *in vivo* applications/studies one uses only the term magnetic resonance spectroscopy (MRS) or magnetic resonance imaging (MRI). The outcome of MR experiments can e.g. be a spectrum containing metabolites of interest or e.g. an image of a specific part/organ of the body (see Fig.1). In basic/clinical research and clinical applications MRI and MRS are applicable to a wide range of different research and/or disease related questions and problems.

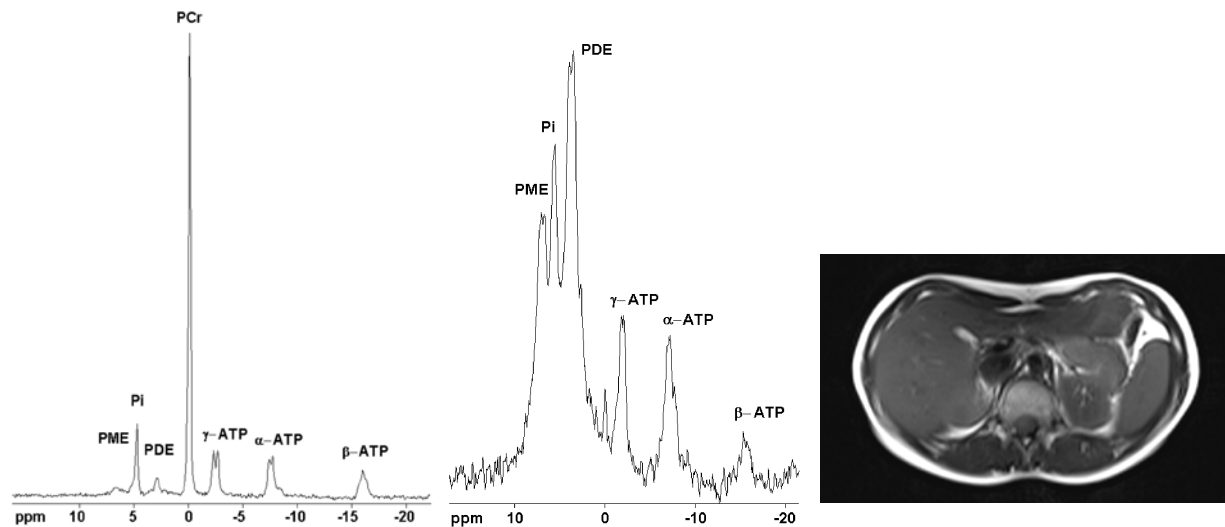


Figure 1: ^{31}P MRS spectra of human skeletal thigh muscle (left) and human liver (middle). T₁-weighted image of the abdominal region of a healthy lean volunteer at the height of the liver used to determine e.g. visceral fat (right).

The muscle spectrum shows a high phosphocreatine (PCr) signal (repetition time = 15s, 48 averages). The liver spectrum with negligible PCr-signal at 0 ppm (repetition time = 5s, 48 averages, apodization 15Hz). The β -ATP signal is in both spectra reduced due to the limited bandwidth of the 90° adiabatic excitation pulse. PME: phosphomonoesters Pi: inorganic phosphate, PDE: phosphodiester, PCr: phosphocreatine, and ATP: adenosine triphosphate with the three phosphates α , β , γ .

NMR/MR is based as already mentioned on the existence of a spin of a nuclei. Nuclei without a spin quantum number I , respectively $I = 0$ are not detectable by NMR (these are e.g. ^{12}C , ^{16}O , ^{32}S etc.). NMR effects can be studied in a strong external field. The classical description of the NMR concept is not adequate to explain the quantum mechanical spin. In the following the quantum mechanical description of the NMR concept is used. A vector quantity is printed in bold.

NMR detectable nuclei contain an angular momentum P and because of their electric charge also a magnetic moment μ . In quantum mechanics P is limited to discrete values. This holds also for μ and the z-coordinate of μ .

$$P = \sqrt{I(I+1)} \hbar \quad (1.1)$$

P is the angular momentum, I the spin quantum number, and \hbar the Planck's constant h over 2π ($\hbar = h/2\pi$).

$$\mu = \gamma P = \gamma \sqrt{I(I+1)} \hbar \quad (1.2)$$

μ is the magnetic moment and γ the gyromagnetic ratio. The gyromagnetic ratio, i.e. the ratio of magnetic and angular momentum is a nucleus specific property (see Tab.1).

$$\mu_z = \gamma m \hbar \quad (1.3)$$

μ_z is the z-coordinate of the magnetic moment and m the magnetic quantum number. It is also limited to discrete values (quantization of direction, $m = I, I-1, \dots -I$).

The exchange of electromagnetic radiation with the nuclei is characterized by absorption and emission of photons. Each nucleus, respectively atom or molecule has its own energy state and can change between different energy levels according the different electronic, vibrational, or rotational states. Absorption of photons brings the nuclei into a higher energy state. By emission of photons the nuclei fall back into a lower energy level. These energy levels take again only discrete values. The magnetic energy E of a magnetic moment is:

$$E = -\mu_z B_0 = -m\gamma\hbar B_0 \quad (1.5)$$

B_0 is a (strong) external magnetic field that makes the NMR effect detectable. The difference between energy levels of nuclei is described by ΔE (see Fig.2). The frequency of a photon is proportional to its energy.

$$\Delta E = \gamma\hbar B_0 = h\nu_0 \quad (1.6)$$

Isotope	Spin	γ ($10^7 \text{ rad T}^{-1} \text{ s}^{-1}$)	ν_0 at 3T (MHz)	Natural abundance (%)	Relative sensitivity
^1H	1/2	26.752	127.7	99.96	1.00
^2H	1	4.107	19.6	0.02	$1.45 \cdot 10^{-6}$
^{13}C	1/2	6.728	32.1	1.11	$1.76 \cdot 10^{-4}$
^{15}N	1/2	-2.712	12.9	0.37	$3.86 \cdot 10^{-6}$
^{17}O	5/2	-3.628	17.3	0.04	$1.08 \cdot 10^{-5}$
^{19}F	1/2	25.181	120.2	100.00	0.83
^{31}P	1/2	10.841	51.8	100.00	$6.65 \cdot 10^{-2}$
^{129}Xe	1/2	-7.452	35.6	26.44	$5.71 \cdot 10^{-3}$

Table 1: Shows properties of some common nuclei detectable by NMR. γ is the gyromagnetic ratio, ν_0 the precession or Larmor frequency.

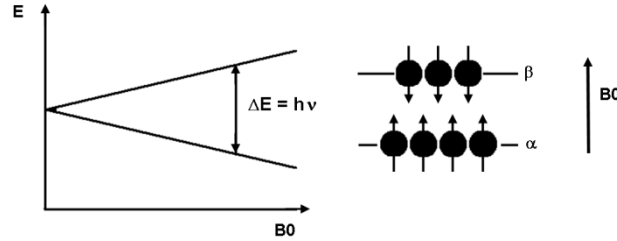


Figure 2: Shows the magnetic energy E of a nucleus with spin $1/2$ dependent on the external magnetic field strength B_0 . Magnetic moments of spins in state α (lower energy level) are aligned in the positive direction of B_0 . In state β (higher energy level) the magnetic moments are in antiparallel direction with B_0 . The energy difference ΔE describes the amount of electromagnetic radiation that is absorbed or ejected. In NMR this electromagnetic radiation is in the range of radiofrequencies.

From equation 1.6 the Larmor equation can be derived. It describes the connection between the precession (Larmor) frequency ν_0 and the external magnetic field B_0 .

$$\nu_0 = \frac{\omega_0}{2\pi} = \left(\frac{\gamma}{2\pi}\right) B_0 \quad (1.7)$$

ω_0 is the angular frequency and is associated with the Larmor frequency as follows $\omega_0 = \nu_0 2\pi$. Nuclei with spin $1/2$ can be in two different spin states α (spin state of lower energy and parallel alignment with B_0) and β (spin state of higher energy and antiparallel alignment with B_0). The α energy level has a slightly higher population of spins. The ratio of the populations between the two different spin states is described by the Boltzmann equation:

$$\frac{N_\beta}{N_\alpha} = e^{-\frac{\Delta E}{k_B T}} \quad (1.8)$$

N_α , N_β are the number of spins in the two spin states α and β . k_B is the Boltzmann constant and T the absolute temperature. The sum of the single magnetic moments results in a macroscopic magnetization M_0 along the positive B_0 direction because of the higher population in level α :

$$M_0 = N_\alpha \mu_z + N_\beta \mu_z \approx N_{tot} \left(\frac{\gamma^2 \hbar^2 B_0}{4k_B T}\right) \quad (1.9)$$

N_{tot} are the number of individual spins. A further milestone in the history of NMR was the change of the acquisition of a spectrum from the continuous wave form technique to a pulsed NMR technique combined with a Fourier transformation²⁶. Instead of excite each frequency separately and look for a possible resonance, all frequencies were excited at once with a very short radiofrequency pulse (rf-pulse). The so gained signal contains all resonances and can be transformed by a so called Fourier transformation into a spectrum of separated resonances. The signal or resonances are acquired in time domain $f(t)$. The time signal can be resolved into the single resonances by a Fourier transformation into a frequency domain signal $F(\nu)$. The Fourier transformation from time to frequency domain is described as follows:

$$F(\nu) = \int_{-\infty}^{+\infty} f(t) e^{-i2\pi\nu t} dt \quad (1.10)$$

The macroscopic magnetization M_0 described before can be used to illustrate some simple NMR experiments. The individual magnetic moments of M_0 precess with the Larmor frequency ν_0 about the B_0 field in e.g. the z -direction. An additional smaller field B_1 (rf-pulse) applied in e.g. the x -direction disturbs this magnetization. In a coordinate system that rotates with frequency ν_1 around the z -direction (rotated system denoted by ') the magnetic magnetization

M_0 is excited along the z-y'-plane (see Fig. 3). An rf-pulse that rotates the macroscopic magnetization M_0 onto the positive y'-axis is called a 90°_x pulse. This simple one-pulse sequence generates an FID (free induction decay). Rotation of M_0 onto the negative z-axis inverts the macroscopic magnetization (and the Boltzmann distribution) and is achieved by a so-called 180°_x or 180°_y inversion pulse.

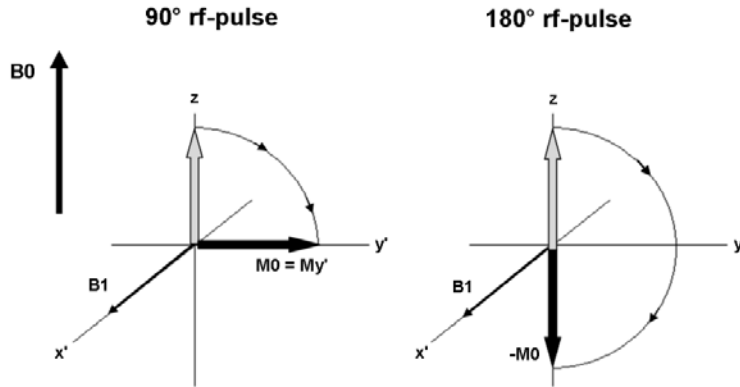


Figure 3: Schematic drawing of the magnetic magnetization M_0 after a 90° and a 180° rf-pulse (black arrows) in a rotating coordinate system (rotation around the z-axis with frequency ν_1 according to the B_1 field, indicated with x' and y'). B_0 is the external magnetic field and B_1 the magnetic field of the applied rf-pulse.

NMR became important in chemistry and medicine because not only the different nuclei (e.g. H, C) are distinguishable from each other, but also the same nuclei (e.g. protons) at different positions in a molecule. The resonance frequency ν_0 not only depends on the gyromagnetic ratio γ and the B_0 field, but also on the chemical environment of a nuclei induced by the surrounding nuclei. This is an important characteristic and is called 'chemical shift', which makes the different nuclei, respectively molecules distinguishable from each another²⁷. The relatively weak absorption and emission of electromagnetic radiation of nuclei (caused by the unfavorable Boltzmann distribution) makes NMR spectroscopy a less sensitive method compared to other spectroscopy methods (ultraviolet or infrared spectroscopy). However this fact is also an advantage because it makes NMR to a non-invasive method, which allows repetitive/longitudinal measurements in patients.

After a perturbation (e.g. 90° or 180° pulse) the system, respectively M_0 , returns into its initial state. This process can be described by transversal and longitudinal relaxation processes as follows:

$$M_z(t) = M_0(1 - e^{-\frac{t}{T_1}}) \quad (90^\circ \text{ pulse}) \quad (1.11a)$$

$$M_z(t) = M_0(1 - 2e^{-\frac{t}{T_1}}) \quad (180^\circ \text{ pulse}) \quad (1.11b)$$

$$M_{xy}(t) = M_{xy}(0)e^{-\frac{t}{T_2}} \quad (1.12)$$

The relaxation processes contain two time constants. T_1 is the longitudinal relaxation time and T_2 the transversal relaxation time.

The repetition time (TR) of an experiment is usually set according to the relaxation times T_1 and T_2 . To measure T_1 relaxation times one uses an ‘inversion recovery’ experiment. The resonances are at the beginning inverted by a 180° non-selective inversion pulse. Non-selective pulses affect the whole spectrum or at least all resonances within a certain bandwidth, while selective pulses affect only a single resonance. After the non-selective inversion pulse a certain time is waited called the inversion time (T_I) before the final 90° detection pulse. Spectra for different T_I are acquired. This relaxation curve is described by equation (1.11b) and the T_1 parameter can be fitted to this curve.

The breakthrough of NMR in clinical practice came with the invention of magnetic resonance imaging (MRI) by Mansfield²⁸ and Lauterbur²⁹ in 1973. Additional to the strong static magnetic field they applied lower position dependent magnetic fields (gradients), which allowed the recognition of the spatial location of the molecules in form of an image. Usually using clinical MR scanners one wants to have an ‘image’ with the information of the location of the sample or organ of interest before one starts with the experiment. MRI is therefore a useful tool. It is also widely used without spectroscopy in medicine (e.g. brain tumors, cancer). In this thesis the focus is set on spectroscopy. Imaging is only used on the edge for e.g. acquiring whole body images with separated fat-tissue compartments.

The additional lower position dependent magnetic fields to the strong magnetic field B_0 , which allowed the recognition of the spatial location of the molecules in form of an image are called gradients. The additional application of gradients changes the B_0 field as follows:

$$\mathbf{B}(\mathbf{r}) = B_0 + \mathbf{r}\mathbf{G} \quad (1.13)$$

$$\omega(\mathbf{r}) = \gamma\mathbf{B}(\mathbf{r}) = \gamma B_0 + \gamma\mathbf{r}\mathbf{G} \quad (1.14)$$

\mathbf{G} is the magnetic field gradient vector and \mathbf{r} the position vector.

To get an image of a 3D object one needs to encode all three dimension independently. This can be a time consuming process. Therefore one reduces the problem from three dimensions to two and only selects a ‘slice’ out of the object. This can be done, if an additional magnetic field (gradient) is applied simultaneously with a selective rf-pulse. The thickness of the slice is then dependent on the strength of the magnetic field gradient and the bandwidth of the rf-pulse. The bandwidth is the frequency range that can be excited with an rf-pulse.

After a slice is selected the MR signal needs to be still encoded in two directions. This is done by frequency encoding and phase encoding. In one direction (e.g. x-direction) the frequency is altered according to the distribution of the MR signal. In the y-direction the phase of the spins is changed according to their spatial location.

In view of image contrast it is useful to look at spin-echoes instead of the first free induction decays (FID’s). The formation of an echo can be achieved with a simple sequence of a 90° - followed by a 180° pulse (see Fig. 4). The 90° pulse excites the magnetization into the xy-plane. There the signal is dephasing. During this process a 180° pulse is applied, which reverses the dephasing into a rephasing. The rephased signal forms the echo. This simple but useful sequence was invented 1950 by Hahn³⁰.

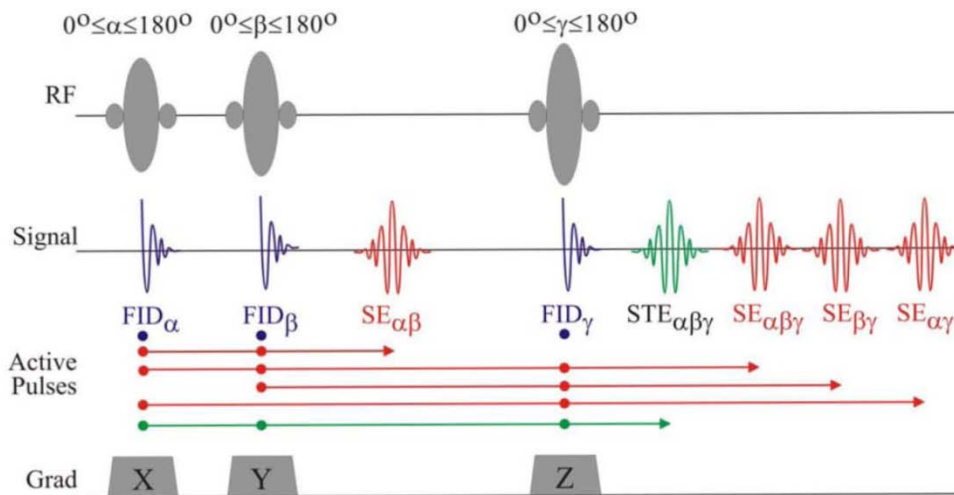


Figure 4: All the detectable signals (free induction decays, spin-echoes, and stimulated echoes) that are produced by three subsequent radiofrequency (RF) pulses. Hahn described these signals in a seminal paper in 1950³⁰. If the three pulses are combined with gradients, i.e., with variations of the magnetic field strength, the three spatial dimensions can be used to select a specific volume in space, a so-called voxel. Every radiofrequency pulse that does not have a pulse angle of exactly 0 or 180 degrees generates a free induction decay (FID). Two pulses can, in addition, be source for a spin-echo (SE). Three pulses can either re-form a spin echo or generate a stimulated echo (STE). In volume selection sequences, it is crucial to destroy all unwanted signal combinations by so-called crusher gradients. (Courtesy of C.Boesch)

Image contrast is influenced by the two parameters TE (echo time, time between application of the 90° pulse and the peak of the echo) and TR (repetition time) due to the fact that different tissues (e.g. fat, muscle, water) have different T_1 and T_2 relaxation times. Relaxation times of water ($T_1 > 4000$ ms, $T_2 > 2000$ ms) are much longer than for fat ($T_1 \sim 260$ ms, $T_2 \sim 70$ ms). There are three main different contrast types, T_1 weighted images (short TR and TE values, fat is bright means high signal intensity), T_2 weighted images (long TR and TE values, fat is dark means low signal intensity), and proton density weighted images (the more protons a tissue contains the brighter is this part).

To acquire the body images for $VISS$ a T_1 weighted TSE (turbo spin echo sequence) was used. In difference to the spin echo sequence the turbo spin echo sequence has instead of only one 180° pulse a train of 180° pulses. This has the advantage of reducing the scan time.

1.2 Mitochondria, ^{31}P saturation- and inversion transfer

Mitochondria are energy producing structures in the cells and act as so-called 'power plants' of the cells (see Fig. 5). In a wide range of degenerative and metabolic diseases, cancer and aging, the energy production of the mitochondria (especially mitochondrial activity) is a key parameter understanding the underlying biochemical mechanisms of these disorders³¹.

Mitochondrial activity can be assessed by different methods, e.g. measurement of oxygen (O_2) consumption^{32,33}, ^{13}C (tricarboxylic acid cycle (TCA) flux) and/or ^{31}P (magnetization transfer) MRS^{34,35}. All methods measure indirectly or directly mitochondrial activity.

Mitochondrial activity can be calculated directly from the net oxidative ATP synthesis rate. In the ATP synthesis/hydrolysis reaction Pi (inorganic phosphate) and ADP (adenosine diphosphate) form ATP (adenosine triphosphate), respectively the terminal phosphate of ATP becomes Pi ($\text{ADP} + \text{P}_i \rightarrow \text{ATP}$). The ATP synthesis rate or ATP turnover essentially results from two pathways: aerobic contribution from mitochondria (oxidative ATP synthesis rate or mitochondrial

oxidative phosphorylation) and anaerobic contribution from glycolysis (glycolytic ATP synthesis rate). In human skeletal muscle the part of aerobic to anaerobic contribution is about 90% to 10%³⁶ and in human liver its estimated to be 25% to 75%¹⁷.

Mitochondrion

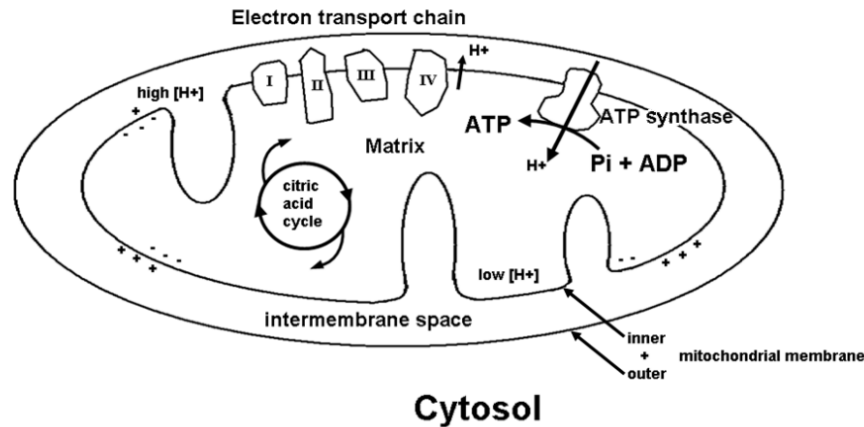


Figure 5: Mitochondrion in the cytosol with schematic view of the citric acid cycle, electron transport chain, and ATP synthesis. Protons are pumped through electron transfer in the respiratory chain from the matrix to the intermembrane space. Membrane potential and pH gradient create a proton motive force that starts up ATP synthesis.

Reaction rates and fluxes of biochemical reactions can be measured by MRS *in vivo*. ³¹P MRS has been used since the earliest days of *in vivo* NMR to study metabolism³⁷⁻³⁹, and in particular to measure the mitochondrial production of ATP. This is evaluated from ³¹P MRS of the high-energy phosphates ATP and Pi. There have been conceptually different approaches developed to evaluate mitochondrial function from ³¹P MRS measurement of high-energy phosphates.

One relies on measuring the initial phosphocreatine (PCr) recovery^{36,40} rate after an exercise which is proportional to *maximal* aerobic ATP synthesis at the end of exercise.

The other is performed at rest using the approach of magnetization transfer. In magnetization transfer experiments like saturation transfer (ST)¹⁴ and inversion transfer (IT)¹⁵ the magnetic equilibrium is disturbed, but not the chemical equilibrium. The idea is to disturb (and label) one side of a biochemical reaction (e. g. γ -ATP) with a saturation or inversion of a resonance) and look at the effect (i.e. the time evolution) on the other side (e.g. Pi).

With the ST experiment, the flux from Pi to ATP is measured, which represents the unidirectional flux of oxidative ATP synthesis. ST is the most used and best studied magnetization transfer technique to determine ATP synthesis. Most studies are investigated in skeletal muscle^{41,42}. An earlier study showed the feasibility to use ST in the perfused rat liver⁴³. So far only two studies exist in the human healthy and insulin resistant liver^{17,21}.

From the IT experiment the forward and backward flux of the oxidative ATP synthesis can be calculated. Due to the more parameters that have to be fitted it is the less robust method compared to ST. In an IT experiment the γ -ATP resonance is selectively inverted. This results first in a signal decrease and then a recovery of the Pi resonance. It has been applied in rabbit skeletal muscle⁴⁴ or rat hearts⁴⁵ to study the creatine kinase reaction. So far IT hasn't been applied in human skeletal muscle and liver to study ATP synthesis.

However a recent debate has been raised, suggesting that the saturation transfer method largely overestimates oxidative mitochondrial ATP synthesis because it neglects contributions from the glycolytic exchange flux⁴⁶⁻⁴⁸. Comparing PCr recovery and ST in young healthy subjects indeed confirmed the anomalously high results from saturation transfer³⁶, but the authors showed correlation between the two measurements, and argued that resting ST

measurements could therefore still provide an indicator of mitochondrial oxidative capacity. IT is less sensitive method than ST and a comparison of the two methods could help to distinguish between the different measured pools (glycolytic, oxidative, small exchanging pools) contributing to the ATP synthesis rate.⁴⁹

1.3 Volume determination, VISS method

Further the determination of tissue volumes or volumes of specific organs is often required in studies in connection with metabolism and insulin resistance. The amount and distribution of fat depots, e.g. visceral adipose tissue (VAT), subcutaneous adipose tissue (SCAT) or whole body fat (WBF) is correlated with metabolic diseases as insulin insensitivity or are of importance as cardiovascular risk factors. The volume of an organ, e.g. liver is of interest to determine the total amount of metabolites as [concentration x volume] in that specific organ.

MRI is well suited for the determination of such volumes^{23,50,51}. Based on MR images the volume of fat depots or organs is calculated. Traditionally T₁-weighted images⁵² are acquired, but recently newer techniques as chemical-shift imaging (DIXON^{53,54}, IDEAL^{55,56}) came up.

There exist automated, semi-automated, and manual segmentation methods⁵⁷⁻⁶⁰ to determine specific volumes. Automated algorithms are often very specific to one type of volume, e.g. VAT, but are not applicable to determine liver volume. Manual segmentation methods usually take a very long time to analyze the data.

3 Tesla MR systems are increasingly used, but inhomogeneity of the radiofrequency field in the abdominal region jeopardizes a threshold-based (see Fig. 6A) estimation of VAT and WBF. The complex structure of the volume (e.g. VAT), partial volume effect, image inhomogeneity and image contrast of non-fat volumes jeopardizes the calculation of the mentioned tissue or organ volumes. There is a need for accurate and fast volume determination programs, which are applicable to variable volumes with different characteristics, e.g. complex structure of VAT vs. a low contrast organ as the liver.

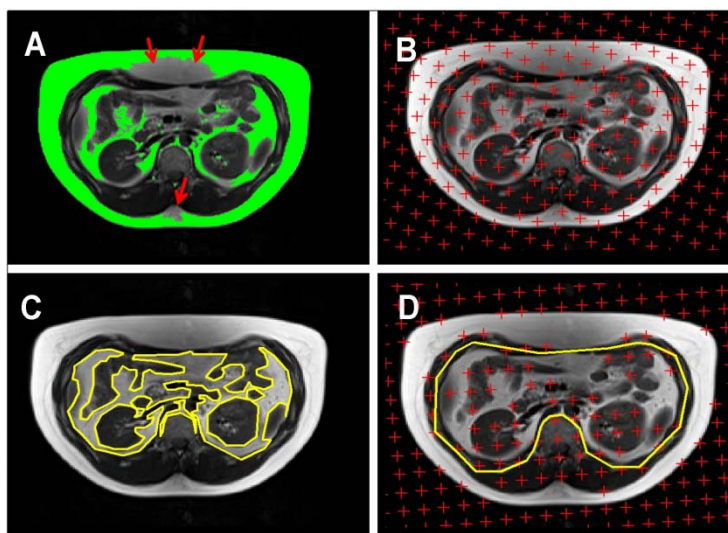


Figure 6⁶¹ : Determination of visceral fat and/or subcutaneous fat in a subject with a body mass index of 31.1 kg/m² using a threshold-only technique (A), point-counting-only (B), and the manual planimetric (contour-only) method (C). While threshold-only has difficulties to cope with inhomogeneities in the image (red arrows), point-counting-only is time consuming if the number of points is high, and manual contour-only methods are complex in highly fragmented tissue such as VAT. (D) In contrast, the VISS method can combine the advantages of the three methods, where the preparation of the images with contour and threshold helps to limit the number of points which need to be handled.

1.4 Specific aims and hypothesis, importance and relevance, novelty

The main focus was set on the development of methodological tasks. The major aim was the development of non-invasive MR spectroscopy methods to determine mitochondrial activity in skeletal muscle and liver tissue using ^{31}P MRS on a 3 Tesla MR scanner. Therefore two magnetization transfer methods (saturation transfer and inversion transfer) were then implemented to measure ATP synthesis exchange rate. A study to compare the two different methods was then applied to healthy volunteers in skeletal muscle and liver. It is hypothesized that both methods lead to equivalent results of ATP synthesis rate.

Mitochondrial activity is in some specific diseases as e.g. insulin resistance a key parameter to understand the underlying biochemical mechanisms. Inversion transfer hasn't been applied so far in human skeletal muscle or liver neither a comparison is done between the two methods saturation and inversion transfer.

The other objective was to program a software (*VISS*) for the determination of variable volumes (e.g. VAT, WBF, single organs) combining the strengths of three volume estimations: (a) threshold²³ (b) manual planimetric methods⁶⁰, and (c) point counting⁶² (see Fig. 6). It is hypothesized that with *VISS* volumes of different characteristics can be measured accurately and in a sufficient short time. Insulin resistance can be connected with obesity. Therefore in many studies about insulin resistance fat compartments, e.g. VAT, are evaluated. Also the intra-hepatocellular lipids (IHCL) or other metabolites as glycogen are often of interest in connection with insulin resistance. To calculate the absolute concentration of a metabolite in an organ also its volume has to be known. *VISS* is in contrast to many other software easily applicable to variable volumes with different characteristics.

2. Results

2.1 ATP synthesis in human liver and skeletal muscle using ³¹P MRS

Reference:

Buehler T et. al. Applying ³¹P saturation and inversion transfer in human liver and skeletal muscle to measure ATP synthesis exchange rate constants. NMR Biomed. (2012) (*in preparation, based on abstract "Determination of ATP synthesis exchange rates in human liver and skeletal muscle using ³¹P magnetization transfer" in section List of Publications*)

Manuscript:

See prepared manuscript for submission with preliminary results in section Original Manuscripts.

2.2 Determination of body compartments with VISS

Reference:

Buehler T, Ramseier N, Machann J, Schwenzer NF, Boesch C. Magnetic Resonance Imaging based Determination of Body Compartments with the Versatile, Interactive, Sparse Sampling (VISS) Method. J. Magn. Reson. Imag. (*accepted for publication April 2012*)

Manuscript:

See section Original Manuscripts.

2.3 Effect of growth hormone replacement therapy on fat compartments

Reference:

Egger A*, **Buehler T***, Boesch C, Diem P, Stettler C, Christ ER. The Effect of Growth Hormone Replacement Therapy on Different Fat Compartments: A Whole Body Magnetic Resonance Imaging Study. Eur. J. Endocrinol. 164: 23-29 (2011).
(*A Egger and T Buehler contributed equally to this work)

Manuscript:

See section Original Manuscripts.

2.4 Effect of β -alanine intake on muscle carnosine

Reference:

Stellingwerff T, Anwander H, Egger A, **Buehler T**, Kreis R, Decombaz J, Boesch C. Effect of two β -alanine dosing protocols on muscle carnosine synthesis and washout. Amino Acids: Epub ahead of print: DOI: 10.1007/s00726-011-1054-4. (2011)

Manuscript:

See section Original Manuscripts.

Summary:

Carnosine is a dipeptide consisting of the two amino acids alanine and histidine with proton buffering function during muscle performance. It can be observed with ¹H MRS. Its augmentation and storage through β-alanine (BA) intake was questioned. Therefore a study was designed with three different dosing regimes (placebo, low-dose, and high-dose) over 8 weeks supplementation and an additional washout phase of again 8 weeks. The absolute increase of muscle carnosine is dependent upon the total consumed BA, but does not rely on the baseline muscle carnosine, the muscle type, or the daily amount of supplemented BA.

Contribution to this paper:

I was substantially involved in the ¹H MRS examinations for carnosine and taurine in tibialis anterior and gastrocnemius muscle. At the ISMRM (International Society for Magnetic Resonance in Medicine) in 2010 I gave an oral presentation about this study⁶³. Additionally I had a share in literature research (especially dose response) and in proof-reading of this paper.

2.5 Effect of fructose and galactose on liver glycogen synthesis after exercise

Reference:

Decombaz J, Jentjens R, Ith M, Scheurer E, **Buehler T**, Jeukendrup A, Boesch C. Fructose and Galactose Enhance Post-Exercise Human Liver Glycogen Synthesis. *Med.Sci.Sports Exerc.* 43(10):1964-71 (2011)

Manuscript:

See section Original Manuscripts.

Summary:

Change of glycogen stores in exercise and fatigue are of interest. The effect of different carbohydrates on liver glycogen synthesis in humans is questioned. Therefore a study was designed with well-trained male cyclists consuming 3 drinks of carbohydrates (GLU = MD+glucose, FRU = MD+fructose, and GAL = MD+galactose, MD = maltodextrin) after exhausting workload on a bike. Liver glycogen concentration increased at faster rates with FRU and with GAL than with GLU. Liver volumes increased significantly with FRU and with GAL, but not with GLU. The increasing content of glycogen is nicely represented in the increasing volume of the liver: while GLU leads to a small increase in glycogen and liver volume, FRU and GAL show a significant increase in liver volume, corresponding to an increase in glycogen.

Contribution to this paper:

I was partially involved in the volumetry of the liver. In 2011 I presented a part of this study at the ESMRMB (European Society for Magnetic Resonance in Medicine and Biology) as an electronic poster⁶⁴. Additionally I had a share in proof-reading of this paper.

2.6 Effects of a whey protein on IHCL in obese female

Reference:

Bortolotti M, Maiolo E, Corazza M, van Dijke E, Schneiter P, Boss A, Carrel G, Giusti V, Le KA, Chong DGQ, **Buehler T**, Kreis R, Boesch C, Tappy L. Effects of a whey protein supplementation on intra-hepatocellular lipids in obese female. *Clin.Nutr.* 30: 494-498 (2011).

Manuscript:

See section Original Manuscripts.

Summary:

Hepatic steatosis is improved by intake of high protein diets in rodent models and high fat fed humans. The effect of a protein supplementation on intra-hepatocellular lipids (IHCL), and fasting plasma triglycerides in obese non diabetic women was questioned in this study. Intake of high protein diet decreased significantly IHCL (by 21%), fasting plasma triglycerides (by 15%), and total cholesterol (by 7%). The diet led to a slight increase of fat free mass. The other examined parameters, visceral fat, total liver volume, glucose tolerance, creatinine clearance and insulin sensitivity, remained unchanged. Hepatic steatosis and plasma lipid profiles are improved by a high protein diet in obese non diabetic patients, but with no severe effects on glucose tolerance or creatinine clearance.

Contribution to this paper:

I was partially involved in the volumetry of the visceral fat and the liver. Additionally I had a share in proof-reading of this paper.

3. Discussion

The aim of the thesis was to develop methodological tasks to investigate mitochondrial activity in human liver and skeletal muscle and to develop software to determine body compartments and/or the volume of single organs. Mitochondrial activity or e.g. the distribution and/or the amount of visceral adipose tissue (VAT) are important key data in combination with insulin resistance³¹.

Magnetization transfer techniques (saturation transfer (ST) and inversion transfer (IT)) were developed to determine the ATP synthesis rate as a measure of mitochondrial activity in human liver and skeletal muscle. Despite the challenges of volume selection and motion of the organ, the implementation of ST and IT in the liver was reliable, with reasonable signal-to-noise, and with only little contamination from abdominal wall muscles.

The overall spectra quality in skeletal muscle experiments was good. Spectral resolution in liver examinations was not always sufficient. Therefore 2 out of 10 experiments in the liver had to be repeated, respectively had to be replaced. To improve spectra quality e. g. the number of repetitions (averages) can be increased. Since ST and IT experiments are already time intensive examinations (~1.5 hours duration) this is only possible by reducing the repetition time (TR). This is not always possible, because of the relatively long relaxation times of phosphorus metabolites⁶⁵. In the case of the liver the relatively long set TR of 5s due to fitting robustness can be reduced to 3-4s in further done experiments using ST and IT. Motion triggering of the experiments in the liver may also improve spectra quality.

ATP synthesis exchange rates (k_{AB}) evaluated with ST in this thesis in skeletal thigh muscle are comparable with values evaluated in previous studies in human skeletal calf muscle⁴⁶. Even k_{AB} varies in different muscles¹⁶ they are about in the same range. ST measurements in the liver led to similar k_{AB} values as found in literature^{17,21}.

To my knowledge there exist so far no IT experiments in human skeletal muscle and liver to measure the ATP synthesis rate. k_{AB} values evaluated from IT are significantly higher than from ST. With a Monte Carlo simulation of k_{AB} it was shown that the overestimation is due to an insufficient inversion pulse and/or insufficient precision of measurement data. Improvement of both would make the data analysis of inversion transfer experiments more reliable. To use IT experiments in further studies its accuracy has to be enhanced, e.g. by improving sufficiency of selective inversion pulse and/or measurement precision. For liver as well as for skeletal muscle the inversion of the γ -ATP resonance is incomplete (on average -19% for skeletal muscle and -30% for liver). The inversion pulse is also not perfectly selective, which causes rf-bleedover (spillover). The spillover rate is typically 0.93 in skeletal muscle and 0.82 in liver. The γ -ATP and Pi curve have an actual measurement precision (standard deviation) of 2.4% (Pi) and 3.9% (γ -ATP) for the skeletal muscle and 5.7% (Pi) and 8.7% (γ -ATP) for liver evaluated from the experiments.

With the here presented ST experiment it is not possible to calculate the net ATP synthesis, because of the lack of information about the backward exchange rate constant k_{BA} in comparison to the IT experiment. A longer measurement time for the volunteer/patient to gain the information about k_{BA} with ST is almost not acceptable.

Besides the mentioned drawbacks of the two methods they have the advantage of being non-invasive methods (in comparison to biopsies), which allows e.g. repetitive measurements in longitudinal studies. ST is in addition generally accepted as reliable method to measure biochemical reactions such as the ATP synthesis. Especially in less good accessible organs as the liver such non-invasive methods are of advantage to prevent the patient from an invasive intervention.

IT experiments allow in comparison to the presented ST experiment the determination of the net ATP synthesis flux. But therefore the measurement precision and the precision of single elements in the sequence (e.g. inversion pulse) have to be sufficient enough for data fitting (determination of the kinetic parameters). IT has also the advantage of being the less complex sequence according to sequence programming. It could be an alternative, if it is not possible to implement a very long saturation pulse on specific scanners as needed for a ST experiment.

Insulin resistance is connected with obesity. Therefore in many studies about insulin resistance fat compartments, e.g. VAT or whole body fat (WBF), are evaluated. The intra-hepatocellular lipids (IHCL) or other metabolites as glycogen are often of interest in connection with insulin resistance. The volume of the organs has to be known for absolute quantification of the concentration of these metabolites. Therefore the other main task of the thesis was to program a MATLAB® software called *VISS* method (versatile, interactive sparse sampling method) for the determination of variable volumes (e.g. VAT, single organs) combining the strengths of three volume estimations: (a) threshold (b) manual planimetric methods, and (c) point counting.

Body compartments, especially fragmented VAT depots, are determined accurate and feasible with the *VISS* method. A reasonable agreement is found between and within the different raters (inter- and intra-observer variability). This is also in agreement with published methods⁶⁶ and with a reference volumetric method²³. Additionally the total body mass (TBM) was estimated from the different evaluated body compartments and its specific densities. TBM calculated from MRI agrees well with body weight that was determined by a scale.

A simple contour line is used to separate broad regions such as intra- vs. extra-abdominal region. A threshold based on a histogram quickly determines a major part of the points that have to be deleted (broad fat-water separation). Then the sparse data can be corrected easily by manual interaction. In comparison to a correction of the threshold technique, the removal or adding of a few points per slice is very flexible and fast. While threshold-only methods require compromises by the operator in different parts of the images as soon as rf-inhomogeneity reduces the intensity of fat voxels to that of voxels with water/non-fat-organs, the proposed *VISS* method is more transparent and leads to acceptable results. The combination of contour methods, threshold, and point-counting is at least as reliable as established threshold methods, in particular in complex shaped and inhomogeneous images. In addition the *VISS* method has been used for the volumetric determination of single organs, e.g. the liver²², which led also to reliable results. The strength of the *VISS* method is its reliable application to volumes with different characteristics.

Since the DICOM format of the read in pictures is not always the same and can differ from scanner to scanner, the read in process happens separately over an excel sheet, that has to be prepared by the user.

4. Outlook

The main focus was set on the development of methodological tasks. Their application and verification to a disease model, e.g. insulin resistant patients, patients with non-alcoholic fatty liver disease (NAFLD)⁶⁷ or a more severe state non-alcoholic steatohepatitis (NASH)⁶⁸ would be a further step. However a debate came up whether mitochondrial activity can be measured over basal ATP synthesis flux or not^{69,70}. This would have to be clarified.

Saturation transfer (ST) and inversion transfer (IT) experiments are both reliable experiments to evaluate ATP synthesis rates in human skeletal muscle and liver. For IT experiments some improvements have to be done to increase spectrum quality (mainly in the liver). This could be done by motion triggered measurements in the liver, which is moving due to breathing. Spectra quality can probably be improved more efficiently by reducing rf-bleedover and/or increase of inversion ability of the selective inversion pulse used in this experiment. As soon as the experiment quality of IT is sufficient enough, both methods can be used to evaluate glycolytic and oxidative contribution, and parts from small exchanging pools (e.g. ADP) to the ATP synthesis as stated in Balaban et. al.⁴⁹.

Volume determination with the *VISS* method is feasible and fast and it is applicable to variable volumes with different characteristics (e.g. VAT or single organs). *VISS* is so far a software used in-house. If one would make it accessible to users outside of the institute for testing, it's value and impact could be increased or at least still possible existing bugs could be fixed.

References

1. Eckel RH, Grundy SM, Zimmet PZ. The metabolic syndrome. *Lancet* 2005; **365**: 1415-1428.
2. van Loon LJ, Goodpaster BH. Increased intramuscular lipid storage in the insulin-resistant and endurance-trained state. *Pflugers Arch.* 2006; **451**: 606-616.
3. Patti ME, Corvera S. The Role of Mitochondria in the Pathogenesis of Type 2 Diabetes. *Endocr.Rev.* 2010; **31**: 364-395.
4. Batsis JA, Nieto-Martinez RE, Lopez-Jimenez F. Metabolic syndrome: from global epidemiology to individualized medicine. *Clin.Pharmacol.Ther.* 2007; **82**: 509-524.
5. Grundy SM. Metabolic syndrome: a multiplex cardiovascular risk factor. *J.Clin.Endocrinol.Metab.* 2007; **92**: 399-404.
6. Boesch C. Magnetic Resonance Spectroscopy: Basic Principles. In: Edelman RR, Hesselink JR, Zlatkin MB, Cruess JV (eds) *Clinical Magnetic Resonance Imaging*. Saunders, Elsevier: Philadelphia, PA 2005.
7. Boesch C. Molecular aspects of magnetic resonance imaging and spectroscopy. *Mol.Aspects Med.* 1999; **20**: 185-318.
8. Heerschap A, Houtman C, in 't Zandt HJ, van den Bergh AJ, Wieringa B. Introduction to in vivo ³¹P magnetic resonance spectroscopy of (human) skeletal muscle. *Proc.Nutr.Soc.* 1999; **58**: 861-870.
9. Leibfritz D, Dreher W. Magnetization transfer MRS. *NMR Biomed.* 2001; **14**: 65-76.
10. Kuchel PW. Spin-exchange NMR spectroscopy in studies of the kinetics of enzymes and membrane transport. *NMR Biomed.* 1990; **3**: 102-119.
11. Rudin M. Measurement of exchange reactions in vivo using NMR magnetization transfer techniques. *Magn.Reson.Med.Biol.* 1989; **2**: 177-195.
12. Szendroedi J, Roden M. Mitochondrial fitness and insulin sensitivity in humans. *Diabetologia* 2008; **51**: 2155-2167.
13. Petersen KF, Dufour S, Befroy D, Garcia R, Shulman GI. Impaired mitochondrial activity in the insulin-resistant offspring of patients with type 2 diabetes. *N.Engl.J.Med.* 2004; **350**: 664-671.
14. Forsen S, Hoffman RA. Study of Moderately Rapid Chemical Exchange Reactions by Means of Nuclear Magnetic Double Resonance. *J.Chem.Phys.* 1963; **39**: 2892-2901.
15. Brown TR, Ugurbil K, Shulman RG. ³¹P nuclear magnetic resonance measurements of ATPase kinetics in aerobic Escherichia coli cells. *Proc.Natl.Acad.Sci.U.S.A.* 1977; **74**: 5551-5553.
16. Befroy DE, Petersen KF, Shulman GI, Rothman DL. Localized ³¹P saturation transfer reveals differences in gastrocnemius and soleus rates of ATP synthesis in-vivo. *Proc.Intl.Soc.Magn.Reson.Med.* 2008; **16**: 2565.
17. Schmid AI, Chmelik M, Szendroedi J, Krssak M, Brehm A, Moser E, Roden M. Quantitative ATP synthesis in human liver measured by localized (³¹P) spectroscopy using the magnetization transfer experiment. *NMR Biomed.* 2008; **21**: 437-443.
18. Despres JP, Lemieux I. Abdominal obesity and metabolic syndrome. *Nature* 2006; **444**: 881-887.
19. Kullberg J, Brandberg J, Angelhed JE, Frimmel H, Bergelin E, Strid L, Ahlstrom H, Johansson L, Lonn L. Whole-body adipose tissue analysis: comparison of MRI, CT and dual energy X-ray absorptiometry. *Br.J.Radiol.* 2009; **82**: 123-130.

20. Pietrobelli A, Tato L. Body composition measurements: from the past to the future. *Acta Paediatr.Suppl.* 2005; **94**: 8-13.
21. Schmid AI, Szendroedi J, Chmelik M, Krssak M, Moser E, Roden M. Liver ATP synthesis is lower and relates to insulin sensitivity in patients with type 2 diabetes. *Diabetes Care* 2011; **34**: 448-453.
22. Decombaz J, Jentjens R, Ith M, Scheurer E, Buehler T, Jeukendrup A, Boesch C. Fructose and Galactose Enhance Post-Exercise Human Liver Glycogen Synthesis. *Med.Sci.Sports Exerc.* 2011; **43**: 1964-1971.
23. Machann J, Thamer C, Schoedt B, Haap M, Haring HU, Claussen CD, Stumvoll M, Fritsche A, Schick F. Standardized assessment of whole body adipose tissue topography by MRI. *J.Magn.Reson.Imaging* 2005; **21**: 455-462.
24. Purcell EM, Torrey HC, Pound RV. Resonance absorption by nuclear magnetic moments in solids. *Phys.Rev.* 1946; **69**: 37-38.
25. Bloch F, Hansen WW, Packard M. Nuclear induction. *Phys.Rev.* 1946; **69**: 127.
26. Ernst RR, Anderson WA. Application of Fourier Transform Spectroscopy to Magnetic Resonance. *Rev.Sci.Instrum.* 1966; **37**: 93-102.
27. Proctor WG, Yu FC. The dependence of a nuclear magnetic resonance frequency upon chemical compound. *Phys.Rev.* 1950; **77**: 717.
28. Mansfield P, Grannell PK. NMR 'diffraction' in solids. *J.Phys.C: Solid State* 1973; **6**: L422-L426.
29. Lauterbur PC. Image formation by induced local interactions: examples employing nuclear magnetic resonance. *Nature* 1973; **242**: 190-191.
30. Hahn EL. Spin echoes. *Phys.Rev.* 1950; **80**: 580-594.
31. Wallace DC, Fan W, Procaccio V. Mitochondrial Energetics and Therapeutics. *Annu Rev Pathol* 2010; **5**: 297-348.
32. Richardson RS, Saltin B. Human muscle blood flow and metabolism studied in the isolated quadriceps muscles. *Med.Sci.Sports Exerc.* 1998; **30**: 28-33.
33. Carlier PG, Brillault-Salvat C, Giacomini E, Wary C, Bloch G. How to investigate oxygen supply, uptake, and utilization simultaneously by interleaved NMR imaging and spectroscopy of the skeletal muscle. *Magn.Reson.Med.* 2005; **54**: 1010-1013.
34. Befroy DE, Petersen KF, Rothman DL, Shulman GI. Assessment of in vivo mitochondrial metabolism by magnetic resonance spectroscopy. *Methods Enzymol.* 2009; **457**: 373-393.
35. Jucker BM, Dufour S, Ren J, Cao X, Previs SF, Underhill B, Cadman KS, Shulman GI. Assessment of mitochondrial energy coupling in vivo by ¹³C/³¹P NMR. *Proc.Natl.Acad.Sci.U.S.A.* 2000; **97**: 6880-6884.
36. Schmid AI, Schrauwen-Henderling VB, Andreas M, Wolzt M, Moser E, Roden M. Comparison of Measuring Energy Metabolism by Different ³¹P-Magnetic Resonance Spectroscopy Techniques in Resting, Ischemic, and Exercising Muscle. *Magn.Reson.Med.* 2011; DOI 10.1002/mrm.23095.
37. Kemp GJ, Meyerspeer M, Moser E. Absolute quantification of phosphorus metabolite concentrations in human muscle in vivo by ³¹P MRS: a quantitative review. *NMR Biomed.* 2007; **20**: 555-565.
38. Gadian DG, Radda GK, Brown TR, Chance EM, Dawson MJ, Wilkie DR. The activity of creatine kinase in frog skeletal muscle studied by saturation-transfer nuclear magnetic resonance. *Biochem.J.* 1981; **194**: 215-228.

39. Lebon V, Dufour S, Petersen KF, Ren J, Jucker BM, Slezak LA, Cline GW, Rothman DL, Shulman GI. Effect of triiodothyronine on mitochondrial energy coupling in human skeletal muscle. *J.Clin.Invest.* 2001; **108**: 733-737.
40. Haseler LJ, Hogan MC, Richardson RS. Skeletal muscle phosphocreatine recovery in exercise-trained humans is dependent on O₂ availability. *J.Appl.Physiol.* 1999; **86**: 2013-2018.
41. Szendroedi J, Schmid AI, Chmelik M, Toth C, Brehm A, Krssak M, Nowotny P, Wolzt M, Waldhausl W, Roden M. Muscle mitochondrial ATP synthesis and glucose transport/phosphorylation in type 2 diabetes. *PLoS Med.* 2007; **4**: 858-867.
42. Petersen KF, Dufour S, Shulman GI. Decreased insulin-stimulated ATP synthesis and phosphate transport in muscle of insulin-resistant offspring of type 2 diabetic parents. *PLoS Med.* 2005; **2**: e233.
43. Thoma WJ, Ugurbil K. Saturation-transfer studies of ATP-Pi exchange in isolated perfused rat liver. *Biochim.Biophys.Acta* 1987; **893**: 225-231.
44. Hsieh PS, Balaban RS. Saturation and inversion transfer studies of creatine kinase kinetics in rabbit skeletal muscle in vivo. *Magn.Reson.Med.* 1988; **7**: 56-64.
45. Degani H, Laughlin M, Campbell S, Shulman RG. Kinetics of Creatine Kinase in Heart: A 31P NMR Saturation- and Inversion-Transfer Study. *Biochemistry* 1985; **24**: 5510-5516.
46. Kemp GJ. The interpretation of abnormal 31P magnetic resonance saturation transfer measurements of Pi/ATP exchange in insulin-resistant skeletal muscle. *Am.J.Physiol.* 2008; **294**: E640-E642.
47. Befroy DE, Petersen KF, Dufour S, Mason GF, De Graaf RA, Rothman DL, Shulman GI. Impaired mitochondrial substrate oxidation in muscle of insulin-resistant offspring of type 2 diabetic patients. *Diabetes* 2007; **56**: 1376-1381.
48. From AH, Ugurbil K. Standard magnetic resonance-based measurements of the Pi=>ATP rate do not index the rate of oxidative phosphorylation in cardiac and skeletal muscles. *AmJPhysiolCellPhysiol* 2011; **301**: C1-C11.
49. Balaban RS, Koretsky AP. Interpretation of 31P NMR saturation transfer experiments: what you can't see might confuse you. Focus on "Standard magnetic resonance-based measurements of the Pi=>ATP rate do not index the rate of oxidative phosphorylation in cardiac and skeletal muscles". *AmJPhysiolCellPhysiol* 2011; **301**: C12-C15.
50. Abate N, Burns D, Peshock RM, Garg A, Grundy SM. Estimation of adipose tissue mass by magnetic resonance imaging: validation against dissection in human cadavers. *J.Lipid Res.* 1994; **35**: 1490-1496.
51. Hu HH, Nayak KS, Goran MI. Assessment of abdominal adipose tissue and organ fat content by magnetic resonance imaging. *Obes.Rev.* 2011; **12**: e504-e515.
52. Lancaster JL, Ghiatas AA, Alyassin A, Kilcoyne RF, Bonora E, DeFronzo RA. Measurement of abdominal fat with T1-weighted MR images. *J.Magn.Reson.Imaging* 1991; **1**: 363-369.
53. Ma J. Breath-hold water and fat imaging using a dual-echo two-point Dixon technique with an efficient and robust phase-correction algorithm. *Magn.Reson.Med.* 2004; **52**: 415-419.
54. Glover GH, Schneider E. Three-point Dixon technique for true water/fat decomposition with B₀ inhomogeneity correction. *Magn.Reson.Med.* 1991; **18**: 371-383.
55. Reeder SB, McKenzie CA, Pineda AR, Yu H, Shimakawa A, Brau AC, Hargreaves BA, Gold GE, Brittain JH. Water-fat separation with IDEAL gradient-echo imaging. *J.Magn.Reson.Imaging* 2007; **25**: 644-652.

56. Kijowski R, Woods MA, Lee KS, Takimi K, Yu H, Shimakawa A, Brittain JH, Reeder SB. Improved fat suppression using multipeak reconstruction for IDEAL chemical shift fat-water separation: application with fast spin echo imaging. *J.Magn.Reson.Imaging* 2009; **29**: 436-442.
57. Bonekamp S, Ghosh P, Crawford S, Solga SF, Horska A, Brancati FL, Diehl AM, Smith S, Clark JM. Quantitative comparison and evaluation of software packages for assessment of abdominal adipose tissue distribution by magnetic resonance imaging. *Int.J.Obes.* 2008; **32**: 100-111.
58. Demerath EW, Ritter KJ, Couch WA, Rogers NL, Moreno GM, Choh A, Lee M, Remsberg K, Czerwinski SA, Chumlea WC, Siervogel RM, Towne B. Validity of a new automated software program for visceral adipose tissue estimation. *Int.J.Obes.* 2007; **31**: 285-291.
59. Wurslin C, Machann J, Rempp H, Claussen C, Yang B, Schick F. Topography mapping of whole body adipose tissue using a fully automated and standardized procedure. *J.Magn.Reson.Imaging* 2010; **31**: 430-439.
60. Mazonakis M, Damilakis J, Mantatzis M, Prassopoulos P, Maris T, Varveris H, Gourtsoyiannis N. Stereology versus planimetry to estimate the volume of malignant liver lesions on MR imaging. *Magn.Reson.Imaging* 2004; **22**: 1011-1016.
61. Buehler T, Ramseier N, Machann J, Schwenzler NF, Boesch C. Magnetic resonance imaging based determination of body compartments with the versatile, interactive sparse sampling (VISS) method. *submitted* 2012.
62. Roberts N, Barbosa S, Blumhardt CS, Kawoski RA, Edwards RHT. Stereological estimation of the total volume of MR visible brain lesions in patients with multiple sclerosis. *Magn.Reson.Mater.Phys.* 1994; **2**: 1-4.
63. Buehler T, Stellingwerff T, Anwander H, Egger A, Kreis R, Boesch C. The effect of two beta-alanine dosing protocols on muscle carnosine synthesis and washout measured by ¹H-MR spectroscopy. *Proc.Intl.Soc.Magn.Reson.Med.* 2010; **18**: 417.
64. Buehler T, Ith M, Scheurer E, Decombaz J, Boesch C. MRI based volume determination of single organs using the Versatile, Interactive Sparse Sampling (VISS) method. *ESMRMB Annual Meeting* 2011; **28th**: 575.
65. Meyerspeer M, Krssak M, Moser E. Relaxation times of ³¹P-metabolites in human calf muscle at 3 T. *Magn.Reson.Med.* 2003; **49**: 620-625.
66. Arif H, Racette SB, Villareal DT, Holloszy JO, Weiss EP. Comparison of methods for assessing abdominal adipose tissue from magnetic resonance images. *Obesity* 2007; **15**: 2240-2244.
67. Sevastianova K, Hakkarainen A, Kotronen A, Corner A, Arkkila P, Arola J, Westerbacka J, Bergholm R, Lundbom J, Lundbom N, Yki-Jarvinen H. Nonalcoholic fatty liver disease: detection of elevated nicotinamide adenine dinucleotide phosphate with in vivo 3.0-T ³¹P MR spectroscopy with proton decoupling. *Radiology* 2010; **256**: 466-473.
68. Pessayre D, Fromenty B. NASH: a mitochondrial disease. *J.Hepatol.* 2005; **42**: 928-940.
69. van den Broek NM, Ciapaite J, Nicolay K, Prompers JJ. Comparison of in vivo postexercise phosphocreatine recovery and resting ATP synthesis flux for the assessment of skeletal muscle mitochondrial function. *Am.J.Physiol.* 2010; **299**: C1136-C1143.
70. Sleigh A, Raymond-Barker P, Thackray K, Porter D, Hatunic M, Vottero A, Burren C, Mitchell C, McIntyre M, Brage S, Carpenter TA, Murgatroyd PR, Brindle KM, Kemp GJ, O'Rahilly S, Semple RK, Savage DB. Mitochondrial dysfunction in patients with primary congenital insulin resistance. *J.Clin.Invest.* 2011; **121**: 2457-2461.

Acknowledgements

I would like to thank my supervisor Prof. Chris Boesch for the opportunity to join his research group and for the constructive scientific support during the whole duration of this thesis. Especially I would like to mention his willingness for short notice discussions just by knocking on his door without having to wait for a long time for an appointment. And I also would like to thank for the many times sitting together in front of the scanner teaching me MRS skills.

Prof. Peter Bigler has accepted to be the co-referee of my PhD thesis. I would like to thank him for his critical questions and good ideas. He provided useful input for my work. Even as he went into retirement he continued his support to my PhD thesis.

Furthermore, I'm very thankful to Prof. Primus-E Mullis my mentor from the Graduate School for Cellular and Biomedical Sciences of the University of Bern.

The AMSM group members I would like to thank to be such good colleagues. I enjoyed the shared skiing days, the evenings with games or downtown, or even the nice and refreshing talks in the morning coffee breaks.

I would like to thank Andrea Egger, Peter Diem, Christoph Stettler, Emanuel Christ, Nicolas Ramseier, Jürgen Machann, Nina Schwenzer, and Roland Kreis for the contribution to own or shared papers and the good collaboration.

Special thanks go to Jacques Decombaz and Trent Stellingwerff, to Luc Tappy, Murielle Bortolotti, and Fanny Theytaz to let me be a collaborator of their studies.

Our former medical and English students Sabine Koenig, Regula Koenig, Elisabeth Schaller, and Aurelia Rusch-Koelber did a great job in being an operator for the determination of different kinds of body volumes with the *V*/SS method. I would like to thank them for their help.

Last but not least, I would like to thank the Swiss National Foundation for funding.

List of Publications

Original Papers

Accepted:

- Buehler T, Ramseier N, Machann J, Schwenzer NF, Boesch C. Magnetic Resonance Imaging based Determination of Body Compartments with the Versatile, Interactive, Sparse Sampling (VISS) Method. *J. Magn. Reson. Imag.* (accepted for publication April 2012)
IF(2010) 2.747, Ranking 0.673.
- Stellingwerff T, Anwander H, Egger A, Buehler T, Kreis R, Decombaz J, Boesch C. Effect of two b-alanine dosing protocols on muscle carnosine synthesis and washout. *Amino Acids*: Epub ahead of print: DOI: 10.1007/s00726-011-1054-4. (2011)
IF(2010) 4.106, Ranking 0.715.
- Decombaz J, Jentjens R, Ith M, Scheurer E, Buehler T, Jeukendrup A, Boesch C. Fructose and Galactose Enhance Post-Exercise Human Liver Glycogen Synthesis. *Med.Sci.Sports Exerc.* 43(10):1964-71 (2011)
IF(2010) 4.106, Ranking 0.969.
- Bortolotti M, Maiolo E, Corazza M, van Dijke E, Schneiter P, Boss A, Carrel G, Giusti V, Le KA, Chong DGQ, Buehler T, Kreis R, Boesch C, Tappy L. Effects of a whey protein supplementation on intra-hepatocellular lipids in obese female. *Clin.Nutr.* 30: 494-498 (2011).
IF(2010) 3.410, Ranking 0.791.
- Egger A*, Buehler T*, Boesch C, Diem P, Stettler C, Christ ER. The Effect of Growth Hormone Replacement Therapy on Different Fat Compartments: A Whole Body Magnetic Resonance Imaging Study. *Eur.J.Endocrinol.* 164: 23-29 (2011).
IF(2010) 3.482, Ranking 0.661.
(*A Egger and T Buehler contributed equally to this work)
- Buehler T, Raible CC, Stocker TF. The relationship of winter season North Atlantic blocking frequencies to extreme cold or dry spells in the ERA-40. *Tellus Series A - Dynamic meteorology and oceanography* 63A: 212-222 (2011).
IF(2010) 2.062, Ranking 0.647.

Submitted:

- Theytaz F, Noguchi Y, Egli L, Campos V, Buehler T, Hodson L, Patterson BW, Nishikata N, Kreis R, Mittendorfer B, Fielding B, Boesch C, Tappy L. Effects of a Supplementation in Essential Amino Acids on Hepatic Steatosis Induced by Fructose in Healthy Humans. *Am J Clin Nutr.* (submitted January 2012)

In progress:

- Buehler T et. al. Applying ³¹P saturation and inversion transfer in human liver and skeletal muscle to measure ATP synthesis exchange rate constants. *NMR Biomed.* (in preparation, based on abstract "Determination of ATP synthesis exchange rates in human liver and skeletal muscle using ³¹P magnetization transfer" below)

Abstracts

- Buehler T, Ith M, Scheurer E, Decombaz J, Boesch C. MRI based volume determination of single organs using the Versatile, Interactive Sparse Sampling (VISS) method. ESMRMB Annual Meeting 28th: 575 (2011).
- Buehler T, Boss A, Kreis R, Boesch C. Determination of ATP synthesis exchange rates in human liver and skeletal muscle using ^{31}P magnetization transfer. Proc.Intl.Soc.Magn.Reson.Med. 19: 3005 (2011).
- Stellingwerff T, Anwander H, Egger A, Buehler T, Kreis R, Boesch C, Decombaz J. The Effect Of Two b-alanine Dosing Protocols On Muscle Carnosine Synthesis And Washout. Med.Sci.Sports Exerc. 42Suppl: 108 (2010).
- Buehler T, Ramseier N, Machann J, Schwenzer N, Boesch C. Determination of body compartments at 1.5 and 3 Tesla, combining three volume estimation methods. Proc.Intl.Soc.Magn.Reson.Med. 18: 2915 (2010).
- Buehler T, Stellingwerff T, Anwander H, Egger A, Kreis R, Boesch C. The effect of two beta-alanine dosing protocols on muscle carnosine synthesis and washout measured by ^1H -MR spectroscopy. Proc.Intl.Soc.Magn.Reson.Med. 18: 417 (2010).
- Egger A, Boesch C, Stettler C, Ramseier N, Koenig R, Buehler T, Diem P, Christ ER. Comparison of Bio Impedance Analysis and a Magnetic Resonance Based Volume Estimation Method in Healthy Subjects and in Hypopituitary Patients with Growth Hormone Deficiency Before and After Therapy. Scientific Meeting of the Swiss Society of Endocrinology and Diabetology (2009).
- Buehler T, Chong DG, Boesch C. Rapid and accurate volumetric method for inhomogeneous images. ESMRMB Annual Meeting 26th: 505 (2009).
- Buehler T, Chong DG, Boesch C. Determination of whole body fat and visceral adipose tissue, combining three volume estimation methods. Proc.Intl.Soc.Magn.Reson.Med. 17: 2872 (2009).

Declaration of Originality

Last name, first name: Buehler Tania

Matriculation number: 03-102-290

I hereby declare that this thesis represents my original work and that I have used no other sources except as noted by citations.

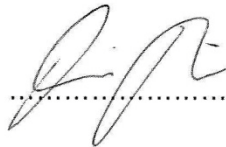
All data, tables, figures and text citations which have been reproduced from any other source, including the internet, have been explicitly acknowledged as such.

I am aware that in case of non-compliance, the Senate is entitled to divest me of the doctorate degree awarded to me on the basis of the present thesis, in accordance with the "Statut der Universität Bern (Universitätsstatut; UniSt)", Art. 20, of 17 December 1997.

Place, date

Signature

Bern, 07.03.2012



.....

Original Manuscripts

Applying ^{31}P saturation and inversion transfer in human liver and skeletal muscle to measure ATP synthesis exchange rate constants

short title: ^{31}P magnetization transfer in human liver and skeletal muscle

Tania Buehler¹, Roland Kreis¹, Chris Boesch¹

¹Department of Clinical Research, University of Bern, Switzerland

Tania Buehler Dipl. Phys.

University Bern, Dept. Clinical Research/AMSM, Pavilion 52, P.O. Box 35, Inselspital, CH-3010 Bern, Switzerland

e-mail: tania.buehler@insel.ch, tania_buehler@gmx.net

phone: ++41-31-632-81-74

fax: ++41-31-632-05-80

Supported by the Swiss National Science Foundation (#310000-118219)

Abstract

^{31}P MRS is a non-invasive and widely used tool for direct and quantitative measurements of human metabolism. In some specific diseases such as insulin resistance, the energy production of the mitochondria (especially mitochondrial activity) is a key parameter in understanding the underlying biochemical mechanisms of the disorder. Therefore two magnetization transfer methods were developed on a 3 Tesla TIM TRIO SIEMENS scanner to determine ATP synthesis rates as a measure of mitochondrial activity in skeletal muscle and liver.

ATP synthesis rates were determined and compared using the two methods saturation transfer (ST) and inversion transfer (IT) in skeletal thigh muscle ($n = 10$) and liver ($n = 10$). The volume selection in the liver was done by suppressing signal from the abdominal wall muscles using spatial saturation bands.

The implementation of IT and ST in the liver was reliable, with reasonable signal-to-noise, and with only little contamination from abdominal wall muscles. The average exchange rate constant k_{AB} in the thigh skeletal muscle is $0.084 \pm 0.017\text{s}^{-1}$ (ST) and $0.140 \pm 0.046\text{s}^{-1}$ (IT), resp. $0.232 \pm 0.079\text{s}^{-1}$ (ST) and $0.463 \pm 0.190\text{s}^{-1}$ (IT) in the liver. The IT measurements overestimate ATP synthesis rates in the liver due to an insufficient selective inversion pulse.

Keywords: ^{31}P MRS; magnetization transfer; saturation transfer; inversion transfer; ATP synthesis; liver; skeletal muscle, insulin resistance

Abbreviations

ADP	adenosine diphosphate
AMARES	advanced method for accurate, robust and efficient spectral fitting of MRS data with use of prior knowledge
ATP	adenosine triphosphate
BMI	body mass index
CV	coefficient of variance
fATP	forward ATP synthesis flux determined by ST and IT
f_{mirror}	mirror frequency of the saturation transfer experiment
f_{Pi}	frequency of inorganic phosphate
$f_{\gamma\text{-ATP}}$	frequency of γ -ATP
IT	inversion transfer
JMRUI	Java Magnetic Resonance User Interface
k_{AB}	forward exchange rate constant of ATP synthesis
k_{BA}	backward exchange rate constant of ATP synthesis
MATLAB	matrix laboratory, a high-performance language for technical computing
MRS	magnetic resonance spectroscopy
$M_{\text{ZA}}(t)$	longitudinal magnetization of pool A (Pi) at time t
$M_{\text{ZA}0}$	equilibrium longitudinal magnetization of pool A (Pi)
$M_{\text{ZA}\infty}$	longitudinal magnetization of pool A (Pi) under long saturation time
$M_{\text{ZB}}(t)$	longitudinal magnetization of pool B (γ -ATP) at time t
$M_{\text{ZB}0}$	equilibrium longitudinal magnetization of pool B (Pi)
$M_{\text{ZB}\infty}$	longitudinal magnetization of pool B (Pi) under long saturation time
NADH	nicotinamide adenine dinucleotide
PCr	phosphocreatine
PDE	phosphodiester
Pi	inorganic phosphate
[Pi]	concentration of inorganic phosphate
PME	phosphomonoesters
P/O ratio	ratio of ATP produced per oxygen atom
SD	standard deviation
ST	saturation transfer
T_1	longitudinal relaxation time
$T_{1\text{A}}$	longitudinal relaxation time of pool A (Pi)
$T_{1\text{A}^*}$	longitudinal relaxation time of pool A (Pi) under saturation/inversion of pool B (γ -ATP)
$T_{1\text{B}}$	longitudinal relaxation time of pool B (Pi)
TI	inversion time
TR	repetition time

INTRODUCTION

The metabolic syndrome describes an exceedingly relevant yet not very well defined disorder that is mainly defined by insulin resistance¹. It comes along with obesity and/or aging and represents a serious risk for the individual patient with increased probability to develop type 2 diabetes and cardiovascular disease, including myocardial infarction and stroke². The prevalence of the metabolic syndrome increased during the last few decades and reached epidemic dimensions. It affects up to 40% of the population².

³¹P MRS has been widely used to study metabolism in skeletal muscle or other organs of the body³. Especially magnetization transfer methods, as saturation transfer and inversion transfer, allow to follow spin exchange in moderately rapid biochemical reactions and to determine exchange rate constants and reaction fluxes⁴. Particularly interesting are reactions in mitochondria, which could lead to a better understanding of insulin resistance and ageing⁵.

Few years ago the hypothesis came up that insulin resistance could be caused by impaired mitochondrial activity⁶. Therefore mitochondrial activity was assessed by the measurement of ATP synthesis using phosphocreatine (PCr) recovery and/or saturation transfer experiments⁶⁻¹⁰. Recently the reliability of the saturation transfer method to measure mitochondrial activity was questioned because it neglects contribution to ATP synthesis from the glycolytic pathway¹⁰⁻¹². In human skeletal muscle the part of aerobic to anaerobic contribution is 90% to 10%⁹ and in human liver its estimated to be 25% to 75%¹³. The high contribution to the aerobic part in skeletal muscle makes saturation transfer still to a reliable method to measure mitochondrial activity. In the liver there is no PCr, and therefore the traditional method of PCr recovery is not applicable in the liver.

Another issue on the saturation transfer method is that its values for ATP synthesis exchange rates are much higher compared to other methods in skeletal muscle^{14,15}. Comparing different techniques in young healthy subjects indeed confirmed the anomalously high results from saturation transfer⁹, but the authors showed correlation between the two measurements, and argued that resting saturation transfer measurements could therefore still provide an indicator of mitochondrial oxidative capacity.

The inversion transfer experiment is a pulsed magnetization transfer experiment and it is also a valuable experiment to determine ATP synthesis rates. It is the less sensitive experiment in comparison with saturation transfer and it neglects contribution from small exchanging pools (e.g. adenosine diphosphate (ADP))¹². From the inversion transfer experiment the forward and backward flux of the ATP synthesis can be calculated. Due to the more parameters that have to be fitted it is the less robust method compared to saturation transfer. But in comparison it measures the forward and backward ATP synthesis flux, from which the net flux can be calculated. It has been applied in rabbit skeletal¹⁶ muscle or rat hearts¹⁷, but for the creatine kinase reaction. So far inversion transfer hasn't been applied in human skeletal muscle and liver.

While magnetization transfer experiments have already been introduced a few decades ago, applications in human and in particular in moving organs still need considerable development¹³. We evaluated saturation and inversion transfer experiments on a 3 T MR system in skeletal muscle and liver for a non-invasive characterization of mitochondrial activity measured by the exchange rate constant and the flux through ATP synthesis ($\text{ADP} + \text{P}_i \rightarrow \text{ATP}$). While saturation vs. inversion transfer in skeletal muscle allowed a comparison with data obtained in a static organ without volume selection, the

measurements in liver had to be developed for reliable volume selection. To our knowledge a comparison of saturation and inversion transfer experiments in human skeletal muscle and liver hasn't been done so far.

EXPERIMENTAL

Human subjects

This study was approved by the local ethics committee and from 22 healthy volunteers written informed consent was obtained. All volunteers underwent two consecutive measurements of approximately 1.5 hours duration each (saturation transfer experiment followed by an inversion transfer experiment) with half an hour break in between. Due to not sufficient quality of liver spectra 2 out of 12 volunteers had to be excluded from the study. 10 volunteers were measured in the right thigh muscle (three male, seven female; mean \pm standard deviation (SD) age 30.3 ± 12.1 years, body mass index (BMI) 23.3 ± 2.5 kg/m²) and 10 in the liver (five male, five female; mean \pm SD age 24.8 ± 3.1 years, BMI 23.0 ± 2.1 kg/m²).

All measurements were done on a 3 Tesla MR system (TIM TRIO, Siemens Healthcare, Erlangen, Germany, syngo MR VB15 software) with horizontal orientation of the bore and 60 cm bore size. For the magnetization transfer experiments a ¹H/³¹P flexible surface coil (RAPID Biomedical GmbH) was used. Prior to the experiment localizer images in all three directions were recorded with the body coil. For the liver additional images in axial direction were recorded in breath hold with the surface coil for setting the spatial saturation bands (see Fig.1).

Localization of the ³¹P signal

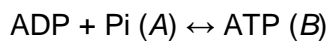
Acquisition was done by using a modified free induction decay product sequence (see Fig. 2). The block pulse for excitation was replaced by a 90° adiabatic excitation pulse (duration 2.56ms; bandwidth 1000 Hz). The volume selection was achieved by the surface coil excitation and in the liver with four additional regional saturation bands (slice selective

sinc pulses) to suppress the signals from muscles of the abdominal wall (see Fig. 1). The coil was placed over the right thigh muscle or the lateral aspect of the liver. In cases where the coil over the liver was misplaced a repositioning of the coil was done. Automatic shimming was performed during free breathing of the volunteer during the first phosphorus sequence. If shimming was not sufficient, shimming was forced to be redone by replacing the adjustment volume.

The repetition time in all ^{31}P experiments was set according to a multiple of measured longitudinal relaxation times (T_1) of ^{31}P metabolites at 3T in skeletal muscle¹⁸ and liver¹³.

Magnetization transfer

Reaction rates and fluxes of biochemical reactions can be measured by NMR spectroscopy *in vivo*. In magnetization transfer experiments like saturation transfer and inversion transfer the magnetic equilibrium is disturbed, but not the chemical equilibrium. The idea is to disturb one side of a biochemical reaction (e. g. γ -ATP) with a saturation or inversion of a resonance) and look at the effect on the other side (e.g. inorganic phosphate (Pi)).



The Bloch equations for a two side biochemical exchange reaction that take T_1 relaxation and biochemical exchange into account look as follows:

$$\frac{\partial M_{ZA}(t)}{\partial t} = \frac{M_{ZA0} - M_{ZA}(t)}{T_{1A}} - k_{AB} \cdot M_{ZA}(t) + k_{BA} \cdot M_{ZB}(t) \quad (1)$$

$$\frac{\partial M_{ZB}(t)}{\partial t} = \frac{M_{ZB0} - M_{ZB}(t)}{T_{1B}} + k_{AB} \cdot M_{ZA}(t) - k_{BA} \cdot M_{ZB}(t) \quad (2)$$

Saturation transfer

In the case of saturation transfer the γ -ATP resonance is selectively saturated (train of rectangular block pulses, 100 ms duration each, 0.12 ms break in between, maximum train length 20 s), which results in a signal decrease of the Pi resonance (see Tab. 1 for detailed sequence parameters). Due to rf-bleedover of the selective saturation pulse the signal $M_{ZA\infty}$ of the Pi resonance is measured with selective saturation at a mirror frequency. The mirror frequency is calculated as follows:

$$f_{mirror} = 2 \cdot f_{Pi} - f_{\gamma-ATP} \quad (3)$$

From the difference of the spectrum saturated at γ -ATP resonance and at mirror frequency, the forward exchange rate constant k_{AB} can be calculated. The saturation of signal B (γ -ATP) simplifies the Bloch equations from above and one gets for the forward exchange rate constant k_{AB} the following equation:

$$k_{AB} = \frac{1}{T_{1A}^*} \cdot \left(1 - \frac{M_{ZA\infty}}{M_{ZA0}}\right), t \rightarrow \infty \quad (4)$$

To evaluate the T_{1A}^* relaxation parameter for Pi under selective saturation of γ -ATP a classical inversion recovery experiment was performed. For the inversion a non-selective adiabatic inversion pulse was used (duration 10 ms, bandwidth 1000 Hz). The total saturation duration was kept constant (e.g. 14 s for muscle and 4.2 s for liver, see Tab. 1), but the saturation duration prior to the inversion pulse was adjusted according to the variable inversion time (TI). T_{1A}^* relaxation times were fitted as single exponentials according to:

$$M_{ZA}(t) = M_{ZA0} \cdot \left(1 - inv \cdot \exp\left(-\frac{t}{T_{1A}^*}\right)\right) \quad (5)$$

The parameter *inv* indicates the grade of inversion of signal Pi and is 2 for complete inversion and 0 for no inversion.

Inversion transfer

In the case of inversion transfer the γ -ATP resonance is selectively inverted (duration 100 ms). The spectrum is acquired after different inversion times (T_I). The inversion time is the time between inversion and acquisition pulse. The inversion of the γ -ATP resonance results first in a signal decrease and then a recovery of the Pi resonance. There is no simplification of the Bloch equations from above when using inversion transfer. The four kinetic parameters (k_{AB} , k_{BA} , T_{1A}^* , T_{1B}^*) have to be fitted by least square curve fitting to the curves of the signals γ -ATP and Pi. See Table 1 for sequence parameters of the inversion transfer experiment.

Data processing, fitting of kinetic parameters, statistical analysis

The JMRUI software¹⁹ was used to process all spectra and evaluate the resonances. Post-processing includes zero and first-order phasing for all spectra and apodization (5Hz) for the liver spectra. The resonances were determined by the AMARES (advanced method for accurate, robust and efficient spectral fitting of MRS data with use of prior knowledge)²⁰ algorithm. PME, Pi, PDE, PCr (only for skeletal muscle), γ -ATP, α -ATP, NADH, and β -ATP resonances were fitted with PME, Pi, PDE, PCr, and NADH as singlets, γ -ATP and α -ATP as duplets, and β -ATP as triplet. Prior knowledge was set as follows: amplitude (estimated), relative phase (fixed, 0 for positive resonances, 180 for negative resonances), shape (Lorentzian). For skeletal muscle line width and frequency was set with soft constraints (soft constraints were evaluated from the 10 summed spectra

with longest Tl or from the 10 summed mirror spectra). For liver line width and frequency was estimated for Pi with fixed shifts to the Pi resonance for the other resonances (fixed shifts were evaluated for each subject from the summed spectra with the two longest Tl 's or from the mirror spectra).

The kinetic parameters T_{1A}^* for saturation transfer and k_{AB} , k_{BA} , T_{1A}^* , and T_{1B}^* for inversion transfer were determined by least square curve fitting using the MATLAB® software. T_{1A}^* for saturation transfer was fitted according to equation (5) with three variables M_{ZA0} , $M_{ZA\infty}$, and inv . The four kinetic parameters and the variables M_{ZA0} , $M_{ZA\infty}$, M_{ZB0} , and $M_{ZB\infty}$ of the inversion transfer experiment were fitted by the Levenberg-Marquardt algorithm²¹ according to the signals of γ -ATP and Pi, which are described by the Bloch-McConnell equations that include terms describing the biochemical exchange (see equations (1) and (2)). Because of the long selective inversion pulse (100ms) and the spatial saturation bands a delay of 55 ms in skeletal muscle and a delay of 75 ms in liver was added to the time axis for fitting. Under the assumption of the equilibrium state k_{BA} was set as follows:

$$k_{BA} = k_{AB} \cdot \frac{M_{ZA0}}{M_{ZB0}} \quad (6)$$

Paired t -tests were used to compare kinetic parameters, [Pi], and forward ATP synthesis flux ($fATP$) from the saturation and inversion transfer experiment. Significance level was set to 0.05. A Bland-Altman analysis was performed to compare the two methods for the kinetic parameter k_{AB} . Coefficient of variance (CV) is calculated for the intra- and inter-subject variability of k_{AB} .

RESULTS

The volume selection of the liver was successful with only small contamination by PCr that originates from muscles in the abdominal wall (see Fig. 1). For skeletal muscle the saturation bands for volume selection are not needed.

The following resonances were evaluated for the liver: PME, Pi, PDE, γ -ATP (duplet), α -ATP (duplet), NADH, and β -ATP (triplet). For skeletal muscle the same set of resonances is determined, but with the additional resonance of PCr. A splitting of the PME and PDE in two resonances is seen only in a few cases in the liver.

In Table 2 the fitted kinetic parameters, concentration of Pi ([Pi]) and the forward ATP synthesis rate ($fATP$) from the saturation and inversion transfer experiment are summarized for liver and skeletal muscle. Significant differences ($P < 0.05$) between the two methods are found for all parameters, except T_{1A}^* in the liver.

The average exchange rate constant k_{AB} (see Fig. 3) in the thigh skeletal muscle is $0.084 \pm 0.017\text{s}^{-1}$ (ST) and $0.140 \pm 0.046\text{s}^{-1}$ (IT), resp. $0.232 \pm 0.079\text{s}^{-1}$ (ST) and $0.463 \pm 0.190\text{s}^{-1}$ (IT) in the liver. Bland-Altman analysis showed an overestimation of the k_{AB} value evaluated with inversion transfer compared to saturation transfer (not shown). The comparison between subjects resulted in a CV of 21% (ST) and 33% (IT) for muscle and 34% (ST) and 41% (IT) for liver (inter-subject variability). The methodological differences (ST vs. IT) yield CV's of 50% in the muscle and 74% in the liver (intra-subject variability).

To understand the overestimation of k_{AB} a closer look was given to the inversion transfer experiment (see Fig. 4). For liver as well as for skeletal muscle the inversion of the γ -ATP resonance is incomplete (on average -19% for skeletal muscle and -30% for liver). The inversion pulse is also not perfectly selective, which causes rf-bleedover (spillover). The spillover rate ($M_{ZA}(0)/M_{ZA0}$) is typically 0.93 in skeletal muscle and 0.82 in liver. A Monte

Carlo simulation was performed to test the influence of inversion (from 0 (half inversion, no signal) to -1 (complete inversion)) and spillover (from 0.5 to 1.0) on k_{AB} (see Fig. 5). The γ -ATP and Pi curve were simulated with a given measurement precision (standard deviation) of 2.4% (Pi) and 3.9% (γ -ATP) for the skeletal muscle and 5.7% (Pi) and 8.7% (γ -ATP) for liver evaluated from the experiments. The simulated data points were fitted according to equation (1) and (2). The number of simulations for each inversion and spillover step was set to 100. The simulated value for k_{AB} according to the given inversion and spillover is about $0.134 \pm 0.069\text{s}^{-1}$ in skeletal muscle and about $0.527 \pm 0.738\text{s}^{-1}$ in liver (see black circles in Fig. 5).

DISCUSSION

Despite the challenges of volume selection and motion of the organ, our implementation of IT and ST in the liver was reliable, with reasonable signal-to-noise, and with only little contamination from abdominal wall muscles.

The spectrum quality in skeletal muscle was good. Spectra quality in liver was sometimes not sufficient enough. Two out of 12 liver volunteers had to be excluded from the study. Motion triggering could probably improve spectra quality. Also a reduction of repetition time (TR) and increase of averages could improve spectra quality in the liver. TR was set longer to be on the safe site for fitting (see Fig 4B).

IT data were fitted with a delay of 55ms in skeletal muscle and 75ms in liver coming from the long selective inversion pulse (100ms) and spatial saturation bands (only in liver) to eliminate 'spillover' from sequence timing. IT data were fitted under the assumption that the organ is in an equilibrium state (see Equation (6)).

ATP synthesis exchange rates k_{AB} evaluated from saturation transfer are comparable with previous studies in skeletal muscle^{14,22} and liver^{8,13} (see Fig.3). k_{AB} from inversion transfer experiments is significantly higher than from saturation transfer experiments in both skeletal thigh muscle and liver. Monte Carlo simulations showed that liver measurements are much more sensitive to an insufficient inversion pulse than skeletal muscle measurements (see Fig. 5). Also the measurement precision influences the accuracy of the fit. E.g. a reduction of 50% of the SD of a measurement in the liver reduces the simulated value of $0.527 \pm 0.738\text{s}^{-1}$ to $0.256 \pm 0.301\text{s}^{-1}$. A 50% better measurement precision in skeletal muscle changes the simulated k_{AB} value from $0.134 \pm 0.069\text{s}^{-1}$ to $0.124 \pm 0.033\text{s}^{-1}$.

Concentrations of Pi are significantly different between saturation and inversion transfer experiments in both organs, but are within the range of previously evaluated values for $[Pi]^{3,23}$.

The forward ATP synthesis flux evaluated from saturation and inversion transfer experiment contains a glycolytic and an oxidative part. Of interest for mitochondrial activity measurements is the oxidative part, which can be estimated from O_2 consumption measurements. In human skeletal muscle the part of aerobic to anaerobic contribution is 90% to 10%⁹ and in human liver it is estimated to be 25% to 75%¹³.

In previous studies a reduction of α -ATP and β -ATP upon the selective saturation of γ -ATP was mentioned in saturation transfer experiments^{12,24}. This could probably allow to estimate parts of small exchanging pools (as ADP). In this study a reduction of α -ATP and β -ATP upon the selective saturation (and inversion) of γ -ATP is also found. It is for saturation transfer and muscle a reduction of 28.8% for α -ATP and 35.5% for β -ATP, respectively 19.6% for α -ATP and 29.5% for β -ATP in the liver. Differences in inversion transfer between longest and shortest inversion time is 26.8% for α -ATP and 18.8% for β -ATP in skeletal muscle and 11.8% for α -ATP and 4.5% for β -ATP in liver. The spectra are acquired with an adiabatic acquisition pulse, which has a too short bandwidth to cover fully the β -ATP resonance at about -16 ppm. Also the influence of possible rf-bleedover on the α -ATP and β -ATP was not evaluated.

In conclusion the saturation transfer experiment in skeletal muscle and liver were comparable with previous work done from other groups. Inversion transfer experiments resulted in significantly higher results for the ATP synthesis exchange rate constant k_{AB} . In liver this overestimation can be explained with insufficient selective inversion pulse (incomplete inversion, spillover) or measurement precision. In skeletal muscle the

insufficient selective inversion pulse has less influence on the k_{AB} . To use inversion transfer experiments in further studies its accuracy has to be enhanced, e.g. by improving sufficiency of selective inversion pulse and/or measurement precision. The experiment time of ~1.5 hours is already high, with the presented saturation transfer experiment it is not possible to calculate the net ATP synthesis flux because of the lack of the information about k_{BA} in comparison to IT. Inversion transfer has also the advantage of being the less complex sequence according to sequence programming, it could be an alternative, if it is not possible to implement a very long saturation pulse as needed for saturation transfer on specific scanners.

Acknowledgements

This work was supported by the Swiss National Science Foundation (SNF Grant #310000-118219).

REFERENCES

1. Eckel RH, Grundy SM, Zimmet PZ. The metabolic syndrome. *Lancet* 2005; **365**: 1415-1428.
2. Batsis JA, Nieto-Martinez RE, Lopez-Jimenez F. Metabolic syndrome: from global epidemiology to individualized medicine. *Clin.Pharmacol.Ther.* 2007; **82**: 509-524.
3. Kemp GJ, Meyerspeer M, Moser E. Absolute quantification of phosphorus metabolite concentrations in human muscle in vivo by ³¹P MRS: a quantitative review. *NMR Biomed.* 2007; **20**: 555-565.
4. Forsen S, Hoffman RA. Study of Moderately Rapid Chemical Exchange Reactions by Means of Nuclear Magnetic Double Resonance. *J.Chem.Phys.* 1963; **39**: 2892-2901.
5. Wallace DC, Fan W, Procaccio V. Mitochondrial Energetics and Therapeutics. *Annu Rev Pathol* 2010; **5**: 297-348.
6. Petersen KF, Dufour S, Befroy D, Garcia R, Shulman GI. Impaired mitochondrial activity in the insulin-resistant offspring of patients with type 2 diabetes. *N.Engl.J.Med.* 2004; **350**: 664-671.
7. Vanderthommen M, Duteil S, Wary C, Raynaud JS, Leroy-Willig A, Crielaard JM, Carlier PG. A comparison of voluntary and electrically induced contractions by interleaved ¹H- and ³¹P-NMRS in humans. *J.Appl.Physiol.* 2003; **94**: 1012-1024.
8. Schmid AI, Szendroedi J, Chmelik M, Krssak M, Moser E, Roden M. Liver ATP synthesis is lower and relates to insulin sensitivity in patients with type 2 diabetes. *Diabetes Care* 2011; **34**: 448-453.
9. Schmid AI, Schrauwen-Henderling VB, Andreas M, Wolzt M, Moser E, Roden M. Comparison of Measuring Energy Metabolism by Different ³¹P-Magnetic Resonance Spectroscopy Techniques in Resting, Ischemic, and Exercising Muscle. *Magn.Reson.Med.* 2011; DOI 10.1002/mrm.23095.
10. van den Broek NM, Ciapaite J, Nicolay K, Prompers JJ. Comparison of in vivo postexercise phosphocreatine recovery and resting ATP synthesis flux for the assessment of skeletal muscle mitochondrial function. *Am.J.Physiol.* 2010; **299**: C1136-C1143.
11. From AH, Ugurbil K. Standard magnetic resonance-based measurements of the $P_i \Rightarrow ATP$ rate do not index the rate of oxidative phosphorylation in cardiac and skeletal muscles. *AmJPhysiolCellPhysiol* 2011; **301**: C1-C11.
12. Balaban RS, Koretsky AP. Interpretation of ³¹P NMR saturation transfer experiments: what you can't see might confuse you. Focus on "Standard magnetic resonance-based measurements of the $P_i \Rightarrow ATP$ rate do not index the rate of oxidative phosphorylation in cardiac and skeletal muscles". *AmJPhysiolCellPhysiol* 2011; **301**: C12-C15.
13. Schmid AI, Chmelik M, Szendroedi J, Krssak M, Brehm A, Moser E, Roden M. Quantitative ATP synthesis in human liver measured by localized (³¹)P spectroscopy using the magnetization transfer experiment. *NMR Biomed.* 2008; **21**: 437-443.

14. Kemp GJ. The interpretation of abnormal ³¹P magnetic resonance saturation transfer measurements of Pi/ATP exchange in insulin-resistant skeletal muscle. *Am.J.Physiol.* 2008; **294**: E640-E642.
15. Befroy DE, Petersen KF, Dufour S, Mason GF, De Graaf RA, Rothman DL, Shulman GI. Impaired mitochondrial substrate oxidation in muscle of insulin-resistant offspring of type 2 diabetic patients. *Diabetes* 2007; **56**: 1376-1381.
16. Hsieh PS, Balaban RS. Saturation and inversion transfer studies of creatine kinase kinetics in rabbit skeletal muscle in vivo. *Magn.Reson.Med.* 1988; **7**: 56-64.
17. Degani H, Alger JR, Shulman RG, Petroff OA, Prichard JW. ³¹P magnetization transfer studies of creatine kinase kinetics in living rabbit brain. *Magn.Reson.Med.* 1987; **5**: 1-12.
18. Meyerspeer M, Krssak M, Moser E. Relaxation times of ³¹P-metabolites in human calf muscle at 3 T. *Magn.Reson.Med.* 2003; **49**: 620-625.
19. Naressi A, Couturier C, Devos JM, Janssen M, Mangeat C, de Beer R, Graveron-Demilly D. Java-based graphical user interface for the MRUI quantitation package. *Magn.Reson.Mater.Phy.* 2001; **12**: 141-152.
20. Vanhamme L, vandenBoogaart A, Van Huffel S. Improved method for accurate and efficient quantification of MRS data with use of prior knowledge. *J.Magn.Reson.* 1997; **129**: 35-43.
21. Degani H, Laughlin M, Campbell S, Shulman RG. Kinetics of Creatine Kinase in Heart: A ³¹P NMR Saturation- and Inversion-Transfer Study. *Biochemistry* 1985; **24**: 5510-5516.
22. Befroy DE, Petersen KF, Shulman GI, Rothman DL. Localized ³¹P saturation transfer reveals differences in gastrocnemius and soleus rates of ATP synthesis in-vivo. *Proc.Intl.Soc.Magn.Reson.Med.* 2008; **16**: 2565.
23. Noren B, Lundberg P, Ressonner M, Wirell S, Almer S, Smedby O. Absolute quantification of human liver metabolite concentrations by localized in vivo ³¹P NMR spectroscopy in diffuse liver disease. *Eur.Radiol.* 2005; **15**: 148-157.
24. Jucker BM, Dufour S, Ren J, Cao X, Previs SF, Underhill B, Cadman KS, Shulman GI. Assessment of mitochondrial energy coupling in vivo by ¹³C/³¹P NMR. *Proc.Natl.Acad.Sci.U.S.A.* 2000; **97**: 6880-6884.

Tables and Figures

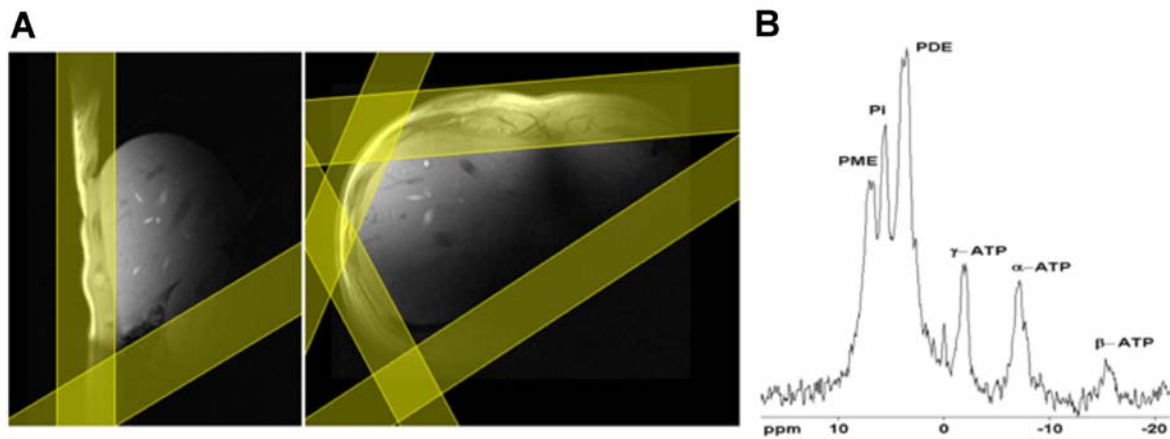


Figure 1: A) Sagittal and axial localizer images of the liver with three regional saturation bands for the abdominal wall muscles and one for the bowel. B) Liver spectrum with negligible PCr-signal at 0 ppm (TR = 5s, 48 averages, apodization 15Hz). The β -ATP signal is reduced due to the limited bandwidth of the 90° adiabatic excitation pulse.

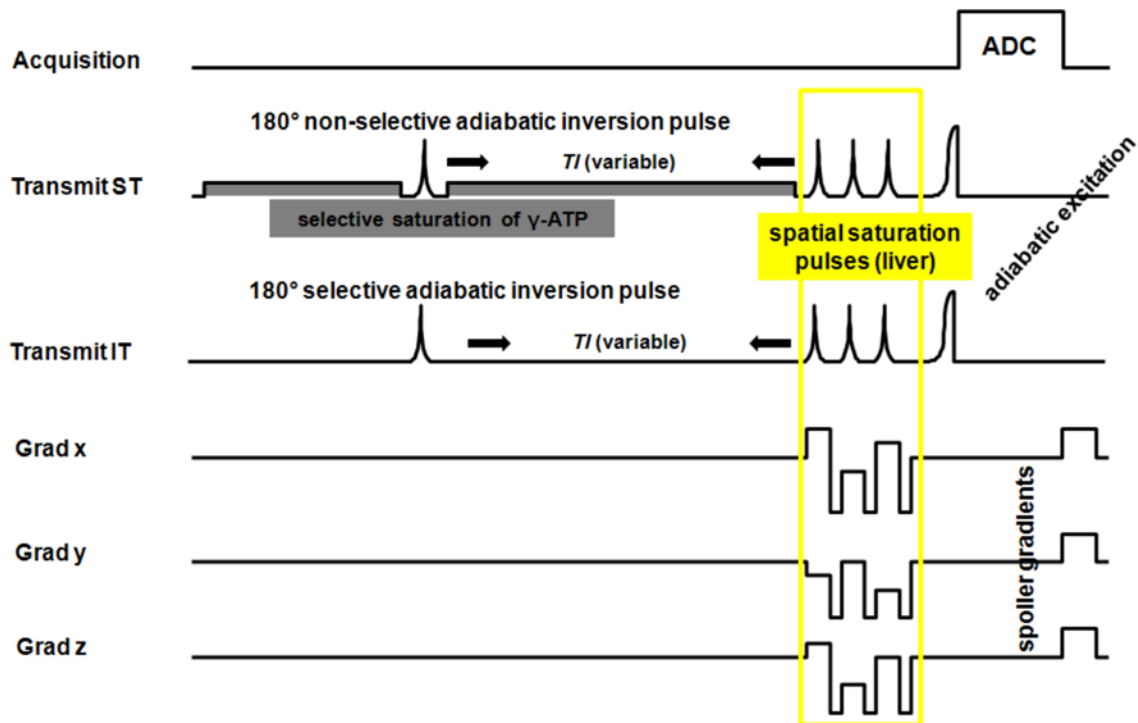


Figure 2: Schematic sequence overview for saturation transfer (Transmit ST) and inversion transfer (Transmit IT). The 180° non-selective adiabatic inversion pulse is only used for the inversion recovery experiment to determine T_{1A}^* in ST. Spatial saturation pulses are only used in the liver experiments to suppress signal from the abdominal wall muscle. The inversion time (T_I) is variable.

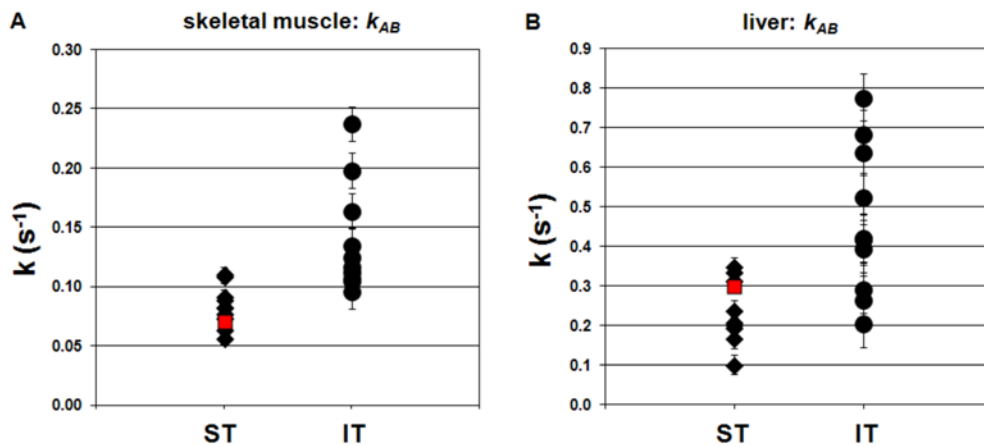


Figure 3: ATP synthesis exchange rate constant k_{AB} measured with the saturation (ST) and inversion (IT) transfer experiment in A) human thigh muscle (n=10, three male, seven female) and B) human liver (n=10, five male, five female). The values in red are literature values^{13,22}.

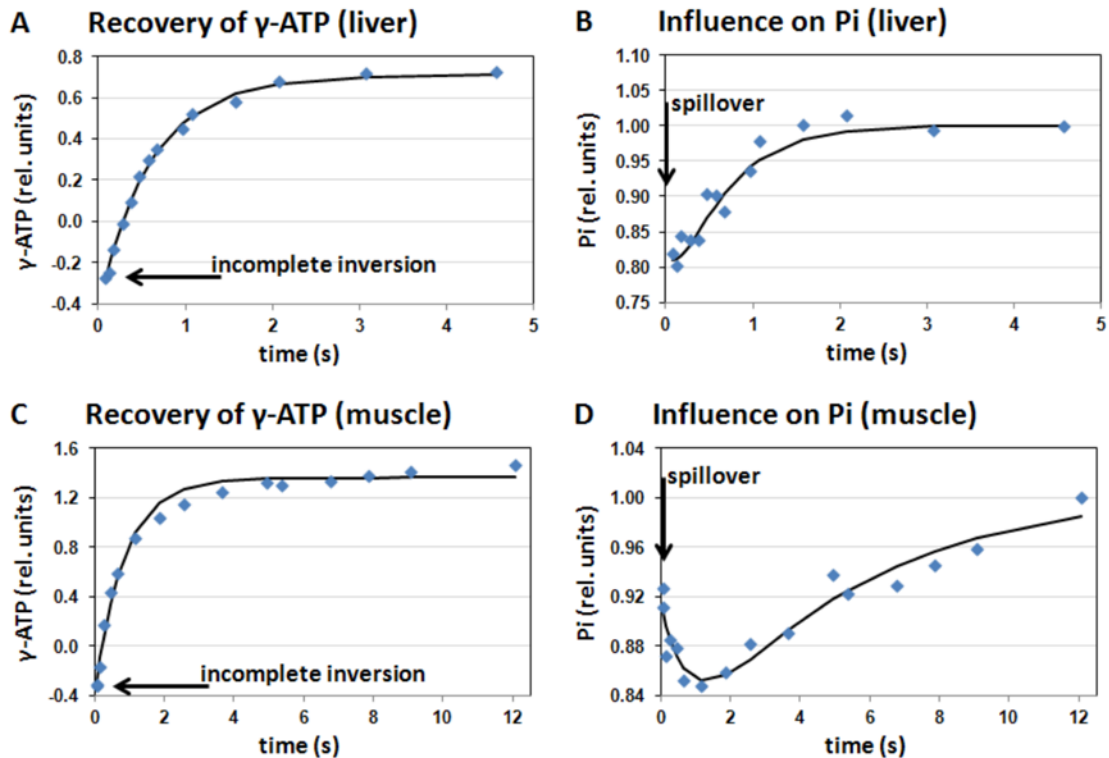


Figure 4: Sample measurement data from an inversion transfer experiment in the skeletal thigh muscle and the liver with fitted curves (solid black lines). The γ -ATP signal is calculated relatively to the Pi signal, where the Pi signal with longest inversion time is set to 1.00. Recovery of the γ -ATP after selective inversion is shown in A) liver and C) skeletal thigh muscle in relative units. Note that the inversion of the γ -ATP is not complete (indicated with black arrows). The influence of the γ -ATP inversion on the Pi signal is shown in B) liver and D) skeletal thigh muscle. Due to rf-bleedover of the selective inversion pulse the Pi signal is reduced at the beginning (see indicated with black arrows, spillover).

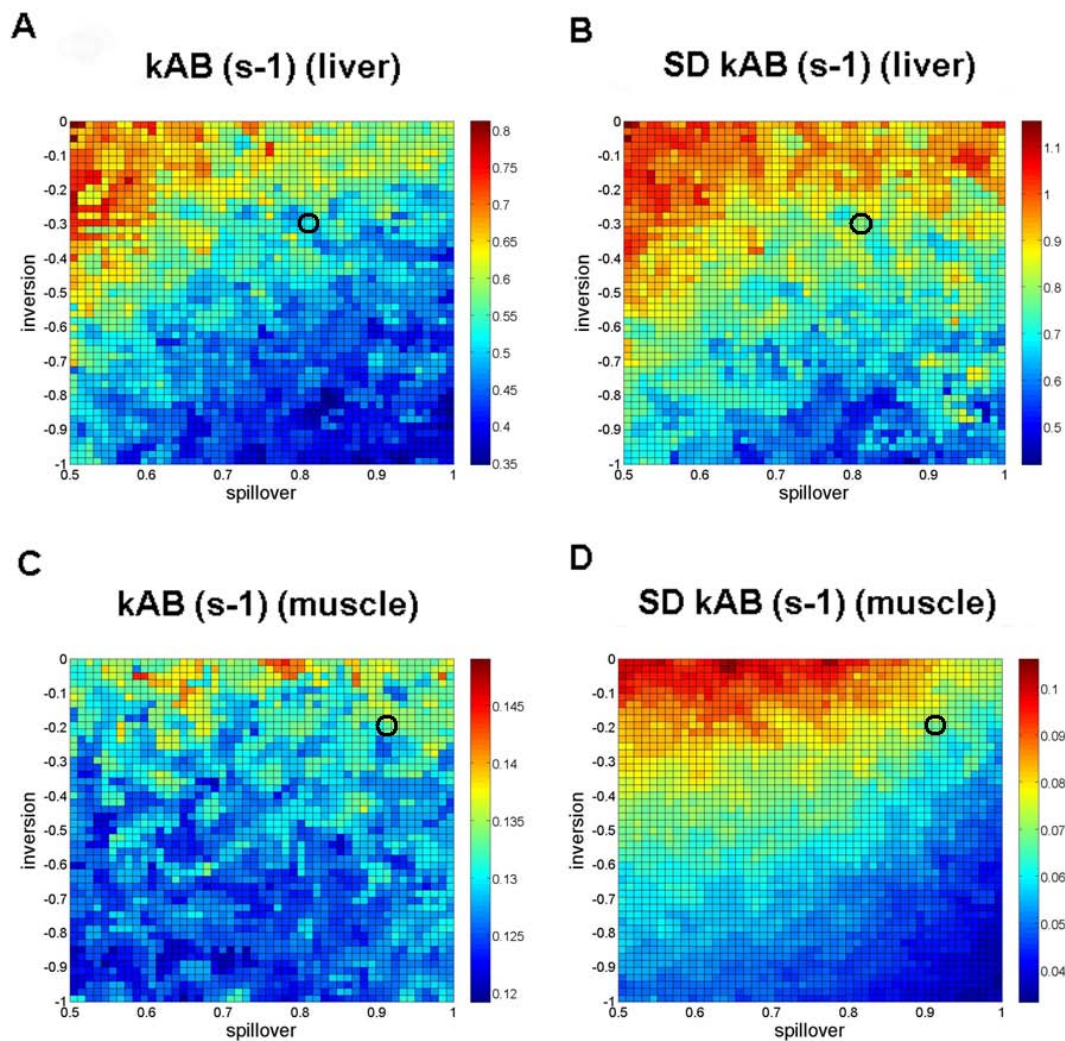


Figure 5: Monte Carlo simulation of kinetic parameter k_{AB} and its standard deviation (SD) from the inversion transfer experiment A) and B) liver and C) and D) skeletal thigh muscle. The γ -ATP and Pi curve were simulated for different inversion and spillover grades. The number of simulations was set to 100, number of inversion and spillover steps to 50 each. The simulated data was afterwards smoothed once by median filtering. The black circles indicate averaged inversion and spillover from measurements.

	Sequence parameter	Saturation transfer	Inversion transfer
Skeletal muscle	TR (s)		15
	Averages		32; 8 for T ₁ [*]
	TI (ms)	13 times between 100-13900 ms	16 times between 0-12000 ms
	Total saturation (ms)	14000ms	–
	Total measurement time (min) (incl. positioning of subject)	70	85
	Typical γ -ATP frequency (Hz)	-113 \pm 5	-113 \pm 5
	Typical mirror frequency (Hz)	-607 \pm 7	–
Liver	TR (s)		8; 5 for T ₁ [*]
	Averages		128; 32 for T ₁ [*]
	TI (ms)	10 times between 100-4100 ms	16 times between 0-4500 ms
	Total saturation (ms)	4200ms	–
	Total measurement time (min) (incl. positioning of subject)	90	90
	Typical γ -ATP frequency (Hz)	-88 \pm 9	-90 \pm 15
	Typical mirror frequency (Hz)	-668 \pm 16	–

Table 1: Sequence parameters for the saturation and inversion transfer experiment in skeletal muscle and liver are shown. Where different parameters are used for the individual inversion recovery experiment, it is indicated with “for T₁^{*}”.

	Variable	Saturation transfer	Inversion transfer
Skeletal muscle	k _{AB} (s ⁻¹)	0.084 \pm 0.017 ^{*1}	0.140 \pm 0.046
	T _{1A} [*] (s)	4.0 \pm 0.4 ^{*2}	7.7 \pm 0.9
	k _{BA} (s ⁻¹)	-	0.090 \pm 0.033
	T _{1B} [*] (s)	-	0.8 \pm 0.2
	[Pi] (mM)	2.96 \pm 0.39 ^{*3}	3.18 \pm 0.38
	fATP (mM/min)	14.6 \pm 2.2 ^{*4}	26.9 \pm 10.2
Liver	k _{AB} (s ⁻¹)	0.232 \pm 0.079 ^{*5}	0.463 \pm 0.190
	T _{1A} [*] (s)	0.6 \pm 0.2	0.5 \pm 0.3
	k _{BA} (s ⁻¹)	-	0.657 \pm 0.356
	T _{1B} [*] (s)	-	0.6 \pm 0.1
	[Pi] (mM)	2.31 \pm 0.44 ^{*6}	2.62 \pm 0.65
	fATP (mM/min)	31.7 \pm 12.3 ^{*7}	75.8 \pm 42.8

Table 2: Kinetic parameters, concentration of Pi ([Pi]) and ATP synthesis rate (fATP) from the saturation transfer and inversion transfer experiment in human skeletal muscle (n=10) and liver (n=10). The data are shown as mean \pm SD. Significant differences between methods (P<0.05): ^{*1} P = 0.011; ^{*2} P = 8•10⁻⁷; ^{*3} P = 0.030; ^{*4} P = 0.005; ^{*5} P = 0.020; ^{*6} P = 0.043; ^{*7} P = 0.020.

MAGNETIC RESONANCE IMAGING BASED DETERMINATION OF BODY COMPARTMENTS WITH THE VERSATILE, INTERACTIVE SPARSE SAMPLING (*VISS*) METHOD

Authors:

Tania Buehler, MS ¹, Nicolas Ramseier, MMed ¹, Juergen Machann, PhD ^{2,3}, Nina F Schwenzer, MD ², Chris Boesch, MD PhD ¹

Author affiliations:

1) Department of Clinical Research, MR-Spectroscopy and Methodology, University of Bern, Bern, Switzerland

2) Section on Experimental Radiology, Department of Diagnostic Radiology, Eberhard-Karls-University of Tübingen, Tübingen, Germany

3) Institute for Diabetes Research and Metabolic Diseases of the Helmholtz Center Munich at the University of Tübingen (Paul Langerhans Institute), Tübingen, Germany

Corresponding Author:

Chris Boesch, MD & PhD

University Bern, Department of Clinical Research (AMSM)

Pavilion 52A Inselspital

P.O.Box 35

CH-3010 Bern, Switzerland

chris.boesch@insel.ch

Phone +41-31-632 81 74

FAX +41-31-632 05 80

Grant support:

Swiss National Science Foundation 310030-118219

Running title:

Versatile, interactive sparse sampling (*VISS*)

ABSTRACT

Purpose: The inhomogeneity of radiofrequency fields at higher field strengths can interfere with established volumetric methods, in particular for the determination of visceral (*VAT*) and subcutaneous adipose tissue (*SCAT*). A versatile, interactive sparse sampling (*VISS*) method is proposed to determine *VAT*, *SCAT*, and also total body volume (*TBV*).

Materials and Methods: *VISS* is based on a separation of major components by contour lines, followed by a sparse sampling algorithm, and eventually a quick manual correction. T1-weighted whole body scans of 24 subjects were evaluated (12 at 1.5T, 12 at 3.0T).

Results: a) Coefficients of variance (*CV*) and intra class correlation coefficients (*ICC*) determined within 3 raters (24 subjects) showed high consistency for *SCAT* (*CV* 2.2%, *ICC* 0.993) and *VAT* (*CV* 4.9%, *ICC* 0.987), b) comparison with an established volumetric method revealed good agreement (Bland-Altman, *VAT* -0.68L to 1.07L, *SCAT* -2.18L to 8.39L), and c) comparison of weights calculated from *TBV* with values measured on a scale resulted in an even better accuracy for *VISS* (Bland-Altman -1.98kg to 4.09kg) than for the reference method (-5.60kg to 1.60kg).

Conclusions: *VISS* is reproducible in particular within the same rater, accurate as compared with established methods, and robust against low contrast and inhomogeneity artifacts.

KEYWORDS

Magnetic Resonance Imaging

Body Compartments

Sparse Sampling Method

Point-Counting Method

Threshold Method

Contour Method

INTRODUCTION

Volumetric measurements *in vivo* are essential for anthropometric and medical investigations, including the determination of the body composition for the distribution of fat depots, for changes of the compartments with nutrition, training and growth, for metabolically active organs such as skeletal muscle or liver, or for changes of bone mineralization with ageing. There are numerous specialized methods to measure specific body volumes such as body impedance analysis, caliper methods, measurements of waist and hip circumference, dual-energy X-ray absorptiometry (DXA), computed tomography (CT), or magnetic resonance imaging (MRI) (1-3). A comparison of the different methods, however, needs to respect the characteristics of the methods which may require changes of the terminology (4).

Total fat volume (*TFV*) of the body and particularly visceral adipose tissue (*VAT*) are of paramount importance as cardiovascular risk factors related to the metabolic syndrome (5). MRI is very well suited to measure soft tissue volumes and numerous anthropometric studies and interventions to better understand fat metabolism have been published (1,4,6-14). Since MRI offers the possibility to manipulate the acquisition for an optimized contrast (15,16), T1-weighted sequences (13), water-suppressed sequences (17), dual flip angle sequences (18), or further developments of the DIXON method (19-23) have been successfully used to evaluate adipose tissue.

In images with sufficient contrast and as long as various tissues have different signal intensities which are unequivocal over the whole image, straightforward volumetric methods can be applied like threshold (6,9,24), contour-only (7), and point-counting-only (25). However, as it is illustrated in Fig.1, all these methods have specific advantages and disadvantages. Mathematical algorithms can help to distinguish the different signal intensities, mostly based on a histogram of the signal intensities. This can be the determination of a dip in the histogram (13) or sophisticated fuzzy c-mean algorithms (26). A limitation of these algorithms is the fact that spatial information is not used and therefore, the method cannot cope with signal inhomogeneities when differences between tissues are smaller than the spatial signal variations. Recent publications extended the classical fuzzy-c-mean algorithm with spatial information (27,28).

In turn, manual or semi-automated drawing of contour lines uses the spatial information (7). However, in the case of highly segmented VAT, the contours are very complicated. For the relatively simply structured subcutaneous adipose tissue (SCAT), several algorithms have been suggested, including snake algorithms (12), point seeds (20) etc. In stereology, point-counting and the acquisition of images according to the Cavalieri principle has been very successful over a long time. It is a sparse sampling method where grids of equally separated points are placed on a volume/area of interest. Since the volume is proportional to the number of grid points, counting of the (sparse) points give an accurate and unbiased estimation of the volume (25,29-33). The method is extremely versatile and can be used for the determination of fat compartments as well as for single organs such as the liver (30,33,34).

While it is necessary to develop automatic methods for larger studies, automatic methods have inherent problems. Different parts of the body require different approaches – while the separation of *VAT* in the abdominal region requires specific algorithms, the separation of muscle tissue in the extremities need other algorithms. In addition, the segmentation of single organs such as the liver typically cannot just base on threshold levels but need some prior knowledge on anatomical situations. In recent publications, this fact has been considered and a series of automatic algorithms have been combined (12,19).

It is well accepted that MRI at 1.5 Tesla is appropriate for volume determination. MRI followed by threshold methods has been successfully used to estimate *TFV* and *VAT* at 1.5 T (9). But in clinics more and more scanners at higher field strengths are used. Inhomogeneity of the radiofrequency field in the abdominal region at 3.0 Tesla jeopardizes the estimation of *VAT* and *TFV* and makes it necessary to find a more robust and accurate method to measure these volumes.

This study suggests a versatile, interactive sparse sampling (*VISS*) method which combines the strengths of three volume determination methods, thus avoiding the inherent weaknesses of the methods: a) threshold techniques are fast but fail as soon as the *RF*-inhomogeneity reduces the signal intensity of fat below that of water in T1-weighted sequences, b) manual planimetric (contour) methods can overcome intensity variations but are almost unfeasible in the visceral region with small areas of fat

between bowel and other abdominal organs, and c) point-counting is an established method in stereology but is rather time consuming, in particular in the fragmented visceral fat. Because the method is based on a sparse sampling scheme, the interactive step is rather easy and time efficient while purely automatic methods (10) often fail and need manual correction. Corrections are almost every time necessary, also in highly sophisticated algorithms (see comparison in (10,11,35)). However, as soon as corrections are needed, *VISS* can compete with other methods since only few points have to be fixed (Fig.2) which is a fast process.

The following shall be tested:

- a) *VISS* has an acceptable consistency within and between raters with intra class correlation coefficients (*ICC*) comparable to literature (35).
- b) *VISS* can be validated against an established volumetric reference method (9) with an agreement close to unity.
- c) *VISS* is comparable with the accuracy of an established volumetric reference (9) when whole body volume is used to calculate body weight.
- d) If *VISS* and the reference threshold method (9) are applied on images that are acquired at different field strength (1.5 T and 3.0 T), *VISS* is less influenced by increasing rf-inhomogeneity at higher field strengths; i.e. *VISS* agrees equally well or even better with the body weight measured by scale than the reference threshold method (9) at higher field strength.

METHODS

Subjects:

In order to test *VISS* on subjects with a large distribution of the body composition and also to be able to detect a potential influence of the inhomogeneity of the radiofrequency field at higher magnetic field strength, 24 subjects were investigated in 2 groups, 12 subjects at 1.5 Tesla and 12 subjects matched for age, height, weight, and body mass index (*BMI*) at 3.0 Tesla.

The 12 subjects measured at 1.5 Tesla (MAGNETOM SONATA; Siemens Healthcare, Erlangen, Germany) were selected from a larger study cohort. Intentionally, these subjects covered a wide range of body mass indices (5 males/ 7 females; age 41.1 +/- 12.3 years; body height 1.72 +/- 0.09; body weight (scale) 87.8 +/- 23.5 kg; *BMI* 29.3 +/- 6.0 kg/m²). The 12 subjects measured at 3.0 Tesla (TIM TRIO; Siemens Healthcare, Erlangen, Germany) were almost perfectly matched with the group at 1.5 Tesla (7 males/ 5 females; age 39.9 +/- 11.1 years; body height 1.71 +/- 0.12; body weight (scale) 86.7 +/- 15.2 kg; *BMI* 29.5 +/- 3.5 kg/m²). The study was approved by the local ethics committees and all participants gave written informed consent prior to the examination.

Imaging:

Imaging parameters were as identical as feasible at the two field strengths, except for optimized contrast parameters (T1-weighted fast spin echo technique with an echo train length of 7, 1.5T: $TR = 486$ ms / $TE = 11$ ms and 3.0 T: $TR = 452$ ms / $TE = 38$ ms). The

body coil was used as combined transmit/receive coil. For the volume determinations, images were taken in axial direction from fingers to toes (slice thickness of 10 mm, 5 slices per sequence, spacing between slices 20 mm, *FOV* 50 cm, acquisition matrix of 256 x 192, 147 phase encoding steps, phase encoding sampled over 75% of the field of view in read direction, field of view reduced in phase direction to 75%, pixel spacing of 2 mm per pixel). Due to the limited range for the motion of the examination tables, the subjects had to take two positions, a first one prone/head-first with outstretched arms, and a second one prone/feet first. A mark was set at the crista iliaca to reposition the subject. The average reposition error is estimated to be within about 20 mm, mainly due to shifted skin, and thus is in agreement with the Cavalieri principle (25) for an unbiased estimation of volumes. This imaging acquisition led to 100 – 130 axial images per subject. In the abdominal region the slices were recorded in breath-hold.

Volume determination by the *VISS* method:

The *VISS* method, which was programmed in MATLAB R2007a (The MathWorks, Natick MA), combines three volume determination methods (Fig.1d, Fig.2):

- a) Contour: a simple contour line (yellow) separates large anatomical regions such as inside vs. outside of the abdominal wall.
- b) Threshold: a regular grid of points is generated by the program; however, the points of the grid are already switched off, if they fall above a pre-defined threshold (Fig.2).
- c) Point-counting: after a quick visual inspection and – if necessary – correction of a few points (Fig.2), the volume is determined based on the number of deleted points (separately inside and outside of the contour line).

Point-counting is a sparse sampling method well established in stereology, where an area is proportional to the number of points within that area (25,29-33). Since the different volumes are proportional to number of counted (deleted) points, the volumes can then be calculated as follows,

$$V = D \cdot d^2 \cdot \sum_{i=1}^n C_i \quad [1]$$

where D is the slice thickness [cm], d the grid size, i.e. the distance between two grid points [cm], C_i the number of deleted grid points within or outside the contour, and n the total number of images that cover the volume of interest. Since images usually are defined by its resolution, d can be calculated as follows,

$$d = \frac{a}{k} \quad [2]$$

where a is the distance between two points in [pixels] and k the image resolution in [pixels/cm].

The accuracy of the point-counting method can be determined (30) and, according to the rules of stereology, the total number of points has to be well above 100 to reduce the influence of the arbitrarily set grid below an acceptable limit, i.e. below approximately 1% (25).

Test of the reliability and reproducibility of *VISS*:

Three raters determined *TBV* (total body volume), *VAT* (visceral adipose tissue), *SCAT* (subcutaneous adipose tissue), and *TFV* (total fat volume, sum of *VAT* and *SCAT*) twice following a detailed instruction of the counting procedure and a test run with data from two subjects. The two training sets were included in the final evaluation but were not

recognizable by the raters. The repetition of measurements was within 1 year for rater 1 and within 1 month for raters 2 and 3. The distance between two grid points was set small enough to obtain more than 100 points for the smallest compartment in a slim subject (typically *VAT*). The threshold to pre-select the volume was set in a histogram of the pixel signal intensities to achieve an optimal separation of the fat and water signal intensity (Fig.2). The separation of *VAT* and *SCAT* with a contour line for each slice was performed for all slices between the one that showed the femur heads and the last one below the first cut of the heart became visible. *TBV* was determined by decreasing the threshold to a value just above the noise level. Therefore, just very few points mainly due to flow or motion artifacts had to be corrected for.

Comparison of *VISS* with an established reference method (9):

In order to validate the results obtained by *VISS*, all 24 data sets were also analyzed with a reference method (9). In order to make the two evaluations comparable, only a single determination using *VISS* first evaluation by rater 1) was compared to the reference method. In brief, the threshold in the reference method was set such that a masked image showed a satisfactory coverage of the fat parts. *VAT* and abdominal *SCAT* are separated by manually drawing two regions of interest. Inclusion and exclusion of tissue was equal in *VISS* and the established method (9); in particular, peripheral lung tissue was not counted while the hilus was counted for the *TBV*. The whole volume determination process (determination of *VAT*, *SCAT*, and *TBV*) for one subject took about 30 minutes for the reference method and 40 minutes for the *VISS* method. Figure 3 shows profiles of *TBV*, *TFV*, *VAT*, and *SCAT* in one subject (male,

30y, 1.64m, 82kg) at 3.0 Tesla, measured by the reference method (9) and by the *VISS* method. *VISS* shows relatively large variations from slice to slice, depending on the grid size. This is to be expected since the number of points counted in a single slice is relatively small (e.g. below 100) and, therefore, the arbitrary positioning of the grid by the program has an influence. However, this variation from slice to slice has no influence on the results as soon as the total number of counted points is sufficient, as it is the case for *TBV*, *TFV*, *VAT*, and *SCAT*.

Calculation of weights from MRI determined volumes:

The following formalism is needed to calculate weights from volumes determined by MRI in order to compare the volumetric methods with weights determined on a scale. The primary target of this study was the volume determination of *VAT* and *SCAT* since these two compartments are relevant for insulin resistance. In order to evaluate the feasibility of *VISS* for a total body compartment analysis and to compare the results with body weight measured on a scale, the total body volume (*TBV*) was also determined and translated into masses. Since fat and fat-free tissues (mainly skeletal muscle and bones) have different gravity densities, it is necessary to determine fat free volume (*FFV*):

$$FFV = TBV - TFV \quad [3]$$

From the various volumes, the masses can be calculated by the relevant gravity densities of $\delta_{FFM} = 1.000 \text{ g/cm}^3$ for fat free mass (*FFM*) according to Visser et al. (38):

$$FFM = \delta_{FFM} * FFV \quad [4]$$

and the masses of the fat compartments (visceral adipose tissue mass $VATM$, subcutaneous adipose tissue mass $SCATM$, total fat mass TFM) using the gravity density $\delta_{lipids} = 0.918 \text{ g/cm}^3$ for lipids (39).

The total body mass (TBM) can now be calculated if the various compartments are summed up:

$$TBM = FFM + TFM \quad [5]$$

Since Heymsfield et al (40) have shown that bone mass (BM) is reasonably well correlated with *body height* (BH), BM could be estimated from BH and gender based on two equations for males and females (according to an erratum in vol.88, page 82, Fig.1 and Fig.2 with the following equations are reversed in (40)):

$$\text{Females:} \quad BM = 3 * 10^{-5} * BH^{2.48} \quad [6]$$

$$\text{Males:} \quad BM = 7 * 10^{-5} * BH^{2.33} \quad [7]$$

This allows estimating the metabolically important lean body mass (LBM):

$$LBM = FFM - BM \quad [8]$$

Statistical analysis:

Statistical analysis has been done in SPSS 18.0 (SPSS Inc. Chicago, IL U.S.A.) and EXCEL 2007 (Microsoft Corporation, Redmond WA U.S.A.). Unpaired t -tests were applied to compare the two groups of subjects who have been measured at 1.5 Tesla and at 3.0 Tesla. Intraclass coefficients (ICC) as well as coefficients of variance (CV) were determined for each of the compartments to assess the reproducibility of the $VISS$ method and in order to compare it with published values. ICC were calculated by the “reliability analysis” in SPSS with the repetitions as variables for the intra-rater ICC of

the different volumes and with the average of the two repetitions from all three raters for the inter-rater *ICC*'s, analogous to a published comparison of different volumetric methods (10,11,35). *CV*'s were calculated in EXCEL from the differences between first and second determination of all three raters for the intra-rater agreement and the difference between each determination and the average of all 3 raters for the inter-rater variability. The standard deviations were divided by the average of the respective volumes for all three compartments. Regression correlation coefficients were calculated in EXCEL to compare measurements at 1.5 T vs. 3.0 T and to test the calculated weights against the weight measured on a scale. The agreement between the two MRI-based methods, and between these methods and the weight determined by a scale was assessed by Bland-Altman analyses (36).

RESULTS

Demographics of the two groups measured at 1.5 T vs. 3.0 T:

Unpaired *t*-tests for age, height, weight, and *BMI* showed no significant differences between subjects measured at 1.5 T and 3.0 T. The group averages as shown in Table 1 also illustrate the similarity of the two cohorts.

Reliability and reproducibility of *VISS*:

Table 1 shows *ICC* and *CV* for the repeated determination of *TBV*, *VAT*, and *SCAT*. The large differences in the average volumes ($TBV > SCAT \gg VAT$) result in larger *CV*'s for *VAT*. Except a slightly smaller inter-rater *CV* for 3.0 T vs. 1.5 T, no obvious differences can be found between the two field strengths, in particular, all confidence limits of the *ICC*'s overlap for a specific compartment. While the raters were able to determine the *TBV* with less than 1% difference between the first and second evaluation (0.63 L), the much smaller *VAT* resulted in a reproducibility of about 5% (0.22 L). As one has to expect, the *CV*'s are larger between raters than within raters with 2.4% (2.08 L) for *TBV* and up to 15.1% (0.67 L) for *VAT*.

The *ICC*'s are generally very high (lowest value 0.962 for the agreement between raters for *VAT*) and reflect the same trend as the *CV*'s with better agreement within the raters as compared to between raters. All confidence limits for the intra- vs. inter-rater *ICC* overlap. Notably, the agreement within and between raters yields either comparable values for 1.5 T and 3.0 T or there is even a trend to better agreement at 3.0 T than at 1.5 T, in particular for *VAT*. However, all confidence limits between 1.5 T and 3.0 T

overlap. In addition, there is less agreement for smaller volumes (*VAT*, lowest *ICC* 0.962) as compared to *SCAT* (lowest *ICC* 0.989) and *TBV* (lowest *ICC* 0.994).

Comparison of *VISS* with a reference method (9):

Figure 4 and Table 2 illustrate the comparison between *VISS* and a reference method (9), using a linear regression analysis and a Bland-Altman plot. The linear regression shows all points for *TBV* indistinguishable from the unity line, however, a numerical analysis reveals (Table 2) an intercept and a slope that is significantly different from the unity line. The Bland-Altman analysis shows that both cohorts at 1.5 T and at 3.0 T have trend to values above zero, the cohort at 1.5 T (blue bar) even reaching significance. The Bland-Altman analyses for *VAT* and *SCAT* show a more balanced picture around zero, still with the cohort at 1.5 T significantly above zero for *SCAT*.

Comparison of *VISS* and the reference method with weight determined by a scale:

In order to test the volumetric measurements with an independent method, the total body mass *TBM* (calculation see appendix) was compared with the weight measured on a scale. Both methods show a high agreement between volumetrically determined weight and the scale Figure 5 and Table 3. *VISS*-determined volumes agree generally better with the scale-determined weight as seen in the Bland-Altman analysis (Table 2) while the reference method results in one regression that deviates from unity (slope in the cohort at 1.5 T). The reference method underestimates the weight if compared with a scale, however, all ranges in the Bland-Altman plot (Figure 5, right column) just include zero.

DISCUSSION

Volumetry of the human body using MRI is highly-relevant with important physiological implications:

- a) The determination of lean body mass, muscle mass, and adipose tissue is important for the calculation of resting metabolic rate and other physiological parameters.
- b) The amount of visceral fat has been identified as a potential cardiac risk factor (5); therefore, methods are required that are capable of separating visceral from subcutaneous fat.
- c) Volumes of distinct organs need to be known to extrapolate metabolite concentrations to total metabolite quantity, e.g. changes of glycogen concentration in liver leads to volume changes (34); therefore, it is necessary to determine liver volume and to multiply metabolite concentration with this volume.

The proposed *VISS* method is a combination of three volumetric methods with a pre-definition of coarse regions, a threshold-based pre-selection of sparse sampling points, and finally a manual correction of very few sampling points. Due to the small number of sampling points and the preparation by the threshold technique, the analysis of a whole body data set (40 minutes) is not much longer than by an established reference method (9) (30 minutes), where the threshold has to be set such that rf-inhomogeneity can be corrected (i.e. underestimation in one part of the image vs. overestimation in another part).

VISS has been tested on whole body data sets from 24 subjects intentionally covering a large range of age, weight, height, and *BMI*. All results are presented for both cohorts

(1.5 T and 3.0 T) together as well as separately. Since it was not technically feasible to scan the same subjects at 1.5 T and 3.0 T, isolated comparisons of *VISS* at the two field strengths are not allowed. In turn, it is appropriate to compare *VISS* against reference methods at the two field strengths. *VISS* and the reference method at least do not show lower accuracy at 3.0 Tesla and thus, it can be concluded that *VISS* can be reliably applied to data sets from the higher field strength.

VISS shows acceptable agreement within and between raters, which compares favorably with a study that compares two established and sophisticated volumetric methods (35), *HIPPO* and *ANALYZE*. The *ICC* for *VAT* determined in this publication (inter-rater *ICC* 0.828 to 0.996, intra-rater *ICC* 0.990 to 0.999) are either in the same range as *VISS* or even lower (inter-rater *ICC* 0.962 to 0.972, intra-rater 0.983 to 0.989). The *ICC* for *SCAT* for these established methods (inter-rater 0.975 to 0.987, intra-rate 0.984 to 0.999) also compare to the *ICC* determined by *VISS* (inter-rater 0.989 to 0.989, intra-rate 0.992 to 0.994). Similar values for *ICC* were found in other studies where available software packages were compared (10,11).

The period between first and second evaluation was much longer for rater 1 (within 1 year) than for raters 2 and 3 (within 1 month), due to additional evaluations that have been performed during completion of the manuscript. The intra-individual *ICC*, however, did not differ for rater 1 vs. raters 2 and 3 (data not shown), supporting the conclusion that even a longer delay between repeated evaluations did not reduce the accuracy.

A comparison of the same data sets analyzed by *VISS* and by a reference method (9) validates the results from *VISS* for *VAT* and *SCAT* with Bland-Altman ranges that include zero. The total body volume *TBV* is larger in the *VISS* analysis (Figure 4) but

still with a high correlation coefficient. Therefore, *VISS* disagrees with the reference method systematically which can be explained by an operator-dependent decision to count small, ambiguous volumes such as hilus of the lung, air-filled cavities etc.

A comparison of the two volumetric methods with the weight determined on a scale (calculation of weight from volumes see appendix) justifies the *TBV* results obtained by *VISS*: While *VISS* shows Bland-Altman plots that include zero, the reference method underestimates the whole body weight (Figure 5). This might also explain the slight discrepancy between the two volumetric methods in Figure 4. It also supports the hypothesis that *VISS* agrees equally well or even better with the body weight measured by scale than the reference threshold method (9) at higher field strength.

MRI has the advantage of excellent soft tissue contrast and, therefore, is predestinated to be used for a direct volume determination of adipose tissue or organs. As long as signal intensity can be used directly to distinguish between different tissues it is easy to define a threshold to discriminate tissues, and thus to calculate volumes. On the other hand, high field MR systems inherently have inhomogeneity problems, particularly but not exclusively in larger regions such as the abdomen as illustrated in Fig.1. As soon as inhomogeneities are present, simple threshold methods are not sufficient. While algorithms exist to smooth *RF*-inhomogeneities in particular in the brain (37), the work is not as far developed for the abdomen and other regions of the body. Typically, operators of threshold programs compensate these inhomogeneities by a certain over- and underestimation that balances out over the whole image as shown in Fig.1.

Fat-water specific sequences (15-23) are helpful to discriminate fat and water and thus, may support the discrimination of *TFV* from other body compartments. However, for the separation of *VAT* vs. *SCAT* or the determination of other volumes, e.g. of the liver, fat-water contrast might not be sufficient to delineate the structures.

Fully automated algorithms (12,19) have been published which are using specific methods in all parts of the body. This is necessary since the determination of fat in the extremities requires different prior knowledge from the delineation of fat in the abdomen. While such automated methods are clearly superior to the proposed *VISS* method in large epidemiological studies, *VISS* has the advantage that it can be applied to single organs (34), e.g. the liver or skeletal muscle, where the achievable contrast is not as high as in fat measurements. While *VISS* has been successfully applied to single organs (34), the methodological background as described in this paper is identical for whole body applications or single organs. In addition, an analysis of five different programs (10) has shown that most of them require manual interaction or are not as accurate as the interactive ones.

The advantages of *VISS* are a result of the sparse data concept, which makes the interaction by an operator easy and fast. As it can be seen in Fig.2, only a few points have to be corrected. If a threshold is preselected inappropriately using the reference technique, a considerable amount of time has to be spent to correct the threshold level. In addition, if two organs with approximately the same signal intensity have to be separated, a pure threshold method is insufficient. *VISS* in turn can measure several tissues of the same signal strength simply by drawing a contour line that separates the

two organs coarsely, as e.g. *VAT* and *SCAT*. In principle, every volume can be measured by this method as long as an operator can distinguish two structures.

The disadvantage of *VISS* is the longer time that is needed (about 40 minutes) to determine a full data set (approximately 100 to 130 images per subject, *VAT*, *SCAT*, and *TBV*) than with the reference method (about 30 minutes). In turn, this difference in time is small and as soon as larger corrections for inhomogeneity in the images are needed, the time difference gets negligible. The needed time to analyze the images is comparable with other manual, semi-automated, or automated programs (10,35).

This study has some limitations:

1) For technical and logistical reasons, it was not possible to measure the very same volunteers in both systems at 1.5 Tesla and 3.0 Tesla, even if the two cohorts were well matched. Therefore, it is not allowed to draw conclusions from a direct and isolated comparison of *VISS* at 1.5 T vs. 3 T. However, it is possible to evaluate the accuracy of *VISS* against two standards (the reference method and a scale) at two different field strengths. To allow such a validation, all results are presented for the two field strengths separately and combined.

2) In order to generate a more detailed model of body compartments, one could introduce even more contour lines and count various tissues separately, such as *VAT*, *SCAT*, skeletal muscle, various organs, bone marrow, etc. However, since this study should demonstrate the feasibility, a detailed separation of various tissues was not attempted. Following the reproducibility study, it became obvious that the rigorousness

of the rater-instructions concerning small but ambiguous compartments (hilus of the lung, air-filled sinuses, bone marrow, etc) is critical and could be improved.

3) Sophisticated image correction algorithms could be used to correct for inhomogeneity artifacts. This would allow using simple threshold algorithms afterwards, however, this would still not allow for a separation of organs with similar signal intensity. 4) The determination of the threshold levels could use some more sophisticated algorithms such as fuzzy c-mean. This has not been programmed so far; however, a combination with the current algorithm would be possible. Since the correction of the few points is easy, the operator anyhow learns to adjust the preparing threshold such that the correction gets easy (e.g. by adjusting the level relatively high such that only deletions are necessary, but not additions of points).

In conclusion, the determination of the various tissues, in particular the fragmented VAT depots, using the *VISS* method is accurate and feasible. It results in reasonable agreement between and within raters, which compares favorably with published methods (35) and with a reference volumetric method (9), and the total body mass agrees well with body weight that is determined by a scale. *VISS* methodology presented in this manuscript can either be used for fat compartments or whole body volume as validated against two standards here. In addition, it has been used for the volumetric determination of single organs, e.g. the liver (34).

A simple contour line helps to separate coarse regions such as intra- vs. extra-abdominal region, while a threshold based on a histogram quickly determines a major part of the points that have to be deleted. Additionally the sparse data can be corrected

easily by manual interaction. In comparison to a correction of the threshold technique, the removal or adding of a few points per slice is very flexible and fast. While threshold-only methods require compromises by the operator in different parts of the images as soon as *rf*-inhomogeneity reduces the intensity of fat voxels to that of voxels with water/non-fat-organs, the proposed *VISS* method is more transparent and leads to acceptable results. The combination of contour methods, threshold, and point-counting is at least as reliable as established threshold methods, in particular in complex shaped and inhomogeneous images.

ACKNOWLEDGEMENTS: for support from Swiss National Science Foundation (#310030-118219), to R.Koenig, S.Koenig and V.Beutler for help with data analysis, D.Chong for helpful tips with MATLAB, and A.Egger for help with data acquisition.

REFERENCES

1. Kullberg J, Brandberg J, Angelhed JE et al. Whole-body adipose tissue analysis: comparison of MRI, CT and dual energy X-ray absorptiometry. *Br J Radiol* 2009;82:123-130.
2. Pietrobelli A, Tato L. Body composition measurements: from the past to the future. *Acta Paediatr Suppl* 2005;94:8-13.
3. Fusch C, Slotboom J, Fuehrer U et al. Neonatal body composition: dual-energy X-ray absorptiometry, magnetic resonance imaging, and three-dimensional chemical shift imaging versus chemical analysis in piglets. *Pediatr Res* 1999;46:465-473.
4. Shen W, Wang Z, Punyanita M et al. Adipose tissue quantification by imaging methods: a proposed classification. *Obes Res* 2003;11:5-16.
5. Despres JP, Lemieux I. Abdominal obesity and metabolic syndrome. *Nature* 2006;444:881-887.
6. Ross R, Leger L, Morris D, deGuise J, Guardo R. Quantification of adipose tissue by MRI: relationship with anthropometric variables. *J Appl Physiol* 1992;72:787-795.
7. Abate N, Burns D, Peshock RM, Garg A, Grundy SM. Estimation of adipose tissue mass by magnetic resonance imaging: validation against dissection in human cadavers. *J Lipid Res* 1994;35:1490-1496.
8. Siegel MJ, Hildebolt CF, Bae KT, Hong C, White NH. Total and Intraabdominal Fat Distribution in Preadolescents and Adolescents: Measurement with MR Imaging. *Radiology* 2007;242:846-856.
9. Machann J, Thamer C, Schnoedt B et al. Standardized assessment of whole body adipose tissue topography by MRI. *J Magn Reson Imaging* 2005;21:455-462.
10. Bonekamp S, Ghosh P, Crawford S et al. Quantitative comparison and evaluation of software packages for assessment of abdominal adipose tissue distribution by magnetic resonance imaging. *Int J Obes* 2008;32:100-111.
11. Demerath EW, Ritter KJ, Couch WA et al. Validity of a new automated software program for visceral adipose tissue estimation. *Int J Obes* 2007;31:285-291.
12. Wurslin C, Machann J, Rempp H, Claussen C, Yang B, Schick F. Topography mapping of whole body adipose tissue using a fully automated and standardized procedure. *J Magn Reson Imaging* 2010;31:430-439.

13. Lancaster JL, Ghiatas AA, Alyassin A, Kilcoyne RF, Bonora E, DeFronzo RA. Measurement of abdominal fat with T1-weighted MR images. *J Magn Reson Imaging* 1991;1:363-369.
14. Ross R, Rissanen J, Pedwell H, Clifford J, Shragge P. Influence of diet and exercise on skeletal muscle and visceral adipose tissue in men. *J Appl Physiol* 1996;81:2445-2455.
15. Bley TA, Wieben O, Francois CJ, Brittain JH, Reeder SB. Fat and water magnetic resonance imaging. *J Magn Reson Imaging* 2010;31:4-18.
16. Hu HH, Nayak KS, Goran MI. Assessment of abdominal adipose tissue and organ fat content by magnetic resonance imaging. *Obes Rev* 2011;12:e504-e515.
17. Armao D, Guyon JP, Firat Z, Brown MA, Semelka RC. Accurate quantification of visceral adipose tissue (VAT) using water-saturation MRI and computer segmentation: preliminary results. *J Magn Reson Imaging* 2006;23:736-741.
18. Kullberg J, Angelhed JE, Lonn L et al. Whole-body T1 mapping improves the definition of adipose tissue: consequences for automated image analysis. *J Magn Reson Imaging* 2006;24:394-401.
19. Kullberg J, Johansson L, Ahlstrom H et al. Automated assessment of whole-body adipose tissue depots from continuously moving bed MRI: a feasibility study. *J Magn Reson Imaging* 2009;30:185-193.
20. Ma J. Breath-hold water and fat imaging using a dual-echo two-point Dixon technique with an efficient and robust phase-correction algorithm. *Magn Reson Med* 2004;52:415-419.
21. Reeder SB, McKenzie CA, Pineda AR et al. Water-fat separation with IDEAL gradient-echo imaging. *J Magn Reson Imaging* 2007;25:644-652.
22. Kijowski R, Woods MA, Lee KS et al. Improved fat suppression using multipeak reconstruction for IDEAL chemical shift fat-water separation: application with fast spin echo imaging. *J Magn Reson Imaging* 2009;29:436-442.
23. Hu HH, Smith DL, Jr., Nayak KS, Goran MI, Nagy TR. Identification of brown adipose tissue in mice with fat-water IDEAL-MRI. *J Magn Reson Imaging* 2010;31:1195-1202.
24. Mitsiopoulos N, Baumgartner RN, Heymsfield SB, Lyons W, Gallagher D, Ross R. Cadaver validation of skeletal muscle measurement by magnetic resonance imaging and computerized tomography. *J Appl Physiol* 1998;85:115-122.

25. Roberts N, Cruz-Orive LM, Reid NMK, Brodie DA, Bourne M, Edwards RHT. Unbiased estimation of human body composition by the Cavalieri method using magnetic resonance imaging. *J Microsc* 1993;171:239-253.
26. Positano V, Gastaldelli A, Sironi AM, Santarelli MF, Lombardi M, Landini L. An accurate and robust method for unsupervised assessment of abdominal fat by MRI. *J Magn Reson Imaging* 2004;20:684-689.
27. Liew AW, Yan H. An adaptive spatial fuzzy clustering algorithm for 3-D MR image segmentation. *IEEE Trans Med Imaging* 2003;22:1063-1075.
28. Positano V, Cusi K, Santarelli MF et al. Automatic correction of intensity inhomogeneities improves unsupervised assessment of abdominal fat by MRI. *J Magn Reson Imaging* 2008;28:403-410.
29. Mazonakis M, Damilakis J, Mantatzis M et al. Stereology versus planimetry to estimate the volume of malignant liver lesions on MR imaging. *Magn Reson Imaging* 2004;22:1011-1016.
30. Mazonakis M, Damilakis J, Maris T, Prassopoulos P, Gourtsoyiannis N. Comparison of two volumetric techniques for estimating liver volume using magnetic resonance imaging. *J Magn Reson Imaging* 2002;15:557-563.
31. Gong QY, Phoenix J, Kemp GJ et al. Estimation of body composition in muscular dystrophy by MRI and stereology. *J Magn Reson Imaging* 2000;12:467-475.
32. Roberts N, Cruz-Orive LM, Bourne M, Herfkens RJ, Karwoski RA, Whitehouse GH. Analysis of cardiac function by MRI and stereology. *J Microsc* 1997;187:31-42.
33. Boesch C, Ith M, Jung B et al. Effect of oral D-tagatose on liver volume and hepatic glycogen accumulation in healthy male volunteers. *Regul Toxicol Pharmacol* 2001;33:257-267.
34. Decombaz J, Jentjens R, Ith M et al. Enhancing effect of fructose or galactose on human liver glycogen synthesis post-exercise. *Med Sci Sports Exerc* 2011;43:1964-1971.
35. Arif H, Racette SB, Villareal DT, Holloszy JO, Weiss EP. Comparison of methods for assessing abdominal adipose tissue from magnetic resonance images. *Obesity* 2007;15:2240-2244.
36. Bland JM, Altman DG. Statistical methods for assessing agreement between two methods of clinical measurement. *Lancet* 1986;1:307-310.
37. Vovk U, Pernus F, Likar B. A review of methods for correction of intensity inhomogeneity in MRI. *IEEE Trans Med Imaging* 2007;26:405-421.

38. Visser M, Gallagher D, Deurenberg P, Wang J, Pierson RN, Heymsfield SB. Density of fat-free body mass: relationship with race, age, and level of body fatness. *Am J Physiol* 1997;272:E781-E787.
39. Boesch C, Machann J, Vermathen P, Schick F. Role of proton MR for the study of muscle lipid metabolism. *NMR Biomed* 2006;19:968-988.
40. Heymsfield SB, Gallagher D, Mayer L, Beetsch J, Pietrobelli A. Scaling of human body composition to stature: new insights into body mass index. *Am J Clin Nutr* 2007;86:82-91.

Table 1: Inter- and intra-observer consistency of *VISS* determined by coefficients of variance (*CV*) and intraclass correlation coefficients (*ICC*) for all 24 subjects and two cohorts at 1.5 T and 3 T, respectively.

TBV		all	1.5 T	3.0 T
Group average	[L]	85.63	85.82	85.44
Group standard deviation	[L]	19.86	23.95	15.85
Intra-rater standard deviation	[L]	0.63	0.63	0.63
Intra-rater <i>CV</i>	[%]	0.7%	0.7	0.7
Inter-rater standard deviation	[L]	2.08	2.08	2.1
Inter-rater <i>CV</i>	[%]	2.4%	2.4%	2.5%
Average intra-rater <i>ICC</i>		0.998	0.997	0.999
(confidence limits)		(0.989 – 0.999)	(0.982 – 0.999)	(0.990 – 1.000)
Inter-rater <i>ICC</i>		0.995	0.994	0.996
(confidence limits)		(0.890 – 0.999)	(0.864 – 0.999)	(0.905 – 0.999)
VAT		all	1.5 T	3.0 T
Group average	[L]	4.46	4.56	4.35
Group standard deviation	[L]	2.50	3.21	1.65
Intra-rater standard deviation	[L]	0.22	0.23	0.20
Intra-rater <i>CV</i>	[%]	4.9%	5.1%	4.7%
Inter-rater standard deviation	[L]	0.67	0.77	0.57
Inter-rater <i>CV</i>	[%]	15.1%	16.8%	13.1%
Average intra-rater <i>ICC</i>		0.987	0.983	0.989
(confidence limits)		(0.959 – 0.995)	(0.867 – 0.996)	(0.963 – 0.997)
Inter-rater <i>ICC</i>		0.968	0.962	0.972
(confidence limits)		(0.856 – 0.989)	(0.775 – 0.991)	(0.871 – 0.993)
SCAT		all	1.5 T	3.0 T
Group average	[L]	33.26	32.63	33.9
Group standard deviation	[L]	12.64	15.08	10.27
Intra-rater standard deviation	[L]	0.75	0.69	0.81
Intra-rater <i>CV</i>	[%]	2.2%	2.1%	2.4%
Inter-rater standard deviation	[L]	2.06	2.09	2.05
Inter-rater <i>CV</i>	[%]	6.2%	6.4%	6.1%
Average intra-rater <i>ICC</i>		0.993	0.992	0.994
(confidence limits)		(0.962 – 0.997)	(0.872 – 0.998)	(0.977 – 0.998)
Inter-rater <i>ICC</i>		0.989	0.989	0.989
(confidence limits)		(0.945 – 0.996)	(0.945 – 0.997)	(0.934 – 0.997)

Table 2: Correlation coefficients, intercepts, slopes, and Bland-Altman ranges from the comparison between the reference method (9) and *VISS* (single evaluation by rater 1) for *TBV*, *VAT*, and *SCAT* in either all 24 subjects or the cohorts of 1.5 T or 3.0 T, respectively. Italic-bold numbers indicate intercept, slopes, or Bland-Altman ranges with confidence limits (not shown in regression analysis) that do not include zero (intercept) or one (slope).

Volume	Cohort	Linear Regression Analysis			Bland-Altman Analysis		
		Correlation R	Intercept	Slope	Average	Lower	Upper
<i>TBV</i>	all	0.997	2.267	1.013	3.33	0.38	6.28
	1.5 T	1.000	4.792	0.996	4.44	3.44	5.44
	3.0 T	0.998	-3.273	1.066	2.22	-0.40	4.84
<i>VAT</i>	all	0.983	-0.048	1.069	0.20	-0.68	1.07
	1.5 T	0.992	0.047	1.092	0.36	-0.51	1.23
	3.0 T	0.967	-0.050	1.023	0.03	-0.75	0.82
<i>SCAT</i>	all	0.983	0.663	1.078	3.11	-2.18	8.39
	1.5 T	0.997	2.094	1.092	4.77	1.06	8.47
	3.0 T	0.987	-3.375	1.142	1.45	-3.21	6.10

Table 3: Correlation coefficients, intercepts, slopes, and Bland-Altman ranges from the comparison between the weights determined from volumes converted by it's specific density against weight determined by a scale in either all 24 subjects or the cohorts of 1.5 T or 3.0 T, respectively. The italic-bold number indicates an intercept where the 95% confidence intervals (not shown in regression analysis) do not include zero.

Method	Cohort	Linear Regression Analysis			Bland Altman Analysis		
		Correlation R	Intercept	Slope	Average	Lower	Upper
VISS	all	0.997	0.502	0.982	1.056	-1.977	4.088
	1.5 T	0.999	-0.937	0.991	1.688	-0.676	4.053
	3.0 T	0.995	2.617	0.965	0.423	-2.783	3.629
Reference	all	0.996	3.137	0.987	-2.005	-5.603	1.593
	1.5 T	0.999	4.614	0.972	-2.265	-4.640	0.110
	3.0 T	0.989	-0.439	1.026	-1.744	-6.311	2.823

FIGURE CAPTIONS

Figure 1

Determination of visceral fat and/or subcutaneous fat in a subject with a body mass index of 31.1 kg/m^2 using a threshold-only technique (A), point-counting-only (B), and the manual planimetric (contour-only) method (C). While threshold-only has difficulties to cope with inhomogeneities in the image (red arrows), point-counting-only is time consuming if the number of points is high, and manual contour-only methods are complex in highly fragmented tissue such as *VAT*. (D) In contrast, the *VISS* method can combine the advantages of the three methods, where the preparation of the images with contour and threshold helps to limit the number of points which need to be handled.

Figure 2

Determination of visceral fat using *VISS* (typically, up to 10 crosses have to be edited manually per slice as shown by the green circles). The threshold can be adjusted manually (upper right corner), however, in contrast to threshold-only methods, this value is uncritical since the following manual correction could cope quickly with wrongly assigned points.

Figure 3

TBV, *VAT*, *SCAT*, and *TFV* (total fat volume, sum of *VAT* and *SCAT*) from a single subject (male, 30y, 1.64m, 82kg) at 3.0 Tesla, showing the results of single slices. While both methods agree very well even for single slices, *VISS* (pink line) shows stronger

noise than the reference method (9) since the number of points in a single slice is not yet sufficient to compensate for the random placement of the grid and the sparse sampling – this is achieved as soon as enough slices are added together. If single slices should be evaluated, a smaller grid can be chosen, resulting in a sufficient number of points (typically >100 over all slices).

Figure 4

Correlation and Bland-Altman analysis of the reference method (9) vs. *VISS* (single evaluation by rater 1). Blue symbols are used for the cohort at 1.5 Tesla while the red symbols represent the cohort at 3.0 Tesla. Upper row: linear correlation between the reference method and *VISS*. The solid line indicates unity. Lower row: Bland-Altman analysis of the same data with confidence limits (difference of *VISS* minus reference method). Three of the Bland-Altman ranges do not include zero. Points showing *TBV* of the cohorts at 1.5 Tesla and at 3.0 Tesla are separated; however, the Bland-Altman ranges of the two cohorts overlap.

Figure 5

Correlation and Bland-Altman analysis of body weight determined by a scale and two volumetric methods (calculations of weights from volumes see Methods), the reference method (9) and *VISS* (single evaluation by rater 1). Blue symbols are used for the cohort at 1.5 Tesla while the red symbols represent the cohort at 3.0 Tesla. The solid line indicates unity. Upper row: linear correlation between the scale and *VISS* or the reference method, respectively. Lower row: Bland-Altman analysis of the same data

with confidence limits (difference volumetric data minus scale). All Bland-Altman ranges include zero but the reference method slightly underestimates the weight. Cohorts at 1.5 Tesla and at 3.0 Tesla overlap for both methods.

Figure 1

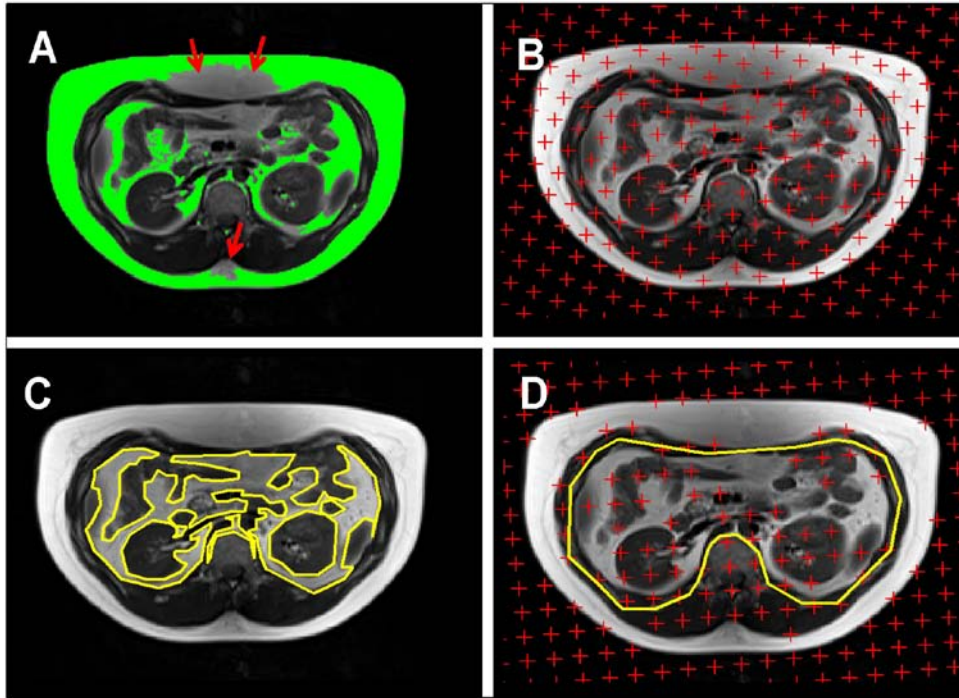


Figure 2

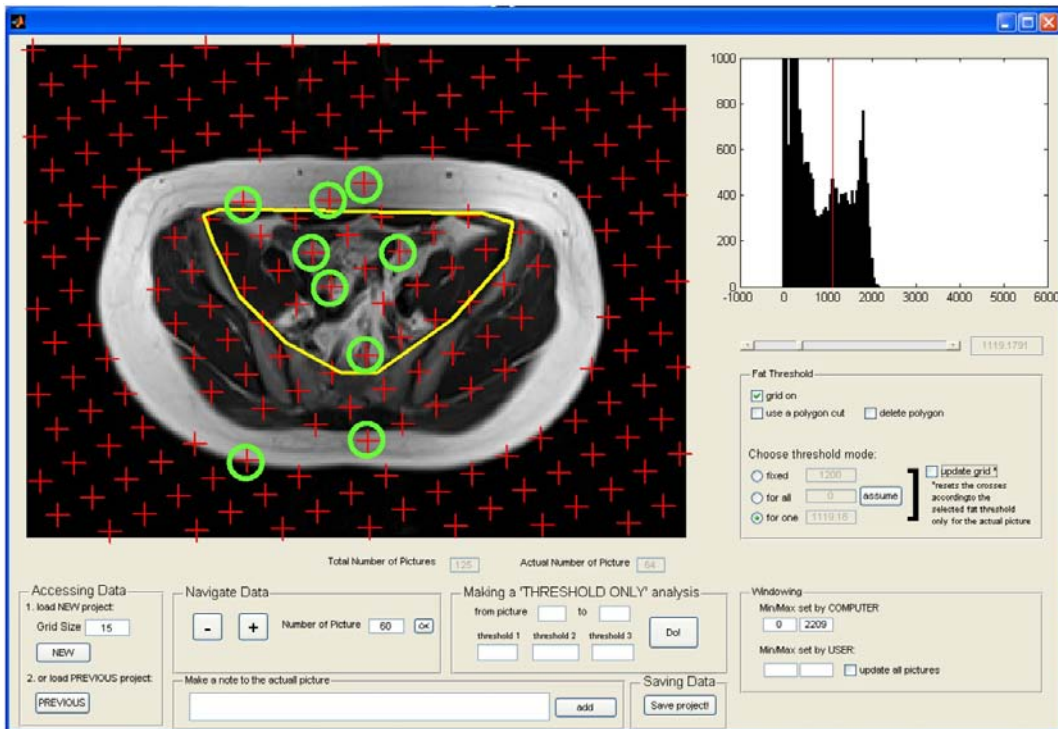


Figure 3

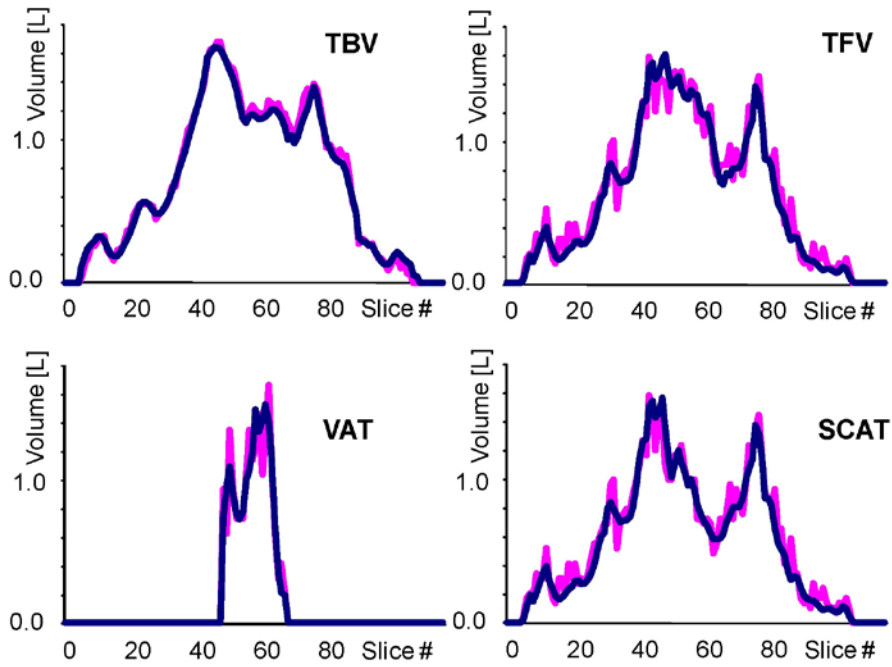


Figure 4

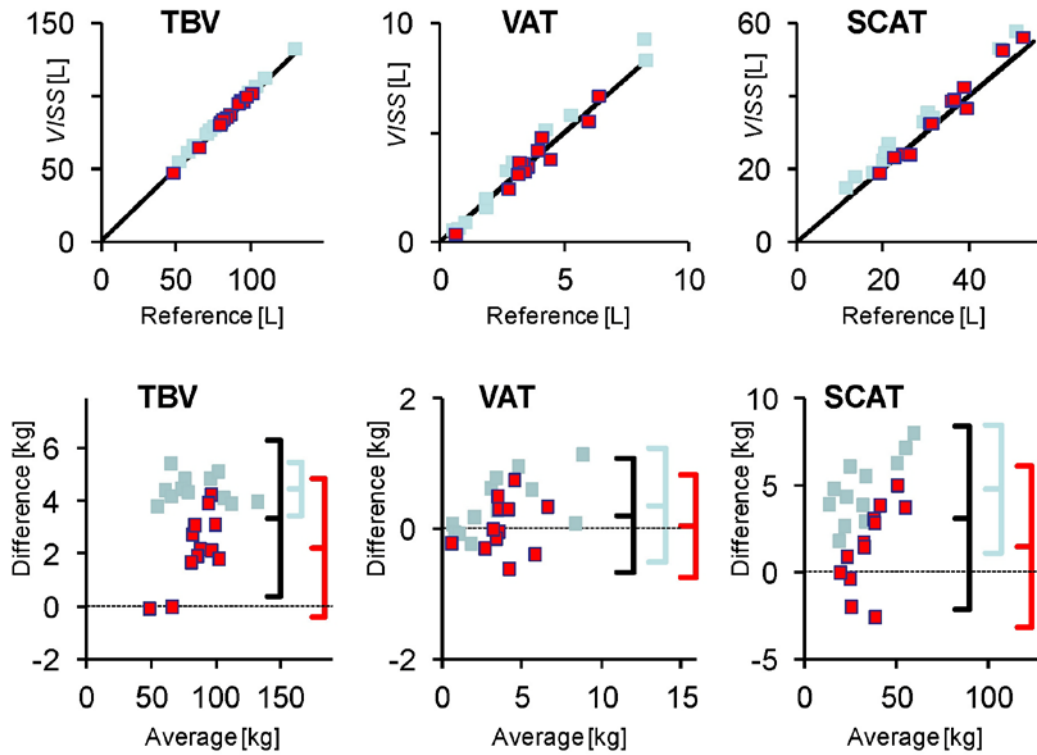
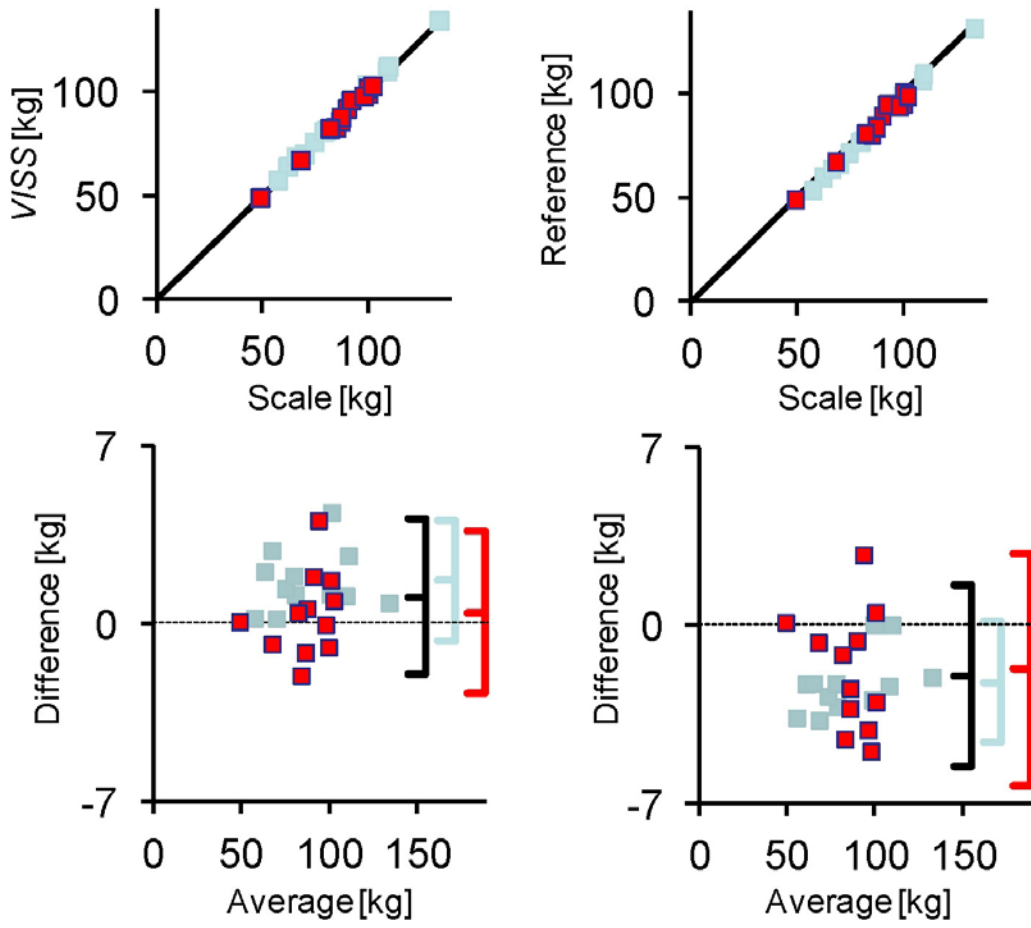


Figure 5



CLINICAL STUDY

The effect of GH replacement therapy on different fat compartments: a whole-body magnetic resonance imaging study

A Egger*, T Buehler^{1,*}, C Boesch¹, P Diem, C Stettler and E R Christ

Division of Endocrinology, Diabetes, and Clinical Nutrition, Inselspital, Bern University Hospital and ¹Department of Clinical Research, University of Bern, CH-3010 Bern, Switzerland

(Correspondence should be addressed to E R Christ; Email: emanuel.christ@insel.ch)

*(A Egger and T Buehler contributed equally to this work)

Abstract

Objective: Patients with GH deficiency (GHD) are insulin resistant with an increase in visceral fat mass (FM). Whether this holds true when sedentary control subjects (CS) are matched for waist has not been documented.

GH replacement therapy (GHRT) results in a decrease in FM. Whether the decrease in FM is mainly related to a reduction in visceral FM remains to be proven. The aim was to separately assess visceral and subcutaneous FM in relation to insulin resistance (IR) in GHD patients before and after GHRT and in sedentary CS.

Methods: Ten patients with GHD were investigated before and 6 months after GHRT. Sedentary CS matched for age, gender, body mass index, and waist were assessed. Exercise capacity was measured as VO_{2max} using an incremental work load on a treadmill. Visceral and subcutaneous FM were measured using whole-body magnetic resonance imaging and IR by the homeostasis model assessment of IR (HOMA-IR) index.

Results: GHD patients had a non-significantly lower VO_{2max} but did not have increased subcutaneous and visceral FM compared with CS. GHRT resulted in a similar relative decrease in subcutaneous and visceral FM. Compared with CS, GHD patients showed a lower HOMA-IR. GHRT tended to increase HOMA-IR.

Conclusion: Matching for waist and separate assessment of visceral and subcutaneous FM may be critical in the evaluation of body composition and IR in GHD patients before and after GHRT.

European Journal of Endocrinology 164 23–29

Introduction

Hypopituitary patients with GH deficiency (GHD) present with altered body composition characterized by an increase in fat mass (FM), predominantly in the visceral compartment, and a decrease in fat-free mass (FFM) and total body water (1, 2). The increase in visceral FM in GHD patients has been linked to an insulin-resistant condition which in turn has been associated with an increased cardiovascular risk (1, 3). GH replacement therapy (GHRT) consistently results in a decrease in FM, and an increase in FFM and body water (1). Interestingly, there is data suggesting that GHRT reduces predominantly visceral FM (4). Short-term GHRT leads usually to a limited increase in insulin resistance (IR) (5) whereas long-term supplementation tends to decrease IR possibly as a consequence of the increase in FFM (6).

A panoply of methods has been used to assess body composition in hypopituitarism with GHD before and

after GHRT including bioimpedance (BIA) (1, 2, 7, 8), 40K labeled water dilution technique (7, 9), computer tomography (CT) (4), and magnetic resonance imaging (MRI) (9) as well as the dual-energy X-ray absorptiometry (DEXA) (1, 7, 10–12). The 40K labeled water dilution technique and BIA assessment depend on total body water and/or electrolyte distribution, which have been shown to be affected by GHD and GHRT (13, 14). This may lead to an overestimation of changes in FFM using these methods (7, 15, 16). DEXA scan does not offer the possibility to differentiate between subcutaneous and visceral FM, a distinction which may be of particular clinical importance in these patients.

The number of methods that reliably determine visceral FM is currently limited. Recent data suggest that abdominal cross-sectional imaging (MRI or CT) is less reliable than whole abdomen scanning in determining visceral FM (16, 17). Furthermore, whole-body MRI has been established for the separate assessment of the different body fat compartments (total, subcutaneous,

and visceral FM) in different scientific settings, including insulin-resistant conditions (18).

In this study, we measured the different fat compartments in hypopituitary patients with GHD (before and after GHRT) and in sedentary control subjects (CS) matched for gender, age, body mass index (BMI), and waist. We hypothesized that GHD patients have predominantly an increase in visceral FM compared with matched CS that will be reduced following GHRT.

Subjects and methods

The study was a prospective single-center open case-control study. It was performed at the University Hospital of Bern, Switzerland. Investigations were done at the Division of Endocrinology, Diabetes and Clinical Nutrition and at the Department of Clinical Research of the University of Bern.

Four women and six men with severe GHD due to pituitary or hypothalamic disease were recruited from the outpatient clinic. GHD was defined as a peak GH of < 3 mU/l during an insulin tolerance test with nadir plasma glucose of < 2.2 mmol/l and hypoglycemic symptoms (19). Patients were included, provided they had been under stable conventional hormone replacement therapy (glucocorticoids, thyroxine (T_4), and sex hormones) as needed for at least 6 months. Exclusion criteria were (former or present) ACTH- or GH-secreting pituitary adenoma, abnormal liver or renal function, active neoplasia, severe cardiovascular disease (unstable coronary artery disease, heart failure New York Heart Association III–IV), diabetes mellitus, hemophilia, therapy with drugs known to affect lipid or glucose metabolism, inability to exercise and contraindications to exposure to a 3-Tesla magnetic field. Additionally, we recruited ten sedentary CS matched for age, gender, BMI, and waist.

The study was performed according to the Declaration of Helsinki, the guidelines of good clinical practice, the Swiss health laws, and the ordinance on clinical research. Approval for the study was obtained from the ethics committee, Bern. Each study subject gave written informed consent.

Study protocol

GHD patients and CS attended the hospital after an overnight fast. In GHD patients with LH/FSH insufficiency, the investigation of body composition was performed in the middle of the dose interval in male patients and during replacement therapy in female patients respectively. In patients with TSH insufficiency, the dose was adjusted to obtain stable free T_4 concentrations in the upper half of the normal range. Body weight was measured on an electronic balance with subjects wearing light clothes and without shoes. Height was assessed by a stadiometer. BMI was

calculated as the weight divided by the square of the height. The waist circumference was measured in the upright position with a flexible tape placed on a horizontal plane at the level of the iliac crest. The measurement was made at the end of a normal expiration. Fasting baseline blood sample was collected; body composition was determined by BIA and immediately afterward by whole-body MRI in a 3-Tesla whole-body system. On a separate visit, a spirometry was carried out in all patients and sedentary CS using an incremental workload on a treadmill with the determination of peak aerobic capacity (VO_{2max}).

Patients with GHD were instructed about self-administration of GH using a pen device (Genotropin-Pen, Pfizer, Switzerland). Usual clinical care was provided (monthly visit with insulin-like growth factor 1 (IGF1) measurements to adjust GH doses). GH dose was gradually increased to obtain IGF1 concentrations in the upper half of the age-adjusted reference range as suggested by the GH Research Society (19). After 6 months of GHRT, weight maintaining diet (total need of calories/d calculated according to the formula of Harris-Benedict, qualitatively consisting of 50% carbohydrate, 30% fat, and 20% protein), and identical physical activity, the same studies were performed in the patients.

Whole-body fat analysis

Images were acquired on a 3T MR system (Tim Trio; SIEMENS, Erlangen, Germany) with the body coil as combined transmit/receive coil. To determine visceral FM, subcutaneous FM, and whole-body volume (WBV), images were taken in axial direction with a T1-weighted fast spin echo technique (TR = 452 ms, TE = 38 ms, echo train length = 7, slice thickness of 10 mm, five slices per sequence, spacing between slices 20 mm, FOV 50 cm, image resolution 2 mm per pixel) from fingers to toes leading to 100–130 axial images per subject. Owing to the limited displacement of the examination table, the subjects were measured in two positions, prone/head-first with outstretched arms and prone/feet-first. A mark was set at the iliac crest to reposition the subject. In the abdominal region, the slices were recorded in breath hold.

Image analysis for volume determination was done by using a home-built program (MATLAB R2007a, The MathWorks, Natick, MA, USA) that is based on an extended point counting method (20) and three sequential steps for the determination of visceral FM and subcutaneous FM: i) the region of visceral fat is separated from subcutaneous fat by a simple contour line, ii) the points for the point counting method are set or deleted by the program based on a threshold value, and iii) visual inspection of the points lets the operator correct for intensity variations resulting from radio frequency (RF) inhomogeneity. For the WBV, no separation by the contour line was applied, and the threshold was set to a minimal value

(above noise level). Thus, except the volume of the lung, all tissues were counted for WBV.

The precision of the volumetric technique had been established in a phantom model with up to eight bottles filled with a known amount of oil between bottles with water (21) (typically 1 l per bottle). Aluminum foil between the bottles generated highly inhomogeneous images, which corresponded to the complexity and inhomogeneity of real abdominal images at higher magnetic field strength. The images were analyzed by three observers twice. The Bland–Altman analysis of the comparison between measured and true volumes resulted in a coefficient of variance (CV) of 4.5%, the comparison between the first and second determination by an observer (intra-observer variability) resulted in a CV of 4.1%, and the comparison between the values determined by the three observers (inter-observer variability) resulted in a CV of 4.2%.

For the study, the analysis of the images was performed at the end of the study by a single operator who was not part of the clinical team, and completely blinded to the group of the volunteers or the treatment status of the patients.

To estimate the accuracy of the WBV, the weight of the subjects was calculated based on a two-compartment model with a fat compartment (density for adipose tissue 0.918 g/ml, (22)) and an FFM (average density for the FFM 1.100 g/ml (23)).

Biochemical analysis

Serum IGF1 was measured by an IRMA (Nichols Institute, San Juan Capistrano, CA, USA), and plasma glucose was measured using the hexokinase method (Hitachi 917, Roche). Insulin was determined by RIA (Linco Research, Labodia, Yens, Switzerland).

Statistical analysis

Statistical analysis was performed in SPSS 17.0 (SPSS, Inc., Chicago, IL, USA). Results are expressed as median \pm interquartile range. Non-parametric Wilcoxon signed-rank test was used to compare unpaired datasets (GHD versus CS), whereas non-parametric Mann–Whitney tests were used to compare paired data (GHD versus GHRT). A Pearson correlation was calculated to compare body weight based on MRI assessment with body weight measured on a scale. A two-sided *P* value of <0.05 was considered significant.

Results

Clinical and biochemical findings

Individual clinical characteristics of the GHD patients are summarized in Table 1. At the end of the study, one of the GHD patients had to be withdrawn due to a discus hernia with a need for a surgical intervention, which was judged not to be related to GHRT (Tables 1–3).

The final dose of GH was attained at 3 months. During the remaining 3 months, a stable GH dose was administered. The median dose was 0.5 mg/day in male patients (range 0.3–0.6 mg/day) and 0.7 mg/day (range 0.5–1.2 mg/day) in female patients.

All except one patient had LH/FSH insufficiency. All the male patients ($n=6$) were substituted with testosterone undecanoas 1000 mg every 10–12 weeks. Two of the female patients with LH/FSH insufficiency were postmenopausal. One of the postmenopausal patients was substituted with a combination including estradiol valeras and cyproteron acetate, one premenopausal female patient was treated with an anticonceptive combination therapy including gestodenum 0.075 mg

Table 1 Clinical characteristics of patients presenting with GHD.

Age (years)	Gender	Diagnosis	Duration hypopit.	Treatment			Hormone deficiencies				
				Surg	DxRT	DA	GH	ACTH	TSH	LH/FSH	ADH
46	M	Hormone-inactive pituitary adenoma	8	+	+		+	+	+	+	
43	M	Hormone-inactive pituitary adenoma	29	+	+		+	+	+	+	
54	F	Epidermoid cyst	8	+			+	+		+	
54	M	Gonadotroph cell adenoma	1	+			+			+	
18	F	Idiopathic GH deficiency	17				+			+	
47	M	Hormone-inactive pituitary adenoma	1	+			+	+	+	+	
30	M	Prolactinoma	3			+	+	+	+	+	
56	F	Hormone-inactive pituitary adenoma	1	+			+		+	+	
32	M	Macroprolactinoma	1			+	+			+	
39	F	Hormone-inactive pituitary adenoma	1	+			+				

Hypopit., hypopituitarism; Surg, surgery; DxRT, pituitary radiotherapy; DA, dopamine agonist; ADH, antidiuretic hormone.

Table 2 Anthropometric, biochemical, and body composition characteristics of GHD before and after therapy (GHRT).

	GHD	GHRT	P values
Males/females	6/4	6/4	
Age (years)	45.5 (32.0–54.6)	46.1 (32.6–55.1)	0.005
Waist (cm) ^a	90.5 (78.9–96.9)	91.0 (77.5–93.5)	0.362
BMI (kg/m ²)	27.2 (22.9–29.0)	27.3 (22.3–29.8)	0.575
Baseline IGF1 (ng/ml)	68.5 (40.3–87.6)	153.0 (112.0–174.3)	0.005
HOMA-IR	0.74 (0.31–1.65)	1.14 (0.62–2.10)	0.169
FM BIA (kg)	21.4 (17.0–28.4)	19.7 (14.5–25.6)	0.047
FFM BIA (kg)	51.6 (43.7–60.0)	54.0 (44.4–65.7)	0.005
Total FM MRI (kg) ^a	19.0 (14.7–25.5)	17.6 (12.0–24.3)	0.008
Subcutaneous FM MRI (kg) ^a	16.0 (13.8–22.7)	14.7 (10.8–21.6)	0.008
Visceral FM MRI (kg) ^a	2.1 (1.3–3.1)	2.0 (1.1–2.6)	0.044
FFM MRI (kg) ^a	47.7 (42.6–59.3)	49.3 (43.9–62.1)	0.015

Results are median and interquartile range. Bold P values, statistically significant.

^aAnalysis based on nine paired datasets.

and ethinylestradiol 0.02 mg replacement therapy. T₄ replacement therapy was necessary in half of the patients. The dose ranged between 0.075 and 0.175 (median 0.1 mg). Cortisol replacement therapy was initiated in half of the patients. The dose of cortisol was adapted to the body weight and administered in two or three doses as done previously (24). The cortisol replacement dose used in the GHD patients was between 15 and 20 mg (median 17.5 mg/day).

Physical fitness as assessed by the determination of VO_{2max} was non-significantly lower in the GHD patients than in the CS (GHD: 37.1 (31.5–40.2) versus CS: 39.9 (38.1–45.9) ml O₂/kg body weight; P=0.10, median and interquartile range).

Additional anthropometric and fasting biochemical results of the GHD patients and CS are shown in Tables 2 and 3.

GHD patients and CS did not differ regarding the matching criteria: gender, age, BMI, and waist. GHRT did not have a significant influence on neither weight, BMI nor waist (Table 2).

GHD patients had significantly lower IGF1 levels than CS. GHRT led to a significant increase in IGF1 levels.

GHD patients showed a lower homeostasis model assessment of IR (HOMA-IR) than CS. GHRT tended to increase HOMA-IR, but the difference did not reach conventional levels of statistical significance.

Bioimpedance

Results of BIA are summarized in Tables 2 and 3. GHD patients and CS did not differ regarding FM and FFM. GHRT led to a significant decrease in FM (P<0.047) in parallel with a significant increase in FFM (P<0.005).

Whole-body MRI

Table 3 and Fig. 1 summarize the results of body composition as assessed by whole-body MRI (Tables 2 and 3 and Fig. 1). GHD patients and CS did not significantly differ with regard to the amount of total

Table 3 Baseline anthropometric, biochemical, and body composition characteristics of GHD patients and matched sedentary controls (CS).

	GHD	CS	P values (CS vs GHD)
Males/females	6/4	6/4	
Age (years)	45.5 (32.0–54.6)	44.4 (30.6–53.6)	0.940
Waist (cm) ^a	91.6 (82.3–100.3)	90.0 (80.5–97.9)	0.821
BMI (kg/m ²)	27.2 (22.9–29.0)	23.9 (22.0–29.2)	0.450
Baseline IGF1 (ng/ml)	68.5 (40.3–87.6)	111.5 (93.8–138.3)	0.001
HOMA-IR	0.74 (0.31–1.65)	1.42 (1.17–2.34)	0.034
FM BIA (kg)	21.4 (17.0–28.4)	16.6 (15.4–30.0)	0.496
FFM BIA (kg)	51.6 (43.7–60.0)	51.7 (40.5–64.0)	0.970
Total FM MRI (kg) ^a	19.2 (14.8–24.8)	18.1 (13.6–25.3)	0.650
Subcutaneous FM MRI (kg) ^a	16.4 (14.0–22.1)	15.2 (12.1–23.4)	0.545
Visceral FM MRI (kg) ^a	2.4 (1.5–3.3)	2.6 (1.3–3.4)	0.940
FFM MRI (kg) ^a	51.1 (43.6–62.8)	50.9 (39.3–65.1)	1.000

Results are median and interquartile range. Bold P values, statistically significant.

^aDifferences between median values of GHD patients by the inclusion of ten patients as compared with Table 2.

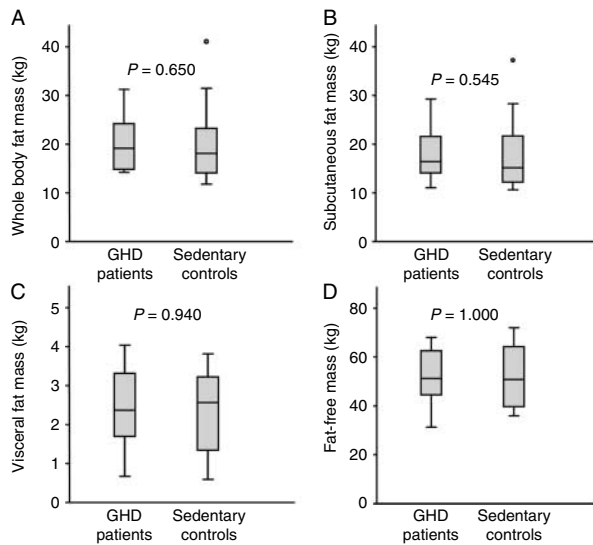


Figure 1 Comparison of body composition of GHD patients and matched sedentary control subjects. (A) Whole-body fat mass, (B) subcutaneous fat mass, (C) visceral fat mass, and (D) fat-free mass. Interquartile ranges are plotted according to Tukey's Hinges (SPSS 17.0). *P* values are shown for the comparison against GHD patients.

body FM, subcutaneous FM, visceral FM, and FFM (Table 3 and Fig. 1A–D).

GHRT led to a significant decrease in total body FM, subcutaneous FM, and visceral FM. The relative decrease in visceral FM (17%) and subcutaneous FM (12%) was similar. In addition, a significant increase in FFM was observed.

Correlations

There was an excellent correlation between the weight calculated from MRI and weight measured on a scale (body weight by scale = $1.032 \times$ weight by MRI $- 0.043$ kg; $R^2 = 0.98$; $P < 0.001$). The absolute calculated body weight based on the MRI method resulted in a mean underestimation of body weight of 2.3 ± 1.9 kg (mean \pm s.d.).

Discussion

The main results of this study are twofold: i) hypopituitary patients with GHD do not have an increase in subcutaneous and visceral FM compared with CS matched for age, gender as well as for BMI and waist, ii) GHRT reduced both subcutaneous and visceral FM to a similar extent.

Using whole-body MRI, total FM and its distribution in the subcutaneous and visceral compartments were not significantly different between GHD patients and sedentary CS. This is in contrast to previous studies (1) and our hypothesis. A possible explanation for this controversial finding may be the fact that this study

included waist circumference as an additional criteria to match the GHD patients. Furthermore, in contrast to previous studies (4, 25), half of our GHD patients had a sufficient corticotrophin axis (Table 1) as assessed by an insulin tolerance test, and the remaining were adequately substituted with hydrocortisone (twice or thrice daily regime) according to a weight-adapted dose regime (24). In this study, the median substitution dose of hydrocortisone was 17.5 mg/day (0.20 mg/kg body weight), significantly lower than in previous studies where daily doses between 25 and 30 mg were reported (4, 25). The fact that the dose of hydrocortisone replacement therapy may have a significant impact on body FM, in particular on visceral FM, is further substantiated by a recent study that reports a significant reduction in total and abdominal FM following a decrease in dose of hydrocortisone from 20–30 to 10–15 mg/day in hypopituitary patients (26).

HOMA-IR scores indicate that GHD patients are unexpectedly less resistant than the sedentary CS. Using different methods of IR measurements, previous studies suggest that GHD patients exhibit an increase in IR compared with CS matched for age, gender, and BMI (27, 28). Based on the small sample size, the current findings have to be interpreted with caution. However, it is tempting to speculate that in the presence of a similar waist circumference and a comparable amount of visceral FM, GHD patients show higher insulin sensitivity due to a lack of GH than CS. Consequently, the reported increase in IR of GHD patients observed in previous studies may rather be a consequence of the choice of CS than the GHD status of the patients. Alternatively, the higher hydrocortisone replacement dose usually administered in previous studies may have been an additional confounding factor. Differences in duration of GHD are unlikely to contribute to these controversial results since the mean duration of hypopituitarism in this study was similar than in previous studies (7 ± 9 years) (1). Similarly, differences in physical fitness do not explain these findings since GHD patients presented with slightly lower VO_{2max} than the matched sedentary CS.

GHRT resulted in a significant decrease in total, visceral, and subcutaneous FM and an increase in FFM. Quantitatively, the changes in total FM and FFM were consistent with previous studies (1). Moreover, in keeping with preceding reports (29), HOMA-IR index tended to increase following GHRT, albeit not reaching the levels of statistical significance. Interestingly, the relative decrease in subcutaneous FM associated with GHRT was accompanied by a comparable relative decrease in visceral FM. This is consistent with the fact that GH receptors are expressed at a quantitatively similar level in subcutaneous and visceral FM suggesting a comparable lipolytic action of GH at both sites (30). In contrast, previous studies proposed a predominant decrease in visceral FM following GHRT (4). Whether the predominant effect on visceral

FM in the preceding studies may at least partly be explained by the established effect of GH on 11- β -hydroxysteroid dehydrogenase type-1 (31), which is likely to be of particular importance in the presence of high substitution dose of cortisone acetate (not used in this study), remains speculative.

The comparison of the weight based on the measured value on a scale and the calculated weight based on the whole-body MRI scan yielded an excellent correlation in the different study populations. However, a slight underestimation of the weight of about 2 kg by MRI scanning was observed. This is most likely due to an inconsistent differentiation of certain tissues such as hilus/lung tissue or air in the abdomen and the fact that the GHD patients and CS were weighted on a scale wearing light clothes. Since the aim of the comparison between MRI volume-based body weight estimation and body weight measured by a scale served as an indicator of the feasibility of the method and was not a primary physiological target, no extra steps were taken into consideration to further reduce this difference.

Our study has certain limitations. The number of participants was relatively small due to the additional matching criteria 'waist' of the CS. Further studies with more patients and CS are warranted to draw firm conclusions. In addition, we did not compare the whole-body FM assessment using whole-body MRI with DEXA, which is the gold standard for the assessment of body composition in endocrine diseases. However, we found an excellent correlation of MR results with the body weight measured on the scale. Furthermore, DEXA scanning is essentially based on the measurement of body composition in two dimension, whereas whole-body MRI scanning allows to assess it in three dimension. Finally, the method is capable of detecting GHRT-induced changes in body composition that are quantitatively comparable to previous results observed using DEXA (7, 11, 12).

In conclusion, this study indicates that GHD patients do not have an increase in visceral FM compared with CS matched for age, gender as well as for BMI and waist. GHRT results in a comparable relative reduction in subcutaneous and visceral FM. Matching for waist and separate assessment of visceral and subcutaneous FM may be critical in the evaluation of body composition and IR in GHD patients before and after GHRT.

Declaration of interest

The authors declare that there is no conflict of interest that could be perceived as prejudicing the impartiality of the research reported.

Funding

The work was funded by grants from the Swiss National Foundation to E R Christ (No. #32000B0-100146) and C Boesch (No. #310000-118219) and by the Independent Pfizer Research Grant (to E R Christ). C Stettler is a PROSPER fellow supported by the Swiss National Science Foundation (Grant Number 3233B0 115212). Pfizer AG Switzerland kindly provided GH. We cordially thank Regula und Sabine Koenig for technical assistance.

Acknowledgements

We thank all the enthusiastic patients and control subjects who agreed to participate in this study.

References

- Carroll PV, Christ ER, Bengtsson BA, Carlsson L, Christiansen JS, Clemmons D, Hintz R, Ho K, Laron Z, Sizonenko P, Sonksen PH, Tanaka T & Thorne M. Growth hormone deficiency in adulthood and the effects of growth hormone replacement: a review. Growth Hormone Research Society Scientific Committee. *Journal of Clinical Endocrinology and Metabolism* 1998 **83** 382–395. (doi:10.1210/jc.83.2.382)
- Amato G, Mazziotti G, Di Somma C, Lalli E, De Felice G, Conte M, Rotondi M, Pietrosante M, Lombardi G, Bellastella A, Carella C & Colao A. Recombinant growth hormone (GH) therapy in GH-deficient adults: a long-term controlled study on daily versus thrice weekly injections. *Journal of Clinical Endocrinology and Metabolism* 2000 **85** 3720–3725. (doi:10.1210/jc.85.10.3720)
- Bengtsson BA. Untreated growth hormone deficiency explains premature mortality in patients with hypopituitarism. *Growth Hormone & IGF Research* 1998 **8** (Supplement A) 77–80. (doi:10.1016/S1096-6374(98)80014-2)
- Bengtsson BA, Eden S, Lonn L, Kvist H, Stokland A, Lindstedt G, Bosaeus I, Tolli J, Sjostrom L & Isaksson OG. Treatment of adults with growth hormone (GH) deficiency with recombinant human GH. *Journal of Clinical Endocrinology and Metabolism* 1993 **76** 309–317. (doi:10.1210/jc.76.2.309)
- Fowelin J, Attvall S, Lager I & Bengtsson BA. Effects of treatment with recombinant human growth hormone on insulin sensitivity and glucose metabolism in adults with growth hormone deficiency. *Metabolism* 1993 **42** 1443–1447. (doi:10.1016/0026-0495(93)90197-V)
- Johannsson G, Marin P, Lonn L, Ottosson M, Stenlof K, Bjorntorp P, Sjostrom L & Bengtsson BA. Growth hormone treatment of abdominally obese men reduces abdominal fat mass, improves glucose and lipoprotein metabolism, and reduces diastolic blood pressure. *Journal of Clinical Endocrinology and Metabolism* 1997 **82** 727–734. (doi:10.1210/jc.82.3.727)
- Koranyi J, Bosaeus I, Alpsten M, Bengtsson BA & Johannsson G. Body composition during GH replacement in adults – methodological variations with respect to gender. *European Journal of Endocrinology* 2006 **154** 545–553. (doi:10.1530/eje.1.02118)
- Christ ER, Cummings MH, Westwood NB, Sawyer BM, Pearson TC, Sonksen PH & Russell-Jones DL. The importance of growth hormone in the regulation of erythropoiesis, red cell mass, and plasma volume in adults with growth hormone deficiency. *Journal of Clinical Endocrinology and Metabolism* 1997 **82** 2985–2990. (doi:10.1210/jc.82.9.2985)
- Snel YE, Doerga ME, Brummer RM, Zelissen PM & Koppeschaar HP. Magnetic resonance imaging-assessed adipose tissue and serum lipid and insulin concentrations in growth hormone-deficient adults. Effect of growth hormone replacement. *Arteriosclerosis, Thrombosis, and Vascular Biology* 1995 **15** 1543–1548.
- Attanasio AF, Howell S, Bates PC, Frewer P, Chipman J, Blum WF & Shalet SM. Body composition, IGF-I and IGFBP-3 concentrations as outcome measures in severely GH-deficient (GHD) patients after childhood GH treatment: a comparison with adult onset GHD patients. *Journal of Clinical Endocrinology and Metabolism* 2002 **87** 3368–3372. (doi:10.1210/jc.87.7.3368)
- Attanasio AF, Shavrikova E, Blum WF, Cromer M, Child CJ, Paskova M, Lebl J, Chipman JJ & Shalet SM. Continued growth hormone (GH) treatment after final height is necessary to complete somatic development in childhood-onset GH-deficient patients. *Journal of Clinical Endocrinology and Metabolism* 2004 **89** 4857–4862. (doi:10.1210/jc.2004-0551)
- Weaver JU, Monson JP, Noonan K, John WG, Edwards A, Evans KA & Cunningham J. The effect of low dose recombinant

- human growth hormone replacement on regional fat distribution, insulin sensitivity, and cardiovascular risk factors in hypopituitary adults. *Journal of Clinical Endocrinology and Metabolism* 1995 **80** 153–159. (doi:10.1210/jc.80.1.153)
- 13 Moller J, Frandsen E, Fisker S, Jorgensen JO & Christiansen JS. Decreased plasma and extracellular volume in growth hormone deficient adults and the acute and prolonged effects of GH administration: a controlled experimental study. *Clinical Endocrinology* 1996 **44** 533–539. (doi:10.1046/j.1365-2265.1996.728550.x)
 - 14 Salomon F, Cuneo RC, Hesp R & Sonksen PH. The effects of treatment with recombinant human growth hormone on body composition and metabolism in adults with growth hormone deficiency. *New England Journal of Medicine* 1989 **321** 1797–1803. (doi:10.1056/NEJM198912283212605)
 - 15 Haymond MW, Sunehag AL & Ellis KJ. Body composition as a clinical endpoint in the treatment of growth hormone deficiency. *Hormone Research* 1999 **51** (Supplement 3) 132–140. (doi:10.1159/000053176)
 - 16 Ludescher B, Machann J, Eschweiler GW, Vanhofen S, Maenz C, Thamer C, Claussen CD & Schick F. Correlation of fat distribution in whole body MRI with generally used anthropometric data. *Investigative Radiology* 2009 **44** 712–719. (doi:10.1097/RLI.0b013e3181afbb1e)
 - 17 Thomas EL, Saeed N, Hajnal JV, Brynes A, Goldstone AP, Frost G & Bell JD. Magnetic resonance imaging of total body fat. *Journal of Applied Physiology* 1998 **85** 1778–1785.
 - 18 Machann J, Thamer C, Schnoedt B, Haap M, Haring HU, Claussen CD, Stumvoll M, Fritsche A & Schick F. Standardized assessment of whole body adipose tissue topography by MRI. *Journal of Magnetic Resonance Imaging* 2005 **21** 455–462. (doi:10.1002/jmri.20292)
 - 19 Sonksen PH & Christiansen JS. Consensus guidelines for the diagnosis and treatment of adults with growth hormone deficiency. Growth Hormone Research Society. *Growth Hormone & IGF Research* 1998 **8** (Supplement B) 89–92. (doi:10.1016/S1096-6374(98)80028-2)
 - 20 Buehler TRN, Machann J, Schwenger N & Boesch C. Determination of body compartments at 1.5 and 3 Tesla combining three volume estimation methods. *Proceedings of the International Society for Magnetic Resonance in Medicine* 2010 **18** 2915.
 - 21 Buehler TCD & Boesch C. Determination of whole body fat and visceral adipose tissue, combining three volume estimation methods. *Proceedings of the International Society for Magnetic Resonance in Medicine* 2009 **17** 2872.
 - 22 Boesch C, Machann J, Vermathen P & Schick F. Role of proton MR for the study of muscle lipid metabolism. *NMR in Biomedicine* 2006 **19** 968–988. (doi:10.1002/nbm.1096)
 - 23 Visser M, Gallagher D, Deurenberg P, Wang J, Pierson RN Jr & Heymsfield SB. Density of fat-free body mass: relationship with race, age, and level of body fatness. *American Journal of Physiology* 1997 **272** E781–E787.
 - 24 Mah PM, Jenkins RC, Rostami-Hodjegan A, Newell-Price J, Doane A, Ibbotson V, Tucker GT & Ross RJ. Weight-related dosing, timing and monitoring hydrocortisone replacement therapy in patients with adrenal insufficiency. *Clinical Endocrinology* 2004 **61** 367–375. (doi:10.1111/j.1365-2265.2004.02106.x)
 - 25 Snel YE, Brummer RJ, Doerga ME, Zelissen PM, Bakker CJ, Hendriks MJ & Koppeschaar HP. Adipose tissue assessed by magnetic resonance imaging in growth hormone-deficient adults: the effect of growth hormone replacement and a comparison with control subjects. *American Journal of Clinical Nutrition* 1995 **61** 1290–1294.
 - 26 Danilowicz K, Bruno OD, Manavela M, Gomez RM & Barkan A. Correction of cortisol overreplacement ameliorates morbidities in patients with hypopituitarism: a pilot study. *Pituitary* 2008 **11** 279–285. (doi:10.1007/s11102-008-0126-2)
 - 27 Johannsson G & Bengtsson BA. Growth hormone and the metabolic syndrome. *Journal of Endocrinological Investigation* 1999 **22** 41–46.
 - 28 Jorgensen JO, Krag M, Jessen N, Norrelund H, Vestergaard ET, Moller N & Christiansen JS. Growth hormone and glucose homeostasis. *Hormone Research* 2004 **62** (Supplement 3) 51–55. (doi:10.1159/000080499)
 - 29 Fowelin J, Attvall S, von Schenck H, Bengtsson BA, Smith U & Lager I. Effect of prolonged hyperglycemia on growth hormone levels and insulin sensitivity in insulin-dependent diabetes mellitus. *Metabolism* 1993 **42** 387–394. (doi:10.1016/0026-0495(93)90092-3)
 - 30 Fisker S, Hansen B, Fuglsang J, Kristensen K, Ovesen P, Orskov H & Jorgensen JO. Gene expression of the GH receptor in subcutaneous and intraabdominal fat in healthy females: relationship to GH-binding protein. *European Journal of Endocrinology* 2004 **150** 773–777. (doi:10.1530/eje.0.1500773)
 - 31 Agha A & Monson JP. Modulation of glucocorticoid metabolism by the growth hormone – IGF-1 axis. *Clinical Endocrinology* 2007 **66** 459–465. (doi:10.1111/j.1365-2265.2007.02763.x)

Received 17 September 2010

Accepted 7 October 2010

Effect of two β -alanine dosing protocols on muscle carnosine synthesis and washout

Trent Stellingwerff · Helen Anwander ·
Andrea Egger · Tania Buehler · Roland Kreis ·
Jacques Decombaz · Chris Boesch

Received: 8 June 2011 / Accepted: 30 July 2011
© Springer-Verlag 2011

Abstract Carnosine (β -alanyl-L-histidine) is found in high concentrations in skeletal muscle and chronic β -alanine (BA) supplementation can increase carnosine content. This placebo-controlled, double-blind study compared two different 8-week BA dosing regimens on the time course of muscle carnosine loading and 8-week washout, leading to a BA dose–response study with serial muscle carnosine assessments throughout. Thirty-one young males were randomized into three BA dosing groups: (1) high–low: 3.2 g BA/day for 4 weeks, followed by 1.6 g BA/day for 4 weeks; (2) low–low: 1.6 g BA/day for 8 weeks; and (3) placebo. Muscle carnosine in *tibialis-anterior* (TA) and *gastrocnemius* (GA) muscles was measured by $^1\text{H-MRS}$ at weeks 0, 2, 4, 8, 12 and 16. Flushing symptoms and blood clinical chemistry were trivial in all three groups and there were no muscle carnosine changes in the placebo group. During the first 4 weeks, the increase for high–low (TA 2.04 mmol/kg_{ww}, GA 1.75 mmol/kg_{ww}) was \sim twofold greater than low–low (TA 1.12 mmol/kg_{ww}, GA 0.80 mmol/kg_{ww}). 1.6 g BA/day significantly increased muscle carnosine within 2 weeks and induced continual rises in already augmented muscle carnosine stores (week 4–8, high–low regime). The dose–response showed a carnosine increase of 2.01 mmol/kg_{ww} per 100 g of consumed BA, which was only dependent upon the total accumulated BA consumed (within a daily intake range of 1.6–3.2 g BA/day). Washout rates were gradual (0.18 mmol/kg_{ww}

and 0.43 mmol/kg_{ww}/week; \sim 2%/week). In summary, the absolute increase in muscle carnosine is only dependent upon the total BA consumed and is not dependent upon baseline muscle carnosine, the muscle type, or the daily amount of supplemented BA.

Keywords β -alanine · Carnosine · Muscle · Synthesis · Washout · Dose–response

Introduction

Carnosine has been described since the 1930s as a potent intra-muscular buffer due to its nitrogen containing side imidazole ring, which can directly accept and buffer H^+ ions at a pKa constant of 6.83 (Bate-Smith 1938), thus slowing the decline in pH during intense exercise (Baguet et al. 2010b). Beyond the imperative role that carnosine plays in intra-muscular buffering during high-intensity exercise, a multitude of other physiological roles for carnosine has been demonstrated with in vitro models, including acting as an antioxidant (Boldyrev et al. 1993), a regulator of muscle excitation–contraction coupling via increasing calcium sensitivity (Batrakova and Rubtsov 1997), a source of histidine for histamine synthesis for wound healing (Flancbaum et al. 1990) and protecting proteins against glycation during aging (Hipkiss 2005). The main source of dietary carnosine in humans is via meat consumption (Abe 2000), of which most omnivores consume \sim 50 to 300 mg of carnosine per day (Baguet et al. 2009) and as much as \sim 500 mg if they consume 100 g of turkey. Conversely, it has recently been demonstrated that vegetarians have \sim 22% lower muscle carnosine content (Everaert et al. 2011). Dietary carnosine is rapidly broken down in plasma due to the presence of the hydrolyzing

T. Stellingwerff (✉) · J. Decombaz
Department of Nutrition and Health,
Nestlé Research Center, Nestec Ltd, PO Box 44,
1000 Lausanne 26, Switzerland
e-mail: trent.stellingwerff@rdls.nestle.com

H. Anwander · A. Egger · T. Buehler · R. Kreis · C. Boesch
University of Bern, Bern, Switzerland

enzyme carnosinase (Asatoor et al. 1970), which yields β -alanine (BA) and L-histidine with minimal carnosine detectable in the plasma (Park et al. 2005). In contrast, carnosine is synthesized in human skeletal muscle and cells of the CNS from the essential amino acid L-histidine and the non-proteinogenic amino acid β -alanine (Bakardjiev and Bauer 1994).

Since the concentration of L-histidine in muscle and plasma is high relative to the low intramuscular concentration of BA, which exhibits a much higher K_m for the enzyme carnosine synthetase (Bakardjiev and Bauer 1994), it was hypothesized that BA may be limiting to carnosine synthesis. Supporting this premise, Harris et al. (2006) were the first to show that prolonged BA supplementation (~ 3 to 6 g/day) in humans results in a significant 40–65% increase in muscle carnosine content and have subsequently shown that this can increase high-intensity exercise performance via total work done at 110% of cycling wattage maximum (Hill et al. 2007), which was recently confirmed by Sale et al. (2011). It has previously been shown that when subjects are given a single BA dose of more than 800 mg (corresponding to ~ 10 mg/kg body weight) there are ever increasing paresthesia symptoms (minor “pins and needles”, skin vasodilation, flushing, over ~ 60 to 120 min; Harris et al. 2006). But, the required acute daily BA needed to increase muscle carnosine is \sim tenfold higher than normal dietary intake. Given this, most studies have implemented small repeated daily doses of ≤ 800 mg (as much as 8 individual doses; up to 6.4 g/day) to minimize paraesthesia symptoms (Derave et al. 2007; Hill et al. 2007; Kendrick et al. 2008). Recently, a commercialized slow-release tablet of BA has been produced and it was demonstrated that a single 1.6 g BA dose resulted in a blunting of the peak plasma curve with no reports of any paresthesia symptoms in any subjects (Decombaz et al. 2011; Harris et al. 2008). However, the efficacy of muscle carnosine synthesis with the slow-release BA tablet remains to be investigated.

Recently, there has been considerable interest from the scientific and clinical research communities relating to the impact that augmented muscle carnosine may have on health and sports performance outcomes (for reviews see: Artioli et al. 2010; Derave et al. 2010; Sale et al. 2010), and all previous studies have shown significant increases in muscle carnosine pre to post-BA supplementation (Baguet et al. 2009, 2010a; Derave et al. 2007; Harris et al. 2006; Hill et al. 2007; Kendrick et al. 2008, 2009). However, only one of these previous studies utilized two different BA doses and showed that a total of 89.6 g BA for 4 weeks resulted in a 7.8 mmol/kg dry mass (dm) increase in muscle carnosine, whereas 145.6 g BA for 4 weeks resulted in a 11.1 mmol/kg dm increase (Harris et al. 2006), suggesting some degree of linearity to the dose-response.

Thus, there remains to be a comprehensive dose–response study examining the effect of several BA doses with serial muscle carnosine assessments throughout to clearly delineate the synthesis and wash-out rates in several muscle groups. Furthermore, no studies have yet examined whether a slow-release BA tablet, which circumvents paresthesia symptoms, is also effective in raising muscle carnosine content and only one previous study has examined standardized clinical chemistry measures pre and post prolonged BA supplementation (Harris et al. 2006). Consequently the optimal BA dosing regimen to augment intramuscular carnosine content remains to be clarified. Therefore, this placebo-controlled, double-blind study was designed to compare two different 8 week BA dosing regimens on the time course of muscle carnosine loading and subsequent 8 week washout. Non-invasive ^1H -magnetic resonance spectroscopy (MRS) was utilized to undertake six serial muscle carnosine measures throughout. Our hypotheses were that carnosine synthesis would show a progressive dose–response dependent upon daily BA intake (either 1.6 or 3.2 g/day) with no signs of intramuscular saturation.

Methods

Subjects

Thirty-one healthy male subjects with a body mass index (BMI) > 18 and < 25 kg/m² participated in this study. Subjects were excluded if they had a soy, fish or crustacean allergy, had extremely adverse paresthesia sensitivity to a pure 400 mg β -alanine (BA) acute supplementation (as assessed during the initial visit) and if they were regular consumers of sports foods/supplements in the last 3 months. Furthermore, subjects were also excluded if their baseline muscle carnosine content was > 1 standard deviation above the average baseline muscle carnosine as assessed by preceding measurements combined from a pilot study and the current study (excluded if the average of *gastrocnemius* (GA) and *tibialis anterior* (TA) eventually was > 8.95 mmol/kg_{ww} (kg wet weight)). Altogether, 43 subjects were initially tested, 9 were excluded due to carnosine contents that were > 1 standard deviation above the average baseline, and 3 withdrew during the course of the experiment for scheduling or personal reasons. There were no differences in average age (24.8 ± 4.5 year), weight (76.1 ± 8.0 kg), height (181.2 ± 6.2 cm) or BMI (23.2 ± 1.8 kg/m²) between any of the three experimental groups. An initial lifestyle questionnaire that examined subjects habitual dietary (meat and fish consumption) and exercise routines and baseline muscle carnosine content showed no relationship (correlation between baseline

muscle carnosine and meat consumption ($r = 0.16$) or training/exercise load ($r = 0.11$). All subjects gave their informed consent, and the study was approved by the local Ethics Committee of the Kanton Bern (KEK #117/08), and registered on ClinicalTrials.gov (#NCT 00813553).

Experimental design

This study was designed as a placebo-controlled, double-blind, randomized, parallel-design, single center study with three intervention groups (Fig. 1). The primary purpose was to examine the dose–response of muscle carnosine synthesis to two different β -alanine supplementation regimes compared to placebo over 8 weeks, and subsequent washout (weeks 8–16). Subjects were computer randomized (Trialsys program) into one of 3 supplementation groups as follows:

1. Group high–low ($n = 10$): High dose BA for 4 weeks (3.2 g BA/day), followed by low dose BA for 4 weeks (1.6 g BA/day), followed by 0 g BA/day for 8 weeks.
2. Group low–low ($n = 11$): low dose BA for 8 weeks (1.6 g BA/day), followed by 0 g BA/day for 8 weeks.
3. Group placebo ($n = 10$): 0 g BA/day for 8 weeks, no washout measurements.

As further described below, muscle carnosine and creatine quantification by ^1H -MRS was performed at baseline (week 0) and at weeks 2, 4, 8, 12 and 16 in both GA and TA lower leg muscle groups for the HL and LL groups. After week 8, all ^1H -MRS data were entered into a controlled database prior to knowing what subjects were in the PL group, who did not have any further ^1H -MRS measures made on week 12 or 16. A questionnaire based self-assessment of possible paraesthesia symptoms was conducted during the MRS measurement visits at weeks 0, 2, 4

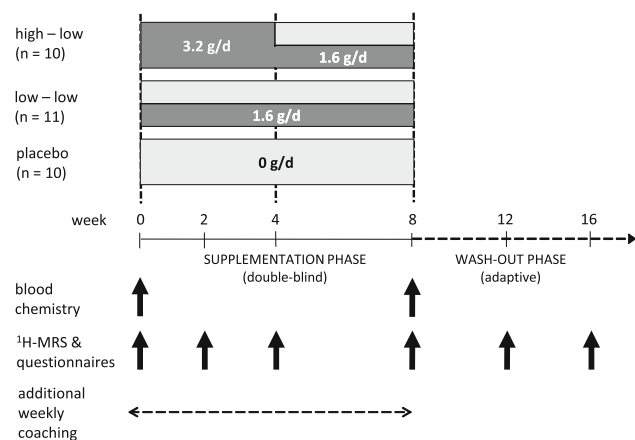


Fig. 1 Schematic representation of study protocol, which was a placebo-controlled, double-blind, randomized, parallel-design, single center study with three groups supplementing either β -alanine or placebo over 8 weeks: (1) high–low; (2) low–low; and (3) placebo

and 8 (Fig. 1). A wide range of standard blood parameters (for full list and lab normal reference values see Table 1) were also assessed by the clinical chemistry laboratory at Inselspital-Bern University Hospital from a 15 ml blood draw at baseline and post-supplementation (week 8). The Inselspital clinical chemistry lab is accredited STS 259 according to the international norm ISO/IEC 17025.

β -alanine and placebo supplements

The BA and the placebo were prepared in two batches in the form of identical $\sim 1,200$ mg tablets by Natural Alternative International, Inc. (NAI). Active or placebo blister packs of tablets were then filled by an external non-study related certified co-packer using blinded study coding lists. Each active tablet contained 800 mg of β -alanine, along with hydroxypropyl, methylcellulose, stearic acid, magnesium stearate and silicon dioxide, in a novel controlled slow-release form. Batch BA purity and individual tablet dose was determined by ion exchange chromatography and quantified using dual wavelength photometric detection following ninhydrin post column derivatization (Biochrom 30, Biochrom Ltd, Cambridge, UK; PEEK Li columns, Laborservice Onken GmbH, D-Gründau), and each tablet was measured to be 92–98% of target theoretical 800 mg dose. All subjects consumed two daily servings of 2-tablets/serving (4 tablets/day) throughout the entire 8 weeks supplementation period with meals. Subjects met with investigators regularly to receive their blister pack of supplements (Fig. 1), and compliance was verbally checked each week and ensured by subjects returning the empty blister packs. Subject's compliance to consuming all required supplements was nearly 100%.

MRS acquisition and spectral fitting

Each subjects planned versus actual visit for their MRS scan was extremely precise, with 91% of MRS scans being achieved on scheduled days ($n = 151$), 97% within 2 days of schedule ($n = 10$), and the rest of the scans achieved within 5 days of scheduled date ($n = 5$). For MRS scheduling/availability, nearly all measurements were done at the same time of the day. As outlined above, a time course of carnosine and creatine concentrations in both TA and GA muscles was measured by ^1H -MRS using a 3 Tesla MR system (TRIO, SIEMENS Erlangen, Germany). Following the acquisition of a localizer series by the body coil for the adjustment of the spectroscopy voxel relative to the tibia plateau, a high-resolution imaging series of the calf (Fast spin echo, echo train 19, TR = 2660 ms, TE 13 ms, slice 4 mm, pixel 0.625 mm \times 0.625 mm) was acquired for the definitive placement of the MRS voxel (Fig. 2a, b). A standard flexible surface coil was used to obtain the

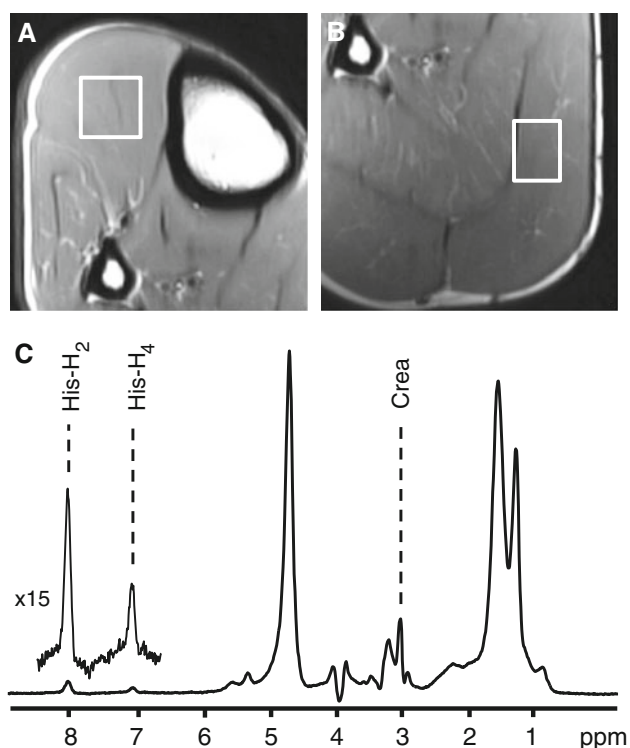


Fig. 2 MR images with localized volume of interest (white box) in *m. tibialis anterior* (a) and *m. gastrocnemius* (b). Image c shows a water-suppressed ^1H -MR spectrum obtained from an $18 \times 18 \times 30 \text{ mm}^3$ voxel located in the *m. tibialis anterior* (male, 22 years). The labeled resonances are Histidine- H_2 (His- H_2 , used for quantification of carnosine), Histidine- H_4 (His- H_4), and central line of the creatine- CH_3 resonance (Crea, triplet due to dipolar coupling)

high-resolution images and subsequent PRESS spectra (“point-resolved-spectroscopy”, TR = 3000 ms, TE = 30 ms). The default voxel size was set to $18 \times 18 \times 30 \text{ mm}$ (Left–Right, Anterior–Posterior, Head–Feet), but was adjusted in LR and AP direction in the case of small TA or GA muscles or fatty infiltrations (Fig. 2a, b). Ninety-six scans with the central frequency at the carnosine- H_2 position (8.0 ppm, PRESS sequence of the vendor adapted) were followed by an unsuppressed water scan ($n = 1$) with the central frequency shifted to the water position to correct for the chemical shift displacement and to acquire exactly the same voxel for the metabolites and the water standard. A second spectrum with a smaller voxel and the central frequency shifted to creatine was acquired at the same position to measure the region between 0.5 and 4.5 ppm. During the measurement, the leg was fixed in all three directions by a home-built fixation device. Quantitation of the carnosine- H_2 and the water resonance was done in jMRUI-3.0 (Naressi et al. 2001) by a batch job with optimized prior knowledge (known relations between resonances and limitations for the fitting process) without human interaction: (1) Removal of the resonances between 0 and 6.0 ppm by a HLSVD process (Hankel-Lanczos

Singular Value Decomposition) (2) Copy of the unsuppressed water resonance multiplied by 0.001 to $-1,000 \text{ Hz}$ from the original position in the spectrum. This resonance was then used to fix the line-width of the carnosine resonances (3) Fitting of the spectra using the AMARES algorithm with the following prior knowledge: line-width carnosine-8 = line-width water * 0.83. This ratio was determined from an unrestricted automatic fit from all spectra. Phase and frequency of the resonances were limited with soft constraints. The carnosine- H_2 (Fig. 2c) resonance at 8.0 ppm was used for quantitation since it is less affected by dipolar coupling, resulting in broadening and apparent T2 shortening, than the carnosine- H_4 resonance (Baguet et al. 2009; Boesch and Kreis 2001; Derave et al. 2007; Ozdemir et al. 2007; Schroder and Bachert 2003). Calculation of absolute carnosine concentrations [$\text{mmol}/\text{kg}_{\text{ww}}$] was based on the unsuppressed water signal and on corrections for the effect of relaxation times (Ozdemir et al. 2007). The central peak of the creatine- CH_3 resonance (Fig. 2c) was quantified without preceding application of HLSVD to estimate relative changes of muscular creatine. The coefficients of variances (CV) were determined previously and in pilot testing, and for carnosine was 8.0% and for creatine to be 12.8% (data not shown).

Paresthesia symptoms questionnaires

Any paresthesia side-effects (e.g., flushing, vasodilation, tingling) and any associated mood-related influences were monitored by a series of questionnaires (Fig. 1). These questionnaires included a body surface symptoms score (SSS), profile of mood states (POMS) and a state anxiety inventory (SAI), and are fully described by Decombaz et al. (2011). The flushing symptoms questionnaire (FSQ) was developed specifically for this study, and was a 10-question retrospective questionnaire focusing on any unusual skin or paresthesia symptoms, and the intensity and duration of symptoms, in the previous 24 h. Questions on “warmth”, “redness”, “pins and needles” and “itching” on a 5-point scale (from none to weak to moderate to strong or extremely strong) were included. The SSS questionnaire was about identifying potential unusual sensations in relation to spatial characteristics on the body surface. It was developed to identify the body site locations most affected by unusual sensations. It consisted of a schematic image of the body, front and back sides, with 23 areas marked by rectangular areas. Subjects were instructed to identify as many areas where symptoms were perceived, or to select the closest rectangle if symptoms fell outside. For POMS, a German adaptation (Albani et al. 2005) of the abridged POMS (Shacham 1983) was used. It consists of 37 descriptors, each belonging to one of 6 different mood states: depression, anxiety-tension, anger-hostility, fatigue-

inertia, confusion, and vigor activity. The Spielberger version of the SAI was used (Spielberger et al. 1983) containing 20 statements of which half comprise positive feelings and half comprise negative feelings. The SAI is the sum of all scores and ranges from 20 to 80. The higher the SAI, the more anxious the subject is.

Statistics

A univariate general model was used to detect an influence of the muscle type and any differences that could have occurred with the arbitrary assignment to the treatment groups. An analysis of covariance (ANCOVA, covariate being the level at week 0) was performed on log-transformed data between treatments at weeks 2, 4, and 8, followed by a post-hoc comparison of the groups with Bonferroni correction. A paired *t* test was used to compare blood clinical chemistry outcomes. For the dose–response analysis, a univariate general linear model (full factorial with “starting levels” as covariate and the factors “muscle”, “treatment regime”, “accumulated BA”, including all interaction terms) was used to detect significant differences for absolute and relative dose response. All statistical analysis was performed with PASW 18.0.0 (SPSS Inc., Chicago, IL, USA). All data are reported as mean \pm standard deviation (SD) with significance assumed at $p < 0.05$, unless otherwise indicated.

Results

Muscle carnosine synthesis and washout

The time course of GA and TA carnosine synthesis and washout are highlighted in Fig. 3a, b, respectively. Baseline carnosine at week 0 was not different between the three groups for either TA (5.75 ± 1.09 mmol/kg_{ww}; range: 3.97–7.48) or GA muscles (8.84 ± 1.54 mmol/kg_{ww}; range: 5.32–11.89), but TA had significantly lower ($p < 0.001$) baseline carnosine than GA. There was no significant increase in muscle carnosine in the placebo trial for either muscle group.

Week 2 Although highly variable, already after 2 weeks, the high–low treatment regime [total of 44.8 g β -alanine (BA)] lead to a significant increase in carnosine in both muscles ($17.4 \pm 9.6\%$ in TA, $p < 0.001$; $9.7 \pm 10.8\%$ in GA, $p = 0.030$). In addition, just 22.4 g of total BA consumed (low–low group) significantly increased carnosine in TA muscle ($11.8 \pm 7.4\%$, $p = 0.005$), and there was a trend for an increase in GA ($8.1 \pm 11.5\%$, $p = 0.082$).

Week 4 During the first 4 week, the low–low group supplemented a total of 44.8 g BA, while high–low group supplemented double that amount (89.6 g BA). Accordingly, there was a \sim twofold greater increase (TA $p = 0.011$ vs. GA $p = 0.030$) in muscle carnosine in both muscle groups for the high–low group (TA 2.04 mmol/kg_{ww} vs. GA 1.75 mmol/kg_{ww} increase) compared to the low–low group (TA 1.12 mmol/kg_{ww} vs. GA 0.80 mmol/kg_{ww} increase).

Week 8 At the end of 8 weeks, low–low resulted in a 21.9 ± 14.4 and $35.5 \pm 13.3\%$ increase in carnosine in TA and GA muscles, respectively. Equally, high–low BA supplementation resulted in a 30.3 ± 14.8 and $44.5 \pm 12.5\%$ increase in carnosine in TA and GA muscles, respectively, which was significantly greater ($p < 0.001$ for each muscle) than placebo. However, differences between the two treatment regimes high–low versus low–low at 8 weeks were no longer statistically significant (GA $p = 0.261$, TA $p = 0.269$).

Washout From weeks 8 to 16, the decay rates were modest and between 0.09 and 0.22 mmol/kg_{ww} per week (~ 2 to 3% of the baseline value per week) with the muscular carnosine levels remaining $\sim 40\%$ of the BA-induced increase after the 8 weeks wash-out period (Fig. 3).

Muscle carnosine dose–response regression analysis and correlations

Given the current study’s design of multiple BA doses and muscle carnosine measures over time, an in-depth dose–response analysis using a univariate general linear model was undertaken examining the absolute (mmol/kg_{ww}; Fig. 4a) and relative (%; Fig. 4b) increase in muscle carnosine content compared to the total grams of BA consumed. Thus, eight separate dose–response analyses could be made (two doses, two muscle groups at weeks 2, 4 and 8). A univariate general model (full factorial model with the covariate “starting levels” and factors “muscle”, “consumed BA dose”, “treatment regime”, and all interaction terms) of the absolute carnosine levels (Fig. 4a) revealed a highly linear dependence with a R^2 of 0.921 and showed that consumed BA dose ($p < 0.001$) and starting carnosine levels ($p < 0.001$) were responsible for $\sim 80\%$ of data variation in absolute carnosine levels. A linear regression of the absolute carnosine increases showed a dose–response of a carnosine increase of 2.01 mmol/kg_{ww}

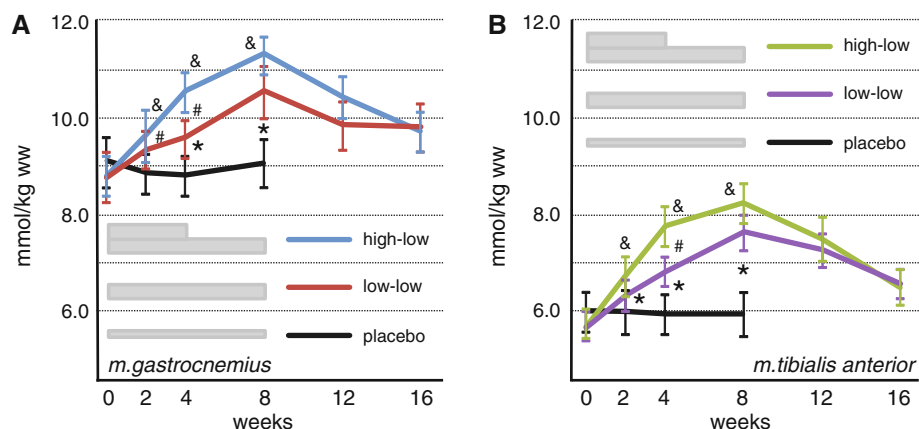


Fig. 3 Synthesis and washout of muscle carnosine concentrations [mmol/kg_{ww}] over time in *m. gastrocnemius* (a) and *m. tibialis anterior* (b) following either β -alanine or placebo over 8 weeks. #low–low

significantly different than placebo, &high–low significantly different than placebo, *low–low significantly different than high–low

per 100 g of consumed BA dose (95% confidence interval 1.83–2.19 mmol/kg_{ww}). From all the other factors, only muscle type showed a tendency to contribute to the dose–response observations, but did not reach significance ($p = 0.055$). In particular, the daily BA treatment regime ($p = 0.941$) was unrelated to the dose–response. In contrast, when the same univariate general model was applied to relative carnosine levels (Fig. 4b), muscle ($p < 0.001$), consumed BA dose ($p < 0.001$), and dose*muscle ($p = 0.004$) were significant while the daily BA treatment regime was still unrelated to the observed dose–response ($p = 0.799$). The differences between the univariate analyses of absolute and relative carnosine increases were due to the fact that there was ~50% more ($p < 0.001$) baseline muscle carnosine in GA versus TA muscle groups (Figs. 3, 5), thus reducing the relative increase in GA.

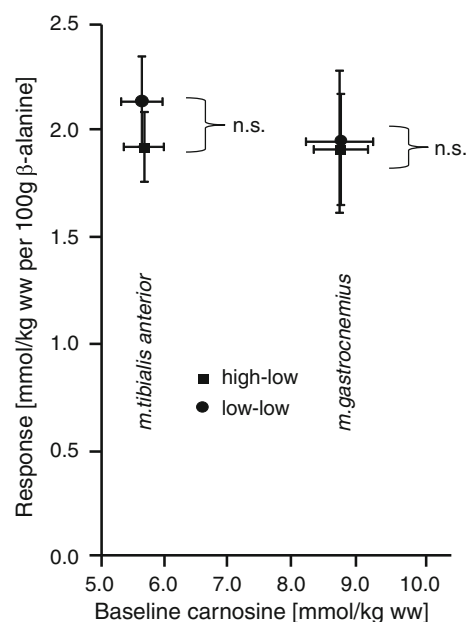


Fig. 5 Average absolute increases in muscle carnosine following two different β -alanine supplementation protocols of either high–low or low–low over 8 weeks in relation to baseline starting muscle carnosine values in *m. gastrocnemius* and *m. tibialis anterior*, respectively. The overlapping error bars indicate that there is neither a difference in carnosine increases between the two treatment regimes nor between the two muscle types

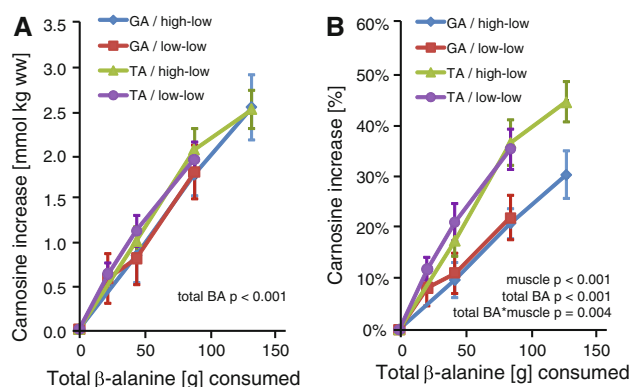


Fig. 4 Dose–response characteristics of β -alanine on the muscle carnosine levels in *gastrocnemius* (GA) and *tibialis anterior* (TA) muscles following two different β -alanine supplementation protocols of either high–low or low–low regime over 8 weeks shown as (a) absolute carnosine increases [mmol/kg_{ww}] and (b) relative carnosine increases (% increase)

Figure 5 shows the average absolute increase in muscle carnosine due to BA supplementation in relation to the baseline pre-BA supplementation muscle carnosine values in both TA and GA muscles. At baseline, GA muscle carnosine was ~3 mmol/kg_{ww} greater ($p < 0.001$) than TA. There was no association between baseline carnosine levels and subsequent muscle carnosine increases with BA supplementation for either muscle group or for the two supplementation regimes ($p = 0.342$ for all data points).

Muscle creatine concentrations

Creatine was also accessed by means of ¹H-MRS (data not shown). There was no treatment or time effect on muscle creatine (central resonance fitted in individual spectra) throughout the entire intervention, as the placebo group had similar values compared to either high–low or low–low.

Blood clinical chemistry

Pre- and post-supplementation analysis of whole blood and plasma parameters for each treatment group revealed no significant effects of time or any treatment (Table 1). At baseline, there were no differences between the groups and when collapsed there were 3.8% of measurements that were outside clinical norms (2.9% above norms, 0.9% below norms). There was no significant difference between treatment groups post-BA supplementation (low–low vs. high–low), and when collapsed together 5.3% of

measurements was outside norms (4.4% above norms, 0.9% below norms), with no significant difference from pre-supplementation ($p = 0.215$). No clear trend was shown and the variations between subjects were larger than any effect of treatment.

Chronic paresthesia symptom and mood assessments

The FSQ and the SSS questionnaires assessed any unusual body surface paresthesia symptoms and the location of the symptoms, respectively, while the POMS and SAI investigated any associated mood/temperament associated with such symptoms. The percentage of unusual sensation via FSQ (ten questions per assessment, with six separate tests, Fig. 1) was generally very low, and even without correction for multiplicity, there was no statistical difference between the groups (16.4, 11.6 and 20.0% reported unusual symptoms for placebo, low–low and high–low, respectively). Of these unusual symptoms, the SSS questionnaire

Table 1 Blood hematology and clinical chemistry for each treatment group pre and post 8 week β -alanine or placebo supplementation

Parameter	Normal ref. range	High–low ($n = 10$)		Low–low ($n = 11$)		Placebo ($n = 10$)	
		PRE	POST	PRE	POST	PRE	POST
Na (mmol/l)	132–142	140.8 ± 1.8	141.2 ± 1.3	141 ± 1.6	141.7 ± 1.7	140.7 ± 1.3	140.6 ± 1.4
K (mmol/l)	3.5–4.7	3.8 ± 0.4	3.8 ± 0.3	3.9 ± 0.1	3.9 ± 0.4	3.8 ± 0.3	3.9 ± 0.3
Creatinine (mol/l)	59–104	81.5 ± 7.6	83.9 ± 13.6	79.6 ± 10.5	80.2 ± 7.3	75.8 ± 8	78.3 ± 8.7
Urea (mmol/l)	2.9–7.7	5.6 ± 0.9	5.9 ± 1.1	5.5 ± 1.4	5.8 ± 1.2	5.5 ± 0.9	5.1 ± 1.0
Total protein (g/L)	60–82	74.4 ± 3.7	76.4 ± 2.3	76.3 ± 2.8	76.5 ± 4.1	75.7 ± 4.2	77.3 ± 3.3
Albumin (g/L)	30–52	43.6 ± 1.9	43.0 ± 3.7	45.5 ± 2.9	43.9 ± 2.7	45.4 ± 3.4	45.7 ± 2.4
Total bilirubin (μmol/L)	3–26	12.0 ± 6.6	12.1 ± 7.2	13.4 ± 9.0	12.8 ± 4.8	8.3 ± 4.4	11.7 ± 6.9
AST (U/L)	10–41	36.9 ± 28.6	39.3 ± 23.4	23.6 ± 3.4	24.7 ± 2.9	31.0 ± 8.8	30.7 ± 9.3
Alkaline phosphatase (U/L)	36–108	67.4 ± 18.8	67.0 ± 19.3	62.3 ± 16.6	62.2 ± 14.3	64.6 ± 16.7	62.6 ± 17.2
Bicarbonate (mmol/l)	22–29	25.0 ± 2.2	25.0 ± 1.4	25.6 ± 1.3	25.8 ± 2.4	24.6 ± 1.8	25.3 ± 2.1
CS (cardiac) troponin (μg/l)	0.00–0.01	0.01 ± 0.00	0.01 ± 0.00	0.01 ± 0.00	0.01 ± 0.00	0.01 ± 0.00	0.01 ± 0.00
Hgb (g/l)	135–168	155.7 ± 7.1	152.5 ± 6.9	152.1 ± 11.2	151.0 ± 11.3	151.3 ± 7.5	152.0 ± 9.7
Hct (% <i>, l/l</i>)	40–50	45 ± 2	45 ± 2	44 ± 3	45 ± 3	44 ± 2	44 ± 2
RBC (T/l)	4.2–5.7	5.1 ± 0.3	5.0 ± 0.2	5.0 ± 0.3	5.0 ± 0.4	5.0 ± 0.3	5.0 ± 0.3
MCV (fl)	80–98	88.2 ± 2.2	88.8 ± 2.3	88.9 ± 2.3	88.8 ± 2.7	89.3 ± 5.1	89.4 ± 4.9
MCH (pg)	27–33	30.4 ± 1.1	30.4 ± 0.8	30.4 ± 1.2	30.3 ± 1.1	30.6 ± 1.6	30.8 ± 2.3
MCHC (g/l)	320–360	343.6 ± 7.5	343.7 ± 6.1	341.5 ± 5.2	340.5 ± 6.4	342.3 ± 3.7	342.7 ± 7.2
WBC (G/l)	3.5–10.5	7.5 ± 1.7	6.5 ± 1.2	6.8 ± 1.3	6.3 ± 1.0	6.8 ± 2.2	6.6 ± 1.5
Neutrophils (G/l)	1.6–7.4	4.3 ± 1.4	3.5 ± 0.8	4.0 ± 1.1	3.8 ± 1.2	3.7 ± 1.6	3.7 ± 1.3
Eosinophils (G/l)	0.02–0.40	0.21 ± 0.18	0.17 ± 0.11	0.16 ± 0.06	0.15 ± 0.06	0.12 ± 0.11	0.16 ± 0.15
Basinophils (G/l)	0.00–0.15	0.04 ± 0.03	0.03 ± 0.01	0.04 ± 0.03	0.04 ± 0.02	0.03 ± 0.01	0.03 ± 0.01
Monocytes (G/l)	0.20–0.93	0.58 ± 0.15	0.55 ± 0.19	0.56 ± 0.12	0.51 ± 0.12	0.54 ± 0.17	0.55 ± 0.13
Lymphocytes (G/l)	1.1–3.5	2.4 ± 0.7	2.2 ± 0.7	2.0 ± 0.4	1.8 ± 0.5	2.3 ± 0.5	2.2 ± 0.4
Platelets(G/l)	140–380	228.1 ± 49.0	215.6 ± 34.5	233.9 ± 87.0	255.8 ± 105.4	249.1 ± 58.3	243.7 ± 32.5
Gamma-Globulin (kU/l)	0–100	72.3 ± 69.6	96.4 ± 124.2	99.7 ± 241.4	84.5 ± 195.0	56.8 ± 45.6	59.1 ± 54.4

All data reported as mean ± SD

Ref reference, AST aspartate-aminotransferase, Hct hematocrit, Hgb hemoglobin, K potassium, MCH mean corpuscular hemoglobin, MCHC mean corpuscular hemoglobin concentration, MCV mean cell volume, Na sodium, RBC blood cell count, WBC white blood cell count

identified that the most frequent symptom location, independent of treatment, was the arms and shoulders. When analyzing the mood questionnaires (POMS and SAI), although minor, the placebo group reported significantly more negative POMS and SAI ratings compared to either treatment (POMS 0.39–0.27; SAI 2.90–3.05), but there was no difference between low–low or high–low treatments. There were no systematic or significant changes in the POMS or SAI ratings across any treatment group throughout the duration of the study.

Discussion

Since this study utilized different β -alanine (BA) doses and multiple muscle carnosine measures over time, it adds significantly to our dose–response understanding of BA supplementation. The key findings are that, within a wide range of total consumed BA used in this study, the absolute increase in muscle carnosine is only dependent upon the total BA consumed, albeit within a daily intake range of 1.6–3.2 g BA/day. Interestingly, it is not dependent upon baseline muscle carnosine, the muscle type, or the daily amount of supplemented BA. In addition, as little as 1.6 g BA/day can significantly increase muscle carnosine stores already within 2 weeks of supplementation and can induce small, but continual, rises in already augmented muscle carnosine stores.

Muscle carnosine dose–response to BA supplementation

In agreement with the current data, every single previous study has demonstrated significant increases in muscle carnosine during a BA supplementation protocol via either quantification of muscle biopsies (Harris et al. 2006; Hill et al. 2007; Kendrick et al. 2008, 2009) or $^1\text{H-MRS}$ analysis (Baguet et al. 2009, 2010a; Derave et al. 2007). However, this is the first study to examine the synthesis and washout of muscle carnosine with two different BA dosing protocols with multiple muscle carnosine assessments over time. Our study design allowed for a univariate test to examine various factors, such as daily BA treatment regimes, muscle types, and their interaction that may influence the extent of intramuscular carnosine accumulation. The univariate general model clearly demonstrates a highly linear dependency ($R^2 = 0.921$) based on the total grams of BA consumed, when either 1.6 or 3.2 g BA/day are consumed. It is shown that 100 g BA increased the absolute carnosine levels by 2.01 mmol/kg_{ww} (95% confidence interval 1.83–2.19 mmol/kg_{ww}). Thus, the absolute carnosine dose–response is solely dependent upon the total grams of BA consumed, and there is no impact on the muscle type or the

daily BA supplementation regime. These findings result in a greatly simplified BA prescriptive application to augment muscle carnosine. Moreover, the continued apparent linearity (or the non-saturation) of this correlation suggests that maximal muscle carnosine levels that are potentially attainable remain to be identified via a long-term (>6 months) BA dosing study. A limitation of this analysis is the fact that a simultaneous wash-out effect during BA intake has not been considered. However, as discussed below, the washout is very slow and thus should not interfere dramatically with the BA loading. In addition, a linear washout as suggested by Baguet et al. (2009) would just reduce the effect of the intake, which would not principally change the statistical model that has been applied.

$^1\text{H-MRS}$ allows for different muscle groups to be analyzed for carnosine to ascertain whether muscles with more fast-twitch (e.g., GA) or slow-twitch (e.g., TA) muscle fiber profiles display a differential response to BA supplementation. Baseline carnosine content has previously been shown to be greater in muscle with a greater proportion of type II fibers (fast-twitch; e.g., GA) as compared to type I [slow-twitch; e.g., TA (Baguet et al. 2009)] or in single fiber quantification from muscle biopsies of the *vastus lateralis* (Dunnnett and Harris 1995; Hill et al. 2007; Kendrick et al. 2009), which is supported by the current data showing baseline GA carnosine content of ~ 9 mmol/kg_{ww} compared to ~ 6 mmol/kg_{ww} for TA (Fig. 3a, b). However, since muscle fiber orientation influences $^1\text{H-MR}$ spectra (see references in Ozdemir et al. 2007), variations of absolute metabolite levels between different muscles have to be interpreted with caution. C2 resonance of carnosine reduces this influence as compared to the C4 signal. The causative explanation for higher muscle carnosine at baseline and post-BA supplementation in muscle dominated by fast-twitch fibers remain to be clarified. However, given that carnosine contributes to intra-muscular buffering (Bate-Smith 1938), it is interesting to note that sprinters and rowers, as compared to marathon runners, not only have a greater percentage of type II fibers but also greater muscle carnosine concentrations, muscle buffering capacity and high-intensity exercise performance (Parkhouse and McKenzie 1984). Nevertheless, our data are in agreement with others (Baguet et al. 2009) in that we demonstrated the same absolute carnosine increase in both TA and GA muscles (~ 2.5 mmol/kg_{ww}; Fig. 4a). This could suggest that there are no fiber type differences in either the BA transporter, changes in transporter expression throughout the supplementation period, and/or differences in muscle carnosine synthase (Bakardjiev and Bauer 1994), as one might then expect a divergence in fiber type specific muscle carnosine synthesis during BA supplementation. However, these mechanism(s) remain to be elucidated.

We also examined whether there was any relationship between baseline carnosine content and the subsequent increase in carnosine due to BA supplementation. Figure 5 shows that there was no statistically detectable effect that lower baseline carnosine levels lead to greater subsequent muscle carnosine increases ($n = 21$). Conversely, Baguet et al. (2010a) found a positive correlation between high baseline muscle carnosine and the increase in muscle carnosine after supplementation [$n = 8$; (Baguet et al. 2010a)]. This difference may be due to some methodological differences of the studies (inclusion of soleus muscle in the Baguet study, exclusion of subjects with high carnosine levels in the current study). Interestingly, muscle creatine increases have been shown to be negatively correlated to high baseline creatine values (Harris et al. 1992), which suggest a saturation, or “muscle full”, response and helps to potentially explain responders and non-responders to creatine supplementation. Even if most of the published data showing increases in muscle carnosine from BA supplementation do not yet appear to show significant carnosine saturation, perhaps by excluding subjects with high-baseline carnosine in the current study we predisposed all subjects to show significantly large increases in muscle carnosine, thus negating any “ceiling effect” of subjects with high-baseline carnosine. Accordingly, until it is determined what the maximal attainable muscle carnosine levels are with prolonged BA supplementation (muscle saturation point), correlations between baseline carnosine and increases in carnosine appear less relevant. Furthermore, whether continually supplementing with BA until a maximal muscle carnosine saturation point is achieved comes with continued increases in high-intensity exercise performance and positive health/clinical outcomes, or whether there are potential negative side-effects, remains to be elucidated.

For the first time, the current study also measured muscle carnosine changes after just 2 weeks of BA supplementation with the lowest daily BA dose (1.6 g BA/day) reported in the literature. Interestingly, both groups of high–low and low–low received the same 1.6 g BA/day from weeks 4 to 8, and both groups showed a very consistent and almost equal continual carnosine increase of ~ 7 and 11% for high–low and low–low, respectively (average for both muscle groups). Therefore, within the range of muscle carnosine contents found within this study (3.91–12.67 mmol/kg_{ww}) at the point when the lower “maintenance” dose was initiated (week 4), the lowest required BA dose to at least maintain augmented muscle carnosine stores appears to be less than the 1.6 g BA/day, as this dose still caused slow, but significant, increases in muscle carnosine from weeks 4 to 8 (Fig. 3a, b). Whether this low daily dose of BA would also maintain even higher levels of muscle carnosine remains to be investigated.

Although highly variable between subjects, already after just 2 weeks, there were small (~ 8 to 12%), but significant increases in muscle carnosine (Fig. 3a, b). Again, these absolute increases were highly linear and dependent upon total grams of BA consumed, but it remains unlikely that these small increases in carnosine could result in a significant performance and/or health benefit.

To our knowledge, this is also the first study to measure increases in muscle carnosine synthesis after subjects consumed a slow-release BA supplement, to eliminate paresthesia symptoms. It has previously been demonstrated that this slow-release tablet of BA results in a blunting of peak plasma BA with similar area under the curve compared to pure BA (Decombaz et al. 2011; Harris et al. 2008). This slow-release BA still reaches plasma concentrations above the BA transporter K_m of ~ 40 μ M (Bakardjiev and Bauer 1994) and thus would be hypothesized to be effective for muscle carnosine synthesis. Accordingly, this study clearly demonstrates that, despite altered plasma pharmacokinetics, slow-release BA is highly efficacious for muscle carnosine synthesis. Correspondingly, our 89.6 and 134.4 g of total supplemented slow-release BA caused carnosine increases of 37 and 45% in TA muscle with high–low dosing protocol, respectively. This is in near agreement with the 40 and 46% increase that Harris et al. (2006) demonstrated with 89.6 and 145.6 g of non slow-release BA, despite the added variability due to different methods for measuring muscle carnosine.

Muscle carnosine washout

This is the second study to examine post-BA muscle carnosine washout kinetics and confirms that once augmented, muscle carnosine appears to be one of the most stable muscle metabolites ever examined (Baguet et al. 2009). Unlike creatine which has a washout of ~ 4 weeks (Hultman et al. 1996), the washout of augmented skeletal muscle carnosine after the termination of BA supplementation is very slow, as the current data show a washout time of ~ 15 to 20 weeks after a ~ 30 to 45% increase in muscle carnosine. These modest decay rates ($\sim 2\%$ /week; between 0.18 and 0.43 mmol/kg_{ww}/week) resulted in muscle carnosine levels that were still $\sim 50\%$ above baseline values after a 4 week washout period (Fig. 3a, b). This washout rate is $\sim 40\%$ slower than the one observed by Baguet et al. (2009), who showed a washout of ~ 2 to 4% per week. Similar to Baguet’s observation of higher carnosine increase with higher baseline levels, this difference may be due to methodological differences of the studies (exclusion of subjects with high carnosine levels in the current study). In addition, the numbers of included subjects (Baguet, $n = 8$, current study, $n = 21$) may be too small to draw far-reaching conclusions. Taken together, both Baguet

et al. (2009) and this study show that once muscle carnosine is increased, any potential performance and/or health benefits resulting from augmented muscle carnosine would appear to be continually realized up to even 4–6 weeks post-supplementation due to the stability of muscle carnosine levels and the slow washout profile.

Muscle creatine

To our knowledge, this is the first study to concurrently assess muscle creatine stores during a chronic BA supplementation protocol, displaying no effect of BA on creatine concentrations, as there were no treatment or time changes throughout the entire intervention. This result is not surprising given that creatine and BA do not share the same skeletal muscle transporter and elicit unique physiological effects. Accordingly, several studies have demonstrated emerging positive performance outcomes when subjects undertook concurrent BA and creatine supplementation (Hoffman et al. 2006; Stout et al. 2006; Zoeller et al. 2007). However, more well-controlled and well-powered performance studies are required to fully ascertain any synergies with these two supplements.

Effect of β -alanine supplementation on blood chemistry and chronic paresthesia symptoms

Despite the recent upsurge of studies involving BA supplementation, only a single previous study has reported routine blood clinical chemistry and hematology measures to assess safety (Harris et al. 2006). The current studies' high–low group consumed a total of 134.4 g of slow-release BA over 8 weeks, while subjects over 4 weeks in the Harris et al. (2006) study consumed a total of 145.6 g BA. Regardless of the dosing protocol, time period or type of BA, both studies demonstrate no significant changes pre- to post, or between placebo or BA groups, in any of the routine blood parameters (Table 1). It has previously been demonstrated that when subjects are acutely supplemented with BA at levels greater than 800 mg/dose it results in moderate to significant paraesthesia (Harris et al. 2006; Hill et al. 2007). Given this, BA supplementation studies have generally utilized small repeated daily doses of ≤ 800 mg doses to minimize paraesthesia symptoms (Derave et al. 2007; Hill et al. 2007; Kendrick et al. 2008). Recently, a commercialized slow-release tablet of BA has been produced and a single acute 1.6 g dose resulted in a blunting of the peak plasma BA curve with no reports of any paraesthesia symptoms (Decombaz et al. 2011; Harris et al. 2008). In accordance, the current study also found no significant paraesthesia effect between treatments when 1.6 g of slow-release BA was given acutely at study

commencement (week 0). However, to our knowledge, not a single study has examined paraesthesia symptoms when BA is chronically supplemented over weeks, while muscle carnosine is concurrently increasing. Cell culture and rodent studies have demonstrated some impact of altering carnosine (β -alanyl-L-histidine) content on total L-histidine, which may impact precursor availability for histamine production and release (Flancbaum et al. 1990; Shen et al. 2008). Thus, it could be hypothesized that changing carnosine content over time might potentially impact upon associated whole-body histamine kinetics and paraesthesia symptoms. However, this study clearly demonstrates no effect of acute or chronic slow-release BA supplementation on paraesthesia symptoms or blood clinical chemistry and hematology measures over 8 weeks. However, long-term studies (>10 weeks) are still needed to definitively know the maximal muscle carnosine contents, and any potential side-effects from long-term BA supplementation.

Conclusion

Similar to creatine (Kley et al. 2011), BA supplementation to augment muscle carnosine is poised for potential application beyond the niche exercise and performance enhancement field and into other prospective roles in myocellular homeostasis and muscular myopathies as well (Derave et al. 2010; Sale et al. 2010). The impressively linear dose-response, which is not dependent upon daily dose (within 1.6–3.2 g/day) or muscle type, is completely dependent on the total amount of consumed BA. The data of this study result in a greatly simplified BA prescriptive application to augment muscle carnosine, which appear remarkably stable post-supplementation. This study also demonstrates that as little as 1.6 g BA/day can be efficacious to increase muscle carnosine, or at the very least maintain augmented carnosine concentrations, in healthy young subjects. Moreover, slow-release BA does not cause acute or chronic paraesthesia or impact upon blood clinical chemistry over 8 weeks. Hence, the current study brings a much improved understanding of the BA dose-response, minimal efficacious dose for carnosine increases, carnosine washout and data to show both acute and chronic safety in the utilization of slow-release BA.

Acknowledgments This study was supported by Nestec Ltd., Vevey, Switzerland and from the Swiss National Science Foundation (#310000-118219). Special acknowledgement go to: Andreas Boss for study support and assistance; Regula Koenig for MR-data analysis assistance; Laurent Parmentier for dermatological tests; Jacques Vuichoud for analytical support in measuring β -alanine in the supplements; Dominik Grathwohl for statistical advice; and Corina Boschat for blinding and preparation of supplements. Some of the authors (TS, JD) are employees of Nestec Ltd, which is a subsidiary

of Nestlé Ltd. and provides professional assistance, research, and consulting services for food, dietary, dietetic, and pharmaceutical products of interest to Nestlé Ltd. No other conflicts of interest were reported.

References

- Abe H (2000) Role of histidine-related compounds as intracellular proton buffering constituents in vertebrate muscle. *Biochemistry (Mosc)* 65:757–765
- Albani C, Blaser G, Geyer M, Schmutzer G, Brähler E, Bailer H et al (2005) Überprüfung der Gütekriterien der deutschen Kurzform des Fragebogens “Profile of Mood States” (POMS) in einer repräsentativen Bevölkerungsstichprobe. *Psychother Psychiatr Med* 55:324–330
- Artioli GG, Gualano B, Smith A, Stout J, Lancha AH Jr (2010) Role of beta-alanine supplementation on muscle carnosine and exercise performance. *Med Sci Sports Exerc* 42:1162–1173
- Asatour AM, Bandoh JK, Lant AF, Milne MD, Navab F (1970) Intestinal absorption of carnosine and its constituent amino acids in man. *Gut* 11:250–254
- Baguet A, Reyngoudt H, Pottier A, Everaert I, Callens S, Achten E et al (2009) Carnosine loading and washout in human skeletal muscles. *J Appl Physiol* 106:837–842
- Baguet A, Bourgeois J, Vanhee L, Achten E, Derave W (2010a) Important role of muscle carnosine in rowing performance. *J Appl Physiol* 109:1096–1101
- Baguet A, Koppo K, Pottier A, Derave W (2010b) Beta-alanine supplementation reduces acidosis but not oxygen uptake response during high-intensity cycling exercise. *Eur J Appl Physiol* 108:495–503
- Bakardjiev A, Bauer K (1994) Transport of beta-alanine and biosynthesis of carnosine by skeletal muscle cells in primary culture. *Eur J Biochem* 225:617–623
- Bate-Smith EC (1938) The buffering of muscle in rigor: protein, phosphate and carnosine. *J Physiol* 92:336–343
- Batrakova MA, Rubtsov AM (1997) Histidine-containing dipeptides as endogenous regulators of the activity of sarcoplasmic reticulum Ca-release channels. *Biochim Biophys Acta* 1324:142–150
- Boesch C, Kreis R (2001) Dipolar coupling and ordering effects observed in magnetic resonance spectra of skeletal muscle. *NMR Biomed* 14:140–148
- Boldyrev AA, Koldobski A, Kurella E, Maltseva V, Stvolinski S (1993) Natural histidine-containing dipeptide carnosine as a potent hydrophilic antioxidant with membrane stabilizing function. A biomedical aspect. *Mol Chem Neuropathol* 19:185–192
- Decombaz J, Beaumont M, Vuichoud J, Bouisset F, Enslin M, Stellingwerff T (2011) The effect of slow-release β -alanine on absorption kinetics and paresthesia (abstract). *Med Sci Sports Exerc* 43:S2224
- Derave W, Ozdemir MS, Harris RC, Pottier A, Reyngoudt H, Koppo K et al (2007) β -Alanine supplementation augments muscle carnosine content and attenuates fatigue during repeated isokinetic contraction bouts in trained sprinters. *J Appl Physiol* 103:1736–1743
- Derave W, Everaert I, Beeckman S, Baguet A (2010) Muscle carnosine metabolism and beta-alanine supplementation in relation to exercise and training. *Sports Med* 40:247–263
- Dunnett M, Harris RC (1995) Carnosine and taurine contents of different fibre types in the middle gluteal muscle of the thoroughbred horse. *Equine Vet J* S18:214–217
- Everaert I, Mooyaart A, Baguet A, Zutinic A, Baelde H, Achten E et al (2011) Vegetarianism, female gender and increasing age, but not CNBDP1 genotype, are associated with reduced muscle carnosine levels in humans. *Amino Acids* 40:1221–1229
- Flanckbaum L, Fitzpatrick JC, Brotman DN, Marcoux AM, Kasziba E, Fisher H (1990) The presence and significance of carnosine in histamine-containing tissues of several mammalian species. *Agents Actions* 31:190–196
- Harris RC, Soderlund K, Hultman E (1992) Elevation of creatine in resting and exercised muscle of normal subjects by creatine supplementation. *Clin Sci* 8:367–374
- Harris RC, Tallon MJ, Dunnett M, Boobis L, Coakley J, Kim HJ et al (2006) The absorption of orally supplied beta-alanine and its effect on muscle carnosine synthesis in human vastus lateralis. *Amino Acids* 30:279–289
- Harris RC, Jones GA, Wise JA (2008) The plasma concentration-time profile of beta-alanine using a controlled-release formulation (Carnosyn) (abstract). *FASEB J* 22:701.9
- Hill CA, Harris RC, Kim HJ, Harris BD, Sale C, Boobis LH et al (2007) Influence of beta-alanine supplementation on skeletal muscle carnosine concentrations and high intensity cycling capacity. *Amino Acids* 32:225–233
- Hipkiss AR (2005) Glycation, ageing and carnosine: are carnivorous diets beneficial? *Mech Ageing Dev* 126:1034–1039
- Hoffman J, Ratamess N, Kang J, Mangine G, Faigenbaum A, Stout J (2006) Effect of creatine and beta-alanine supplementation on performance and endocrine responses in strength/power athletes. *Int J Sport Nutr Exerc Metab* 16:430–446
- Hultman E, Soderlund K, Timmons JA, Cederblad G, Greenhaff PL (1996) Muscle creatine loading in men. *J Appl Physiol* 81:232–237
- Kendrick IP, Harris RC, Kim HJ, Kim CK, Dang VH, Lam TQ et al (2008) The effects of 10 weeks of resistance training combined with beta-alanine supplementation on whole body strength, force production, muscular endurance and body composition. *Amino Acids* 34:547–554
- Kendrick IP, Kim HJ, Harris RC, Kim CK, Dang VH, Lamb TQ et al (2009) The effect of 4 weeks beta-alanine supplementation and isokinetic training on carnosine concentrations in type I and II human skeletal muscle fibres. *Eur J Appl Physiol* 106:131–138
- Kley RA, Tarnopolsky MA, Vorgerd M (2011) Creatine for treating muscle disorders. *Cochrane Database Syst Rev* 2:CD004760
- Naressi A, Couturier C, Devos JM, Janssen M, Mangeat C, de Beer R et al (2001) Java-based graphical user interface for the MRUI quantitation package. *Magma* 12:141–152
- Ozdemir MS, Reyngoudt H, De Deene Y, Sazak HS, Fieremans E, Delputte S et al (2007) Absolute quantification of carnosine in human calf muscle by proton magnetic resonance spectroscopy. *Phys Med Biol* 52:6781–6794
- Park YJ, Volpe SL, Decker EA (2005) Quantitation of carnosine in humans plasma after dietary consumption of beef. *J Agric Food Chem* 53:4736–4739
- Parkhouse WS, McKenzie DC (1984) Possible contribution of skeletal muscle buffers to enhanced anaerobic performance: a brief review. *Med Sci Sports Exerc* 16:328–338
- Sale C, Saunders B, Harris RC (2010) Effect of beta-alanine supplementation on muscle carnosine concentrations and exercise performance. *Amino Acids* 39:321–333
- Sale C, Saunders B, Hudson S, Wise JA, Harris RC, Sunderland CD (2011) Effect of beta-alanine plus sodium bicarbonate on high-intensity cycling capacity. *Med Sci Sports Exerc*. doi: 10.1249/MSS.0b013e3182188501
- Schroder L, Bachert P (2003) Evidence for a dipolar-coupled AM system in carnosine in human calf muscle from in vivo 1H NMR spectroscopy. *J Magn Reson* 164:256–269
- Shacham S (1983) A shortened version of the profile of mood states. *J Pers Assess* 47:305–306

- Shen Y, Zhang S, Fu L, Hu W, Chen Z (2008) Carnosine attenuates mast cell degranulation and histamine release induced by oxygen-glucose deprivation. *Cell Biochem Funct* 26:334–338
- Spielberger CD, Gorsuch RL, Lushene PR, Vagg PR, Jacobs AG (1983) Manual for the state-trait anxiety inventory (Form Y). Consulting Psychologists Press Inc., Palo Alto, CA, p 36
- Stout JR, Cramer JT, Mielke M, O’Kroy J, Torok DJ, Zoeller RF (2006) Effects of twenty-eight days of beta-alanine and creatine monohydrate supplementation on the physical working capacity at neuromuscular fatigue threshold. *J Strength Cond Res* 20:928–931
- Zoeller RF, Stout JR, O’Kroy JA, Torok DJ, Mielke M (2007) Effects of 28 days of beta-alanine and creatine monohydrate supplementation on aerobic power, ventilatory and lactate thresholds, and time to exhaustion. *Amino Acids* 33:505–510

Fructose and Galactose Enhance Postexercise Human Liver Glycogen Synthesis

JACQUES DÉCOMBAZ¹, ROY JENTJENS¹, MICHAEL ITH², EVA SCHEURER², TANIA BUEHLER², ASKER JEUKENDRUP³, and CHRIS BOESCH²

¹Nestlé Research Center, Lausanne, SWITZERLAND; ²Department of Clinical Research, University of Bern, Bern, SWITZERLAND; and ³School of Sport and Exercise Science, University of Birmingham, Birmingham, UNITED KINGDOM

ABSTRACT

DÉCOMBAZ, J., R. JENTJENS, M. ITH, E. SCHEURER, T. BUEHLER, A. JEUKENDRUP, and C. BOESCH. Fructose and Galactose Enhance Postexercise Human Liver Glycogen Synthesis. *Med. Sci. Sports Exerc.*, Vol. 43, No. 10, pp. 1964–1971, 2011. **Purpose:** Both liver and muscle glycogen stores play a fundamental role in exercise and fatigue, but the effect of different CHO sources on liver glycogen synthesis in humans is unclear. The aim was to compare the effect of maltodextrin (MD) drinks containing galactose, fructose, or glucose on postexercise liver glycogen synthesis. **Methods:** In this double-blind, triple crossover, randomized clinical trial, 10 well-trained male cyclists performed three experimental exercise sessions separated by at least 1 wk. After performing a standard exercise protocol to exhaustion, subjects ingested one of three 15% CHO solutions, namely, FRU (MD + fructose, 2:1), GAL (MD + galactose, 2:1), or GLU (MD + glucose, 2:1), each providing 69 g CHO·h⁻¹ during 6.5 h of recovery. Liver glycogen changes were followed using ¹³C magnetic resonance spectroscopy. **Results:** Liver glycogen concentration increased at faster rates with FRU (24 ± 2 mmol·L⁻¹·h⁻¹, *P* < 0.001) and with GAL (28 ± 3 mmol·L⁻¹·h⁻¹, *P* < 0.001) than with GLU (13 ± 2 mmol·L⁻¹·h⁻¹). Liver volumes increased (*P* < 0.001) with FRU (9% ± 2%) and with GAL (10% ± 2%) but not with GLU (2% ± 1%, NS). Net glycogen synthesis appeared linear and was faster with FRU (8.1 ± 0.6 g·h⁻¹, *P* < 0.001) and with GAL (8.6 ± 0.9 g·h⁻¹, *P* < 0.001) than with GLU (3.7 ± 0.5 g·h⁻¹). **Conclusions:** When ingested at a rate designed to saturate intestinal CHO transport systems, MD drinks with added fructose or galactose were twice as effective as MD + glucose in restoring liver glycogen during short-term postexercise recovery. **Key Words:** ¹³C MAGNETIC RESONANCE SPECTROSCOPY, FATIGUE, RECOVERY, NUTRITION

The liver plays a crucial role in preventing hypoglycemia during exercise (27), and it is generally believed that strategies that enhance liver glycogen after exercise will increase exercise capacity in a subsequent exercise bout (6). Most studies have investigated the role of muscle glycogen after exercise (reviewed in Beelen et al. (1) and Jentjens and Jeukendrup (13)), but very few studies have focused on the potentially very important role of the substrates in the liver. Evidence from early rodent studies suggests that when CHO are available after exercise, liver glycogen resynthesis is the first priority and muscle glycogen synthesis is secondary (7). Only one study has investigated liver glycogen synthesis after exercise in healthy humans. In this study, it was found that a single feeding of glucose or fructose (1 g·kg⁻¹ body mass) was sufficient to initiate liver glycogen synthesis after exercise, without affecting muscle glycogen synthesis (6).

Fructose has been shown to have different effects on liver glycogen metabolism than glucose (22). The bulk of an intravenous or oral fructose load is taken up by the liver and converted to glucose (27). However, although gluconeogenesis is markedly increased with fructose ingestion, this does not result in an increased hepatic glucose output, suggesting that fructose could be stimulating hepatic glycogen synthesis, reducing hepatic glycogenolysis, or both. In line with this, small amounts of intraduodenal or intraportally infused fructose given concurrently with a glucose load stimulated the synthesis and storage of liver glycogen and reduced postprandial hyperglycemia and hyperinsulinemia in dogs (32). There is also evidence that small amounts of fructose stimulate glucokinase and glycogen synthase in the liver, the two rate-limiting enzymes of liver glycogen synthesis (22). Combinations of multiple transportable CHO (i.e., glucose and fructose) have also been shown to result in higher exogenous CHO oxidation rates during exercise (14,15,37); for review, see Jeukendrup (16), suggesting better CHO absorption than from a similar amount of glucose only. Very high exogenous CHO oxidation rates were reported for a mixture of maltodextrins and fructose (37). Wallis et al. (36) suggested that this more rapid CHO delivery could also help postexercise muscle glycogen synthesis, but this did not seem to be the case. Muscle glycogen synthesis rates were equally high with maltodextrin–fructose compared with isoenergetic maltodextrin. One explanation could be

Address for correspondence: Chris Boesch, M.D., Ph.D., Department of Clinical Research/AMSM, University of Bern, Pavilion 52A Inselspital, P.O. Box 35, CH-3010 Bern, Switzerland; E-mail: chris.boesch@insel.ch. Submitted for publication September 2010.

Accepted for publication March 2011.

0195-9131/11/4310-1964/0

MEDICINE & SCIENCE IN SPORTS & EXERCISE®

Copyright © 2011 by the American College of Sports Medicine

DOI: 10.1249/MSS.0b013e318218ca5a

that most of the fructose was directed toward liver glycogen synthesis and not muscle glycogen.

Another CHO that could be beneficial for liver glycogen synthesis is galactose. The liver is the major site of galactose uptake and metabolism in humans and galactose clearance from the blood after a galactose load has been used to assess the general functional capacity of this organ. In the liver, galactose can be converted to glucose and subsequently stored as glycogen or immediately released into the circulation. In rats, formation of glycogen accounts for the great majority of galactose taken up by the liver (26). Accordingly, a study with isolated perfused rat liver (34) showed that galactose stimulated liver glycogen synthesis in the presence of glucose with a concomitant increase in the activity of glycogen synthase and a decrease in the activity of glycogen phosphorylase. However, animal and *in vitro* studies (25,38) have shown that the infusion or ingestion of galactose results in lower liver glycogen synthesis rates compared with after the administration of glucose.

Therefore, combinations of glucose with either fructose or galactose could prove to be attractive possibilities when the aim is to amplify liver glycogen resynthesis in humans after a glycogen-depleting exercise. To our knowledge, this has not been done before. However, energy-dense glucose solutions are hypertonic and may interfere with gastrointestinal (GI) fluid delivery. Maltodextrin (MD), a glucose polymer, tastes less sweet than glucose and has a lower osmolality. Because gastric emptying (33) and metabolic availability (30,37) of glucose polymer drinks are not less than for glucose drinks, MD was used for delivering much energy per unit time. In the present work, we used magnetic resonance (MR) techniques, which have made it possible to non-invasively quantify hepatic glycogen metabolism in humans, to investigate the hypothesis that the postexercise ingestion of MD + fructose or MD + galactose results in an enhanced liver glycogen synthesis compared with the ingestion of a matched iso-osmolar and isocaloric MD + glucose control.

METHODS

Subjects. The study was approved by the local ethics committee and conformed to the Declaration of Helsinki. Ten healthy male endurance-trained volunteers gave their written informed consent to participate. They were characterized as follows: height = 184 ± 2 cm, weight = 74 ± 2 kg, age = 29 ± 1 yr, body mass index = 22 ± 1 kg·m⁻², aerobic capacity ($\dot{V}O_{2\max}$) = 64 ± 1 mL·kg⁻¹·min⁻¹, and maximum power (W_{\max}) = 373 ± 14 W (mean \pm SEM).

Study design. This was a double-blind, triple crossover, randomized clinical trial (recruitment started December 1, 2005). After preliminary testing, each subject completed three experimental trials on separate days at least 1 wk apart. After cycling exercise to exhaustion to deplete body glycogen stores, liver glycogen content was evaluated using ¹³C MR spectroscopy (MRS). This was followed by a 6.5-h recovery period in which subjects consumed one of three CHO drinks (Latin square design) containing a combination of two-thirds of maltodextrin (MD) and one-third of fructose (FRU drink), galactose (GAL drink), or glucose (GLU drink). During recovery, liver glycogen was measured approximately every 2 h; blood was collected for analysis of insulin, glucose, and free fatty acids (FFA); and a questionnaire on GI comfort and sensations was administered (details in the “Experimental trials” section and in Fig. 1).

Preliminary testing. Before study commencement, subjects underwent a medical examination where anthropometric measurements were obtained. Subsequently, an aerobic capacity test was performed using a graded exercise protocol to volitional exhaustion on an electromagnetically braked bicycle ergometer (Excalibur Sport; Lode, Groningen, The Netherlands) to evaluate $\dot{V}O_{2\max}$ and W_{\max} , as described elsewhere (37) with the following modifications. The exercise test started at a work intensity of 100 W for 5 min, after which intensity was increased by 30 W every 2 min until the volunteer could no longer maintain the required pedaling frequency (>60 rpm). HR was recorded continuously using

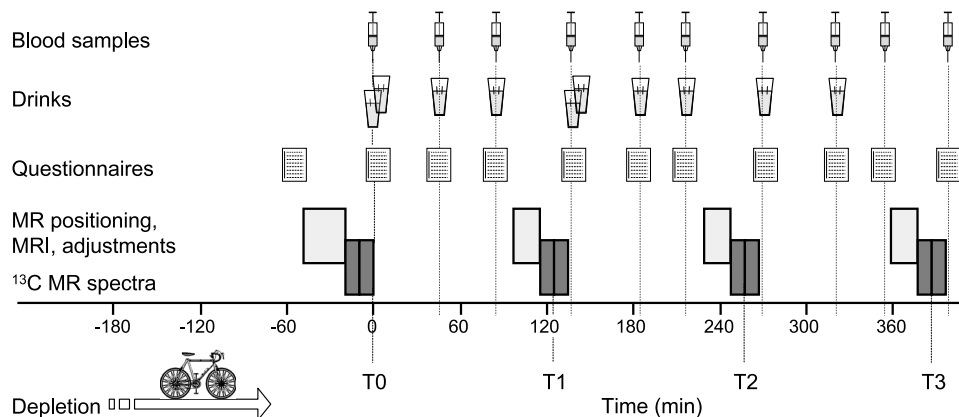


FIGURE 1—Schematic representation of the experiment. The initial depleting exercise was followed by four MR localizer imaging and ¹³C spectroscopy measurements of the liver during recovery at T_0 , T_1 (124 min), T_2 (258 min), and T_3 (392 min). The test drink (one glass = 45 g CHO) was ingested at the time points indicated in the figure. Blood was sampled, and questionnaires on stomach and intestinal sensations were administered in recurring sequences (“Experimental trials” section).

radiotelemetry (Polar Vantage NV; Polar Electro Ltd., Kempele, Finland), whereas oxygen consumption and carbon dioxide production were monitored continuously throughout the test using an online automated gas analysis system (Oxycon Alpha; Jaeger-Toennies, Höchberg, Germany).

Test products. Test drinks were supplied to the experimenter as powder in blinded sachets (one sachet = a 45-g CHO dose). The MD-to-monosaccharide ratio was analyzed in the sample sachets (Nestlé Quality Assurance Laboratory, Croydon, UK) to be 2:1 for each of the FRU, GAL, and GLU mixes. Maltodextrin Glucidex with dextrose equivalent DE12 was obtained from Roquette Frères (Lestrem, France), crystalline fructose Fruiteose S from Galam Ltd. (via Sugro AG, Basel, Switzerland), D-(+)-galactose from Aldrich (Fluka Chemie GmbH, Buchs, Switzerland), and D-(+)-glucose (Roferose ST) from Roquette. On the day of each experimental trial, 10 sachets (450 g) were dissolved in 3 L of water (15% solution) plus some drops of lemon juice to maximize the palatability for each volunteer.

Experimental trials. Subjects kept a dietary and training log 2 d before the first experimental trial. For the subsequent two trials, they were asked to repeat the recorded activities and dietary patterns. In particular, they refrained from strenuous training and had no alcohol consumption the day before a trial. Subjects attended the laboratory in the morning after an overnight fast to undergo a standardized cycling exercise protocol to deplete glycogen stores (19). The exercise started with a 10 min warm-up at 50% W_{max} . Thereafter, the fasted participants cycled for 2-min periods alternating between 90% and 50% W_{max} , until they were no longer able to complete 2 min at 90%. At this point, the high-exercise block was reduced to 80% W_{max} , and the alternating process continued until this intensity could no longer be maintained, after which the high-intensity block was decreased to 70% W_{max} . When the volunteers were no longer able to switch between 70% and 50% at 2-min intervals, they were motivated to maintain the 50% level until complete exhaustion. Water was provided *ad libitum* during the exercise protocol. After exhaustion, participants took a brief shower and returned to the laboratory within 30 min. While supine, a catheter was inserted into an antecubital vein of the forearm to allow for repeated blood sampling. At this time, subjects replied to the questionnaire to evaluate baseline GI sensations. Subsequently, they underwent a basal MR measurement for approximately 45 min (Fig. 1), followed by the initial resting blood sample (7 mL), and the ingestion of the first drink at T_0 (T_0 = zero time). Nine further blood samples and GI questionnaires were collected or administered, respectively, at 45, 85, 140, 185, 220, 275, 320, 355, and 405 min (Fig. 1). The irregular time sequence of blood draws was related to time constraints of the MR measurements because blood sampling could not be done concurrently. T_0 was the time of the end of the baseline MR measurement. For the three subsequent measurements, T_1 (124 min), T_2 (258 min), and T_3 (392 min), the times

were taken half-way during the acquisition of MR spectra (SD = 4 min for the precision of T times).

Beverage ingestion. Test drinks were consumed at the same times as the first eight blood draws (0–320 min). A single dose (45 g, 1 × 300 mL) was given, except at 0 and 135 min, where two doses (2 × 300 mL) were given (Fig. 1). This 2-1-1 schedule was chosen in an attempt to catch up for the time spent in the magnet, where drinking was not possible. Therefore, the effective rate of CHO and fluid intake was 1.5 g·min⁻¹ (90 g·h⁻¹) and 600 mL·h⁻¹ during the first 4 h, but it was 1.15 g·min⁻¹ and 462 mL·h⁻¹ on average during the 6.5-h recovery until the last MR measurement at T_3 .

Magnetic resonance measurements. MR images and ¹H-decoupled natural abundance ¹³C-MR spectra were recorded on a standard 1.5-T GE SIGNA system (General Electric, Milwaukee, WI) equipped with a home-built decoupler console for decoupling and nuclear Overhauser effect build up, as described previously (4,9). The body coil was used to obtain MR images for positioning and volume determination, whereas a double-tuned flexible surface coil (Medical Advance, Milwaukee, WI) was used for ¹³C signal excitation and reception (square surface coil of 11.3 cm × 11.3 cm) and for a localizer ¹H imaging and ¹H decoupling (Helmholtz-type coil, flexible, approximately 16 cm). Volunteers were positioned reproducibly within a few millimeters on an examination bed that had been specifically built for a foregoing study (4) with an analogous acquisition of ¹³C MR spectra in the liver. In addition, the position of the right lower corner of the 12th thoracic vertebra was determined and the relative position of the ¹³C-coil was calculated. In the following sessions, the position of the body was adjusted relative to the right lower edge of the 12th thoracic vertebra. After fixation of the surface coil, one series in axial orientation was repeated to document any change in position during fixation of the surface coil. A typical sequence of spectra is shown in Figure 2.

Quantitation of glycogen. Quantitation of the glycogen signal was obtained in two steps. First, careful positioning of the surface coil helped to obtain the same sensitivity distribution in all sessions for a given subject. Spectra were analyzed using jMRUI (java-based Magnetic Resonance User Interface; http://www.mrui.uab.es/mrui/mrui_Overview.shtml) with the following prior knowledge: fixed position of glycogen, line width relative to the lipid resonances, and two components with different line width (28). Variations of the signal amplification and coil loading were monitored by the simultaneous acquisition from two acetone vials fixed close to the coil center. The acetone resonance showed no systematic variations between volunteers or sessions, such that no correction for coil loading was necessary. The obtained institutional units (IU) are comparable within one volunteer, but they need an individual correction factor depending on the distance between coil and liver. Therefore, in a second step, IU were translated into absolute units (mmol·L⁻¹; 180 g·mol⁻¹) after measuring a 95-mmol·L⁻¹ glycogen solution in a liver-shaped phantom at

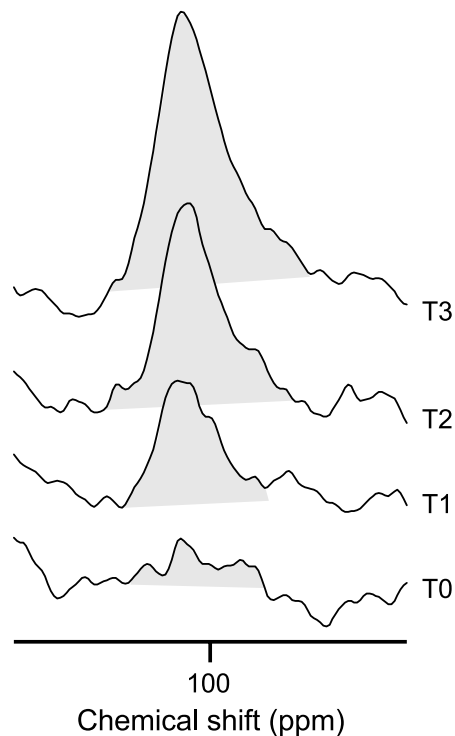


FIGURE 2—Typical sequence of proton-decoupled, natural-abundance ^{13}C spectra obtained by MRS at 1.5 T (8192 scans). Four spectra per session at times T_0 (0 min) to T_3 (392 min) are superimposed and depict the time course of postexercise liver glycogen resynthesis when feeding 450 g CHO during the entire period.

the same distance from the coil center as the liver in the volunteers. These distances had been determined by MRI in volunteers and phantom. Finally, rates of glycogen replenishment during intermediate periods (T_0 to T_1 , T_1 to T_2 , and T_2 to T_3) were calculated after correcting for the individual time intervals between measurements. The glycogen result for one GLU subject at T_2 had to be discarded because of technical problems of the MR scanner.

Quantitation of liver volume. After the acquisition of localizer images, two series of images were taken in axial (13 images, field of view = 40 cm) and coronal (16 images, field of view = 48 cm) directions with a fast-spoiled-gradient sequence (body coil, slice = 8 mm, flip angle = 60° , TE = 1.5 ms, TR = 100 ms, matrix = 512×512). To check for systematic effects of the slice orientation in volume determination, both series were analyzed using a newly developed tool for the evaluation of body composition (5). The determination of liver volumes in the two slice directions showed excellent agreement ($r = 0.957$, slope = 0.88–0.98, 95% confidence interval); therefore, the average of the two measurements was used.

GI questionnaire. The GI questionnaire consisted of 16 questions. Each question started with “Have you suffered from...?” and was answered by ticking a box on a 10-point scale ranging from 1 (*not at all*) to 10 (*very, very much*). Six questions related to upper GI symptoms (general stomach problems, nausea, urge to vomit, belching, heartburn, cramps in the stomach), four questions related to lower GI symptoms

(flatulence, an urge to defecate, cramps in the intestine, diarrhea), and six questions related to central or other symptoms (dizziness, headache, an urge to urinate, a bloated feeling, side aches left, side aches right).

Plasma analysis. Blood was drawn into prechilled tubes and centrifuged. Aliquots of plasma were stored at -20°C until analysis for glucose (enzymatic; Roche Diagnostics, Berthoud, Switzerland) and FFA (enzymatic colorimetric; Wako Bioproducts, Richmond, VA) using an autoanalyzer (XPAND; Dade Behring, Inc., Eschborn, Germany). Plasma insulin was determined by ELISA (IBL; Immuno-Biological Laboratories, Hamburg, Germany). Plasma residues have been used for a metabolomics analysis (published elsewhere) that was not related to the objectives of this study.

Statistics. Statistical analysis of glycogen data was performed with SPSS 18 for Windows (SPSS, Inc., Chicago, IL) using general linear models (GLM), one-sample tests to compare means against zero, and a nonparametric Friedman test to evaluate the responses to the questionnaires on GI sensations. GLM were with fixed factors for treatments, random factors for volunteers, and main interactions. Pairwise comparisons were Bonferroni corrected for multiple tests. Linear regression and the calculation of slopes for determining replenishment rates were performed in Microsoft Excel 2007 (Microsoft Corp., Redmond, WA). One single glycogen result of 120 was missing because of low spectral quality (second postdepletion value for one volunteer with one drink) and was, therefore, not used for the calculation of the slope. A GLM for repeated measures over time was applied to blood concentrations of glucose, insulin, and FFA data, which were log-transformed to achieve approximate normal distribution of the residues. GLM was followed by tests of the within-subject contrasts for treatment \times time. Statistical significance was accepted at $P < 0.05$. The Friedman tests for the 16 questionnaires were Bonferroni corrected such that a significance level of 0.003 was required. Data are presented as means \pm SEM if not stated otherwise.

RESULTS

Glycogen-depleting exercise. The glycogen depletion ride to exhaustion lasted approximately 2 h and was not different between treatments (FRU = 119 ± 2 min, GAL = 116 ± 2 min, and GLU = 118 ± 3 min, NS). The total workload of 1564 kJ (CV = 18%) corresponded to 59% of W_{\max} (CV = 6%) on average (weighted mean of the alternating intensities).

Values at depletion. At exhaustion, the liver glycogen concentration was $99 \text{ mmol}\cdot\text{L}^{-1}$ (CV = 49%), without significant differences between treatments (FRU = $97 \pm 16 \text{ mmol}\cdot\text{L}^{-1}$, GAL = $82 \pm 16 \text{ mmol}\cdot\text{L}^{-1}$, and GLU = $117 \pm 13 \text{ mmol}\cdot\text{L}^{-1}$, NS). Liver volume was 1598 mL (CV = 13%), with a trend ($P = 0.05$) to slight differences between treatments (FRU = 1648 ± 70 mL, GAL = 1540 ± 61 mL, and GLU = 1606 ± 64 mL). Total liver glycogen content before replenishment was 29.2 g (CV = 58%), without

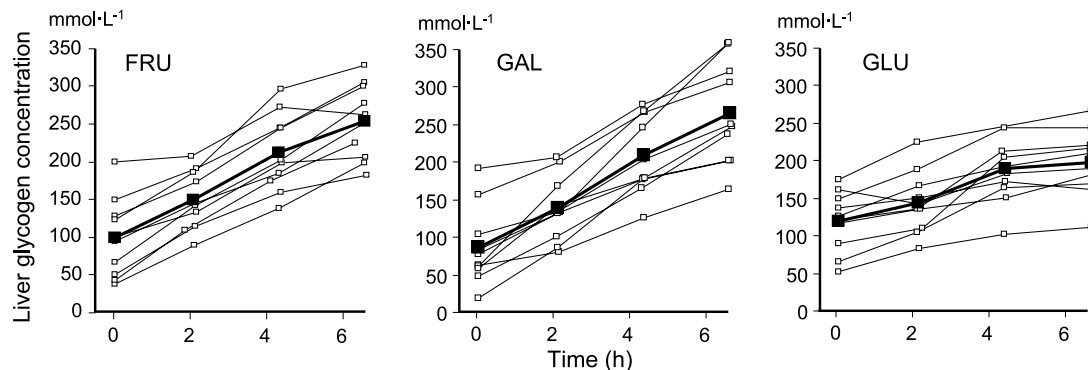


FIGURE 3—Individual liver glycogen concentrations ($\text{mmol}\cdot\text{L}^{-1}$) observed by ^{13}C MRS during postexercise recovery with FRU, GAL, and GLU drinks ($n = 10$). The bold line is the group mean. The GLM indicated a treatment effect ($P < 0.001$). Pairwise comparisons with Bonferroni correction for multiple tests showed significant differences between FRU and GLU ($P < 0.001$) and between GAL and GLU ($P < 0.001$), with concentration changes being slowest after GLU, whereas FRU and GAL were not different (NS).

significant differences between treatments (FRU = 29.6 ± 5.9 g, GAL = 23.6 ± 5.5 g, and GLU = 34.3 ± 4.5 g, NS).

Liver glycogen and volume rates. During recovery, liver glycogen concentration increased consistently in all volunteers (Fig. 3). An analysis of replenishment rates for glycogen concentrations found an overall effect of the treatments ($P < 0.001$) and of the subjects ($P = 0.002$). Furthermore, rates were significantly higher with FRU ($24 \pm 2 \text{ mmol}\cdot\text{L}^{-1}\cdot\text{h}^{-1}$) and GAL ($28 \pm 3 \text{ mmol}\cdot\text{L}^{-1}\cdot\text{h}^{-1}$) compared with GLU ($13 \pm 2 \text{ mmol}\cdot\text{L}^{-1}\cdot\text{h}^{-1}$). Pairwise tests resulted in the following: FRU versus GAL, $P = \text{NS}$; FRU versus GLU, $P < 0.001$; and GAL versus GLU, $P < 0.001$.

Similarly, during replenishment, liver volume significantly increased after FRU ($24 \pm 4 \text{ mL}\cdot\text{h}^{-1}$, $P < 0.001$) and GAL ($22 \pm 3 \text{ mL}\cdot\text{h}^{-1}$, $P < 0.001$), but liver volume remained unchanged after GLU ($3 \pm 3 \text{ mL}\cdot\text{h}^{-1}$, NS; Fig. 4).

Total glycogen content (i.e., glycogen concentrations multiplied by the respective liver volumes) increased significantly after all three drinks (time effect, $P < 0.001$) with FRU ($8.1 \pm 0.6 \text{ g}\cdot\text{h}^{-1}$), GAL ($8.6 \pm 0.9 \text{ g}\cdot\text{h}^{-1}$), and GLU ($3.7 \pm 0.5 \text{ g}\cdot\text{h}^{-1}$) (Fig. 5); however, FRU and GAL led to significantly higher replenishment than GLU (pairwise tests resulted in FRU vs GAL, $P = \text{NS}$; FRU vs GLU, $P < 0.001$;

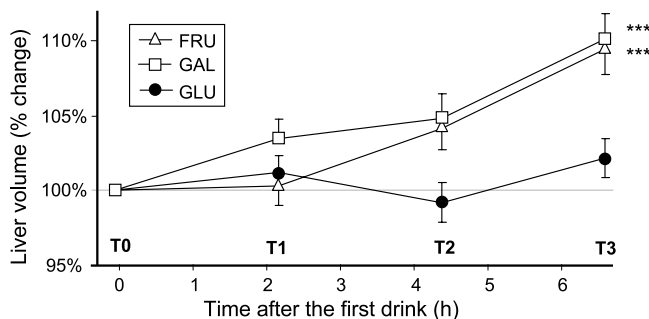


FIGURE 4—Percent change in liver volume determined by MRI at times T_0 to T_3 during postexercise recovery with FRU (triangles), GAL (squares), and GLU (circles) drinks. At the final session (T_3), changes in the liver volumes were different between treatments ($P < 0.001$). Pairwise comparisons with Bonferroni corrections for multiple tests showed increases ($***P < 0.001$) after FRU ($9.5\% \pm 1.7\%$) and after GAL ($10.2\% \pm 1.7\%$) but not after GLU ($2.2\% \pm 1.3\%$, NS). Mean \pm SEM ($n = 10$).

and GAL vs GLU, $P < 0.001$). The increase in liver glycogen content seemed linear for all three treatments for the group averages (FRU $r^2 = 0.964$, GAL $r^2 = 0.976$, GLU $r^2 = 0.886$).

Absolute changes in liver glycogen and volume. The increase in glycogen concentrations within the duration of the experiment (approximately 6.5 h) was significantly different between treatments ($P < 0.001$) and between subjects ($P = 0.005$). The increase was larger after FRU ($154 \pm 14 \text{ mmol}\cdot\text{L}^{-1}$) and GAL ($179 \pm 22 \text{ mmol}\cdot\text{L}^{-1}$) than after GLU ($77 \pm 10 \text{ mmol}\cdot\text{L}^{-1}$). Pairwise tests resulted in the following: FRU versus GAL, $P = \text{NS}$; FRU versus GLU, $P < 0.001$; and GAL versus GLU, $P = 0.001$.

At the end of the recovery period, changes in the liver volumes were significantly different between treatments ($P < 0.001$) and between subjects ($P < 0.001$). An increase occurred after FRU ($153 \pm 27 \text{ mL}$, $P < 0.001$) and GAL ($152 \pm 22 \text{ mL}$, $P < 0.001$) but not after GLU ($35 \pm 21 \text{ mL}$, NS).

The increase in the glycogen content, i.e., differences in glycogen concentrations multiplied by the respective liver

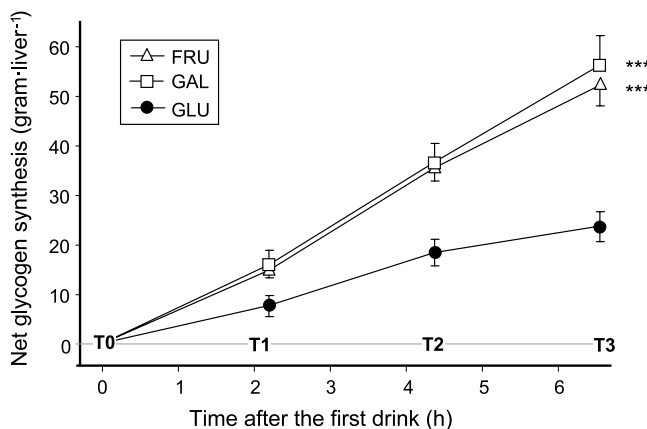


FIGURE 5—Net liver glycogen synthesis (g) determined by MR techniques at times T_0 to T_3 during postexercise recovery with FRU (triangles), GAL (squares), and GLU (circles) drinks. The GLM indicated a treatment effect on rates of gain ($P < 0.001$). Pairwise comparisons with Bonferroni corrections for multiple tests indicated higher rates ($***P < 0.001$) after FRU ($8.1 \pm 0.6 \text{ g}\cdot\text{h}^{-1}$) and after GAL ($8.6 \pm 0.9 \text{ g}\cdot\text{h}^{-1}$) than after GLU ($3.7 \pm 0.5 \text{ g}\cdot\text{h}^{-1}$). Mean \pm SEM ($n = 10$; except for GLU at T_2 , $n = 9$).

volumes, was significantly different between treatments ($P < 0.001$) and between subjects ($P = 0.004$). It reached 52 ± 4 g after FRU and 56 ± 6 g after GAL, as against 23 ± 3 g after GLU.

Plasma variables. Plasma concentrations of glucose and insulin during recovery are shown in Figure 6. In addition to the obvious changes of plasma glucose and plasma insulin with time ($P < 0.001$), the time trends of plasma glucose and insulin were also significantly different for the three treatments (treatment \times time interaction terms, $P < 0.001$, adjusted for sphericity by the Huynh–Feldt correction). A noticeable effect of the treatment was detected by the tests for within-subject contrasts at time 10 ($P < 0.001$) where FRU changed the plasma parameters in 3 of the 10 volunteers significantly. Plasma FFA concentrations decreased in response to CHO ingestion from the resting values (FRU = 0.74 ± 0.15 mmol·L⁻¹, GAL = 0.87 ± 0.05 mmol·L⁻¹, GLU = 0.83 ± 0.05 mmol·L⁻¹) to <0.05 mmol·L⁻¹ at 2 h and onward (time main effect, $P < 0.001$; time \times drink interaction, $P < 0.001$). Tests for within-subject contrasts showed a significant difference at time 10 ($P < 0.001$), with FRU higher than GLU (0.12 ± 0.06 vs 0.01 ± 0.01 mmol·L⁻¹).

Questionnaires. A main effect of the drinks was observed in association with the upper GI tract. Scores during the consumption of GAL were significantly ($P < 0.003$ required to correct for multiple tests) higher than with the

other drinks for general stomach problems ($P = 0.002$), heartburn ($P = 0.001$), and stomach cramps ($P < 0.001$); however, these symptoms remained very modest, with average group maxima not exceeding 1.3 on the 1 to 10 scale at any time point after ingestion of the drinks.

On examination of the time course of the complaints, minor dizziness was reported between exhaustion and consumption of the first drink. Some headaches were observed after exhaustion, which remained stable during the replenishment period, independent of the drinks. The obvious symptom was the occurrence of an urge to urinate, with two peaks coincident with the periods of confinement in the magnet after the consumption of four boluses of a 300-mL drink within 1.5 h (1.2 L).

DISCUSSION

Liver glycogen resynthesis was measured in male cyclists who were fed different CHO mixes during recovery after exhaustive exercise. Our major finding was a doubling of liver glycogen deposition with combinations of MD + fructose or MD + galactose compared with an isoenergetic, iso-osmotic combination of MD + glucose.

Using the biopsy technique, early investigators observed that fructose infusion resulted in greater increases in liver glycogen than glucose (2). More recently using ¹³C MR, Casey et al. (6) fed subjects glucose, sucrose (76 g, one bolus), or a placebo and found only a small net liver glycogen resynthesis during a 4-h period and no difference between glucose and sucrose. The most significant differences between our study and the previous ones (6) are the use of CHO mixes and the larger doses, maximizing the intestinal CHO transport, which resulted in considerable differences in net liver glycogen synthesis rates.

The enhancing effect of FRU on hepatic glycogen synthesis may be partially explained at the level of the intestinal absorption, subsequently to the liver. Postprandially, glucose absorption is increased through the recruitment of the facilitative glucose transporter GLUT2 in addition to the active transporter SGLT1 (18). With the high level of CHO ingestion used in this study (90 g·h⁻¹ in the first 4 h), glucose absorption capacity would have reached saturation (14,17), resulting in submaximal delivery to the liver. In contrast, the intestinal absorption of fructose is GLUT5 dependent and it is readily saturated when fed in isolation, but it is facilitated by the simultaneous ingestion of glucose (35). High consumption (>60 g·h⁻¹) of glucose and fructose blends, which recruit multiple transporters (SGLT1, GLUT2, and GLUT5), have previously been shown to enhance gastric emptying and fluid delivery compared with glucose-only drinks (8,17,31). Accordingly, it could be hypothesized that postexercise CHO delivery to the liver was enhanced with the FRU drink compared with GLU, resulting in increased hepatic glycogen storage. This notion seems to be supported by our observation of unique changes in plasma values with FRU at the final blood draw (85 min after the last drink). Falls in glucose and insulin concentrations (Fig. 6) and the rise in

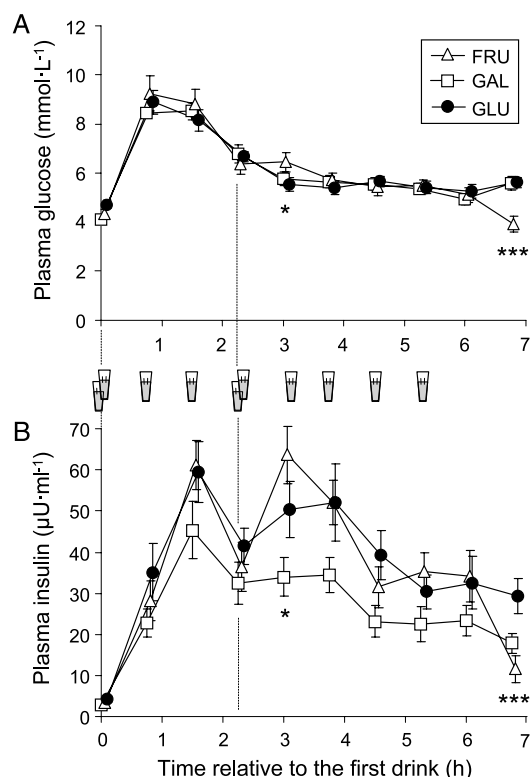


FIGURE 6—Plasma concentrations of glucose (A) and insulin (B) while ingesting one of three drinks during postexercise recovery (one glass = 45 g CHO dose). FRU (triangles), GAL (squares), and GLU (circles). Time points from different series are shifted 3 min apart for better visibility. Within-subjects contrast showed significant differences (treatment \times time, * $P < 0.05$, *** $P < 0.001$). Mean \pm SEM ($n = 10$).

FFA concentration may be the first signals that a post-absorptive situation is reestablishing faster with FRU than with the other blends; however, because this has been observed only in 3 of the 10 volunteers, studies with more subjects would be necessary to confirm this observation.

A factor of potentially larger magnitude in enhancing liver glycogen synthesis is the differential postabsorptive fates of fructose and glucose. Glucose is a relatively poor direct substrate for liver glycogen synthesis (24,27). Much of it is released from the liver into the systemic circulation to be stored as muscle glycogen (3,7). In contrast, fructose is primarily taken up by the liver where it is either phosphorylated and converted to glycogen or metabolized to lactate and pyruvate, which can then be released to the circulation (21). In addition, fructose is a potent acute regulator of liver glucose uptake and glycogen synthesis (29,32) and suppresses net hepatic glycogenolysis (40). Using ^{13}C MR and an euglycemic hyperinsulin clamp, Petersen et al. (29) measured hepatic glycogen synthesis with or without a low-dose fructose infusion ($\sim 40 \text{ mg}\cdot\text{min}^{-1}$) in fasted healthy subjects. These authors observed a threefold increase in the stimulated net rate of hepatic glycogen synthesis with a 13:1 glucose-to-fructose ratio compared with glucose alone (29). This suggests that the amount of fructose that will maximize liver glycogen storage in postexercise feedings lies somewhere between the substantial amount that maximizes intestinal CHO delivery ($>60 \text{ g}\cdot\text{h}^{-1}$) and a catalytic one operating at the hepatic level.

We are not aware of any previous work addressing the role of galactose on quantitative liver glycogen synthesis in humans. This seems to be the first demonstration that replenishment of liver glycogen proceeds twice as fast when one-third of glucose was replaced by galactose in a postexercise CHO drink. Although galactose and glucose are transported equally well by SGLT1 (39), we noticed a slightly higher occurrence of GI problems upstream of the pylorus with GAL (general stomach problems, burns, and cramps) compared with the other drinks. If galactose absorption were competitively inhibited when coingested with glucose (10), a duodenal feedback inhibition (23) could cause upper GI symptoms. Notwithstanding hypothetical absorptive obstacles, hepatic glycogen replenishment was higher with GAL than with GLU, indicating the dominance of hepatic factors over any intestinal limitation. The relatively poor net glycogenic activity reported for galactose when supplied alone has been associated with its weaker insulin stimulation and by urinary galactose loss (25,38). In contrast, our results are consistent with observations of an increased activation of glycogen synthase—in proportion to the rate of infused glucose and independent of insulin—and a decreased glycogen phosphorylase activity when galactose is co-perfused with larger amounts of glucose *in vitro* (34). This suggests that, with GAL, glucose is a major contributor to the neoformed liver glycogen.

Liver size increased during those trials leading to faster glycogen replenishment (FRU and GAL). This enlargement

accounted for a minor fraction ($\sim 9\%$) of glycogen storage, the bulk of the gain being due to liver glycogen concentration changes. Liver volume may change from day to day in relation to exercise, feeding, and hydration, and within a day, a mean diurnal change of 17% in liver size has been reported (20).

In practical exercise and dietary terms, muscle and liver glycogen concentrations may both determine the point of fatigue (11,12). Some information on the relative response of both liver and muscle glycogen replenishment to loading with fructose-containing drinks can be drawn by considering the present study, together with a recent study of muscle glycogen replenishment (36) using comparable study design and subject population during 4 h of recovery. In the study by Wallis et al. (36), recovery drinks were identical with FRU and GLU in the current study, except that free glucose replaced glucose polymers. No significant difference was found in postexercise muscle glycogen accumulation between the CHO treatments (36). Combining the 4-h data of both studies, quantitative estimates of glycogen storage can be derived assuming 10 kg of active muscle mass with a wet-to-dry mass ratio of 4.28 (13). Estimates of whole-body (muscle + liver) glycogen storage amount to 101 g (65 + 36 g) with the fructose-containing drink and 92 g (74 + 18 g) with the glucose-only drink. In other words, whole-body glycogen storage seems to be slightly better when fructose is present.

The effects of these findings on performance are unclear. Of course, hypoglycemia has been described as a possible cause of fatigue during prolonged endurance exercise (12), and hepatic glycogenolysis contributes significantly in the prevention of hypoglycemia. Therefore, having higher liver glycogen stores could be beneficial. CHO drinks containing fructose and galactose could help in situations where athletes have to exercise twice in 1 d with relatively little recovery. Clearly, more research needs to be done to study the possible performance effects as well as to elucidate the underlying mechanisms. Nevertheless, this is the first study in humans to clearly show that CHO blends including fructose and galactose can significantly improve postexercise liver glycogen resynthesis.

In summary, this study demonstrates that ingestion of $\sim 70 \text{ g}\cdot\text{h}^{-1}$ of maltodextrin + fructose (2:1) or maltodextrin + galactose (2:1) drinks consumed during the short-term postexercise recovery results in a twofold increase in the rates of liver glycogen replenishment compared with an isoenergetic, iso-osmotic maltodextrin + glucose control.

The authors thank D. Grathwohl, A. Fracheboud, C. Ammon-Zufferey, A. Blondel-Lubrano, J. Farrar, J.P. Schmid, R. Koenig, E. Schaller, and T. Stellingwerff.

This study was supported by Nestec S.A., Lausanne, Switzerland. The jMRUI software package was kindly provided by the participants of the EU Network programs: Human Capital and Mobility (CHRX-CT94-0432) and Training and Mobility of Researchers (ERBFMRX-CT970160). Part of the salaries were funded by an SNF grant (310000-118219).

The study was instigated and financed by Nestec. J.D. and R.J. were employees of Nestec.

None of the authors had a conflict of interest to declare.

The results of the present study do not constitute endorsement by the American College of Sports Medicine.

REFERENCES

1. Beelen M, Burke LM, Gibala MJ, van Loon LJ. Nutritional strategies to promote postexercise recovery. *Int J Sport Nutr Exerc Metab.* 2010;20(6):515–32.
2. Bergstrom J, Furst P, Gallyas F, et al. Aspects of fructose metabolism in normal man. *Acta Med Scand Suppl.* 1972;542:57–64.
3. Blom PC, Hostmark AT, Vaage O, Kardel KR, Maehlum S. Effect of different post-exercise sugar diets on the rate of muscle glycogen synthesis. *Med Sci Sports Exerc.* 1987;19(5):491–6.
4. Boesch C, Ith M, Jung B, et al. Effect of oral D-tagatose on liver volume and hepatic glycogen accumulation in healthy male volunteers. *Regul Toxicol Pharmacol.* 2001;33(2):257–67.
5. Buehler T, Ramseier N, Machann J, Schwenzler N, Boesch C. Determination of body compartments at 1.5 and 3 Tesla, combining three volume estimation methods (abstract). *Proc Intl Soc Magn Reson Med.* 2010;18:2915.
6. Casey A, Mann R, Banister K, et al. Effect of carbohydrate ingestion on glycogen resynthesis in human liver and skeletal muscle, measured by ^{13}C MRS. *Am J Physiol Endocrinol Metab.* 2000;278(1):E65–75.
7. Conlee RK, Lawler RM, Ross PE. Effects of glucose or fructose feeding on glycogen repletion in muscle and liver after exercise or fasting. *Ann Nutr Metab.* 1987;31(2):126–32.
8. Currell K, Urch J, Cerri E, Jentjens RL, Blannin AK, Jeukendrup AE. Plasma deuterium oxide accumulation following ingestion of different carbohydrate beverages. *Appl Physiol Nutr Metab.* 2008;33(6):1067–72.
9. Fluck CE, Slotboom J, Nuoffer JM, Kreis R, Boesch C, Mullis PE. Normal hepatic glycogen storage after fasting and feeding in children and adolescents with type 1 diabetes. *Pediatr Diabetes.* 2003;4(2):70–6.
10. Holdsworth CD, Dawson AM. The absorption of monosaccharides in man. *Clin Sci.* 1964;27:371–9.
11. Hultman E, Bergstrom J. Muscle glycogen synthesis in relation to diet studied in normal subjects. *Acta Med Scand.* 1967;182(1):109–17.
12. Hultman E, Nilsson LH. Liver glycogen as a glucose-supplying source during exercise. In: Keul E, editor. *Limiting Factors of Physical Performance.* Stuttgart (Germany): Georg Thieme Publ; 1973. p. 179–89.
13. Jentjens R, Jeukendrup A. Determinants of post-exercise glycogen synthesis during short-term recovery. *Sports Med.* 2003;33(2):117–44.
14. Jentjens RL, Jeukendrup AE. High rates of exogenous carbohydrate oxidation from a mixture of glucose and fructose ingested during prolonged cycling exercise. *Br J Nutr.* 2005;93(4):485–92.
15. Jentjens RL, Moseley L, Waring RH, Harding LK, Jeukendrup AE. Oxidation of combined ingestion of glucose and fructose during exercise. *J Appl Physiol.* 2004;96(4):1277–84.
16. Jeukendrup AE. Carbohydrate and exercise performance: the role of multiple transportable carbohydrates. *Curr Opin Clin Nutr Metab Care.* 2010;13(4):452–7.
17. Jeukendrup AE, Moseley L. Multiple transportable carbohydrates enhance gastric emptying and fluid delivery. *Scand J Med Sci Sports.* 2008;20(1):112–21.
18. Kellett GL, Brot-Laroche E, Mace OJ, Leturque A. Sugar absorption in the intestine: the role of GLUT2. *Annu Rev Nutr.* 2008;28:35–54.
19. Kuipers H, Keizer HA, Brouns F, Saris WH. Carbohydrate feeding and glycogen synthesis during exercise in man. *Pflugers Arch.* 1987;410(6):652–6.
20. Leung NW, Farrant P, Peters TJ. Liver volume measurement by ultrasonography in normal subjects and alcoholic patients. *J Hepatol.* 1986;2(2):157–64.
21. Mayes PA. Intermediary metabolism of fructose. *Am J Clin Nutr.* 1993;58(5 suppl):754–65S.
22. McGuinness OP, Cherrington AD. Effects of fructose on hepatic glucose metabolism. *Curr Opin Clin Nutr Metab Care.* 2003;6(4):441–8.
23. Moran TH, McHugh PR. Distinctions among three sugars in their effects on gastric emptying and satiety. *Am J Physiol.* 1981;241(1):R25–30.
24. Newgard CB, Hirsch LJ, Foster DW, McGarry JD. Studies on the mechanism by which exogenous glucose is converted into liver glycogen in the rat: a direct or an indirect pathway? *J Biol Chem.* 1983;258(13):8046–52.
25. Niewoehner CB, Neil B. Mechanism of delayed hepatic glycogen synthesis after an oral galactose load vs. an oral glucose load in adult rats. *Am J Physiol.* 1992;263(1 pt 1):E42–9.
26. Niewoehner CB, Neil B, Martin T. Hepatic uptake and metabolism of oral galactose in adult fasted rats. *Am J Physiol.* 1990;259(6 pt 1):E804–13.
27. Nilsson LH, Hultman E. Liver and muscle glycogen in man after glucose and fructose infusion. *Scand J Clin Lab Invest.* 1974;33(1):5–10.
28. Overloop K, Van Hecke P, Vanstapel F, et al. Evaluation of signal processing methods for the quantification of a multi-exponential signal: the glycogen ^{13}C - ^1H NMR signal. *NMR Biomed.* 1996;9(7):315–21.
29. Petersen KF, Laurent D, Yu C, Cline GW, Shulman GI. Stimulating effects of low-dose fructose on insulin-stimulated hepatic glycogen synthesis in humans. *Diabetes.* 2001;50(6):1263–8.
30. Rowlands DS, Wallis GA, Shaw C, Jentjens RL, Jeukendrup AE. Glucose polymer molecular weight does not affect exogenous carbohydrate oxidation. *Med Sci Sports Exerc.* 2005;37(9):1510–6.
31. Shi X, Summers RW, Schedl HP, Flanagan SW, Chang R, Gisolfi CV. Effects of carbohydrate type and concentration and solution osmolality on water absorption. *Med Sci Sports Exerc.* 1995;27(12):1607–15.
32. Shiota M, Moore MC, Galassetti P, et al. Inclusion of low amounts of fructose with an intraduodenal glucose load markedly reduces postprandial hyperglycemia and hyperinsulinemia in the conscious dog. *Diabetes.* 2002;51(2):469–78.
33. Sole CC, Noakes TD. Faster gastric emptying for glucose-polymer and fructose solutions than for glucose in humans. *Eur J Appl Physiol Occup Physiol.* 1989;58(6):605–12.
34. Sparks JW, Lynch A, Glinsmann WH. Regulation of rat liver glycogen synthesis and activities of glycogen cycle enzymes by glucose and galactose. *Metabolism.* 1976;25(1):47–55.
35. Truswell AS, Seach JM, Thorburn AW. Incomplete absorption of pure fructose in healthy subjects and the facilitating effect of glucose. *Am J Clin Nutr.* 1988;48(6):1424–30.
36. Wallis GA, Hulston CJ, Mann CH, Roper HP, Tipton KD, Jeukendrup AE. Postexercise muscle glycogen synthesis with combined glucose and fructose ingestion. *Med Sci Sports Exerc.* 2008;40(10):1789–94.
37. Wallis GA, Rowlands DS, Shaw C, Jentjens RL, Jeukendrup AE. Oxidation of combined ingestion of maltodextrins and fructose during exercise. *Med Sci Sports Exerc.* 2005;37(3):426–32.
38. Williams CA. Metabolism of lactose and galactose in man. *Prog Biochem Pharmacol.* 1986;21:219–47.
39. Wright EM, Hirayama BA, Loo DF. Active sugar transport in health and disease. *J Intern Med.* 2007;261(1):32–43.
40. Youn JH, Kaslow HR, Bergman RN. Fructose effect to suppress hepatic glycogen degradation. *J Biol Chem.* 1987;262(24):11470–7.



Original Article

Effects of a whey protein supplementation on intrahepatocellular lipids in obese female patients

Murielle Bortolotti^{a,d}, Elena Maiolo^{a,d}, Mattia Corazza^{a,d}, Eveline Van Dijke^{a,d}, Philippe Schneider^{a,e}, Andreas Boss^{b,f}, Guillaume Carrel^{a,e}, Vittorio Giusti^{c,g}, Kim-Anne Lê^{a,h}, Daniel Guee Quo Chong^{b,f}, Tania Buehler^{b,f}, Roland Kreis^{b,f}, Chris Boesch^{b,f}, Luc Tappy^{a,c,*}

^a Department of Physiology, University of Lausanne, 7, rue du Bugnon, 1005 Lausanne, Switzerland

^b Department of Clinical Research/AMSM, University of Bern, Pavilion 52A, Inselspital, P.O. Box 35, 3010 Bern, Switzerland

^c Service of Endocrinology, Diabetes and Metabolism, CHUV, 1011 Lausanne, Switzerland

ARTICLE INFO

Article history:

Received 21 June 2010

Accepted 9 January 2011

Keywords:

Dietary proteins

Non-alcoholic fatty liver disease

Glucose tolerance

Obesity

SUMMARY

Background & aims: High protein diets have been shown to improve hepatic steatosis in rodent models and in high-fat fed humans. We therefore evaluated the effects of a protein supplementation on intrahepatocellular lipids (IHCL), and fasting plasma triglycerides in obese non diabetic women.

Methods: Eleven obese women received a 60 g/day whey protein supplement (WPS) for 4-weeks, while otherwise nourished on a spontaneous diet, IHCL concentrations, visceral body fat, total liver volume (MR), fasting total-triglyceride and cholesterol concentrations, glucose tolerance (standard 75 g OGTT), insulin sensitivity (HOMA IS index), creatinine clearance, blood pressure and body composition (bioimpedance analysis) were assessed before and after 4-week WPS.

Results: IHCL were positively correlated with visceral fat and total liver volume at inclusion. WPS decreased significantly IHCL by $20.8 \pm 7.7\%$, fasting total TG by $15 \pm 6.9\%$, and total cholesterol by $7.3 \pm 2.7\%$. WPS slightly increased fat free mass from 54.8 ± 2.2 kg to 56.7 ± 2.5 kg, $p = 0.005$). Visceral fat, total liver volume, glucose tolerance, creatinine clearance and insulin sensitivity were not changed.

Conclusions: WPS improves hepatic steatosis and plasma lipid profiles in obese non diabetic patients, without adverse effects on glucose tolerance or creatinine clearance.

Trial Number: NCT00870077, ClinicalTrials.gov

© 2011 Elsevier Ltd and European Society for Clinical Nutrition and Metabolism. All rights reserved.

Abbreviations: IHCL, intrahepatocellular lipids; WPS, whey protein supplementation; MR, Magnetic Resonance; ¹H-MRS, ¹H- Magnetic Resonance Spectroscopy; NAFLD, non-alcoholic fatty liver disease; OGTT, oral glucose tolerance test; HOMA, homeostasis assessment model; HOMA IS, HOMA of insulin sensitivity; NEFA, non esterified fatty acids; BOHB, beta-hydroxybutyrate.

* Corresponding author. Department of Physiology, University of Lausanne, 7, rue du Bugnon, 1005 Lausanne, Switzerland. Tel.: +41 21 692 55 41; fax: +41 21 692 55 95.

E-mail addresses: murielle.bortolotti@unil.ch (M. Bortolotti), elena.maiolo@unil.ch (E. Maiolo), mattia.corazza@unil.ch (M. Corazza), eveline_86@hotmail.com (E. Van Dijke), philippe.schneider@unil.ch (P. Schneider), andreas.boss@insel.ch (A. Boss), guillaume.carrel@unil.ch (G. Carrel), vittorio.giusti@chuv.ch (V. Giusti), kimannel@usc.edu (K.-A. Lê), daniel.chong@insel.ch (D.G. Quo Chong), tania.buehler@insel.ch (T. Buehler), roland.kreis@insel.ch (R. Kreis), chris.boesch@insel.ch (C. Boesch), luc.tappy@unil.ch (L. Tappy).

^d Tel.: +41 21 692 55 68; fax: +41 21 692 55 95.

^e Tel.: +41 21 692 55 69; fax: +41 21 692 55 95.

^f Tel.: +41 31 632 8174; fax: +41 31 632 0580.

^g Tel.: +41 21 31 40 642; fax: +41 21 314 43 10.

^h Childhood Obesity Research Center, University of Southern California, 2250 Alcazar Street, CSC #200, Los Angeles, CA 90089. Tel.: +1 323 442 1506.

1. Introduction

Non-alcoholic fatty liver disease (NAFLD) is characterized by an elevated intrahepatocellular lipid (IHCL) concentration. Incidence of NAFLD is frequently increased in obese patients, and is considered as the hepatic component of the metabolic syndrome. It is tightly associated with the metabolic complications of obesity, i.e. insulin resistance, impaired glucose tolerance, and dyslipidemia.^{1,2}

Several reports suggest that a high protein intake may improve NAFLD. In high-fat fed rats, increasing the proportion of protein in the diet reduced hepatic steatosis and dyslipidemia.^{3,4} In healthy human male subjects in whom IHCL concentrations had been nearly doubled by a 4-day hypercaloric, high-fat feeding, increasing the dietary protein intake reduced significantly IHCL concentration.⁵ These observations suggest that a high protein intake may exert beneficial effects in NAFLD patients. We therefore hypothesized that increasing the dietary protein intake in the same range as that which reduced IHCL in high-fat fed subjects⁵ would also reduce IHCL concentrations in obese patients. To evaluate this

hypothesis, we assessed the effects of a 4-week supplementation with 60 g/day whey protein (Whey Protein Supplement : WPS) in obese non diabetic female patients.

2. Research design and method

2.1. Participants

11 obese female patients, aged 38 ± 2 years, were recruited at the obesity clinics of the Centre Hospitalier Universitaire Vaudois (CHUV), Lausanne, Switzerland. They had a mean body weight of 99.7 ± 5.3 kg, a mean height of 1.63 ± 0.02 m, and a mean BMI of 37.6 ± 1.8 kg/m². None had liver or renal disease, nor was on antidiabetic or antilipemic agents. They were sedentary (less than two sessions of physical activity per week). All reported a daily alcohol intake less than 20 g. The experimental protocol was approved by the Ethical Committee of Lausanne University School of Medicine and was registered at ClinicalTrials.gov (Trial Number: NCT00870077, ClinicalTrials.gov). Subjects gave their written informed consent before participating in the study.

2.2. Study design

After inclusion, subjects reported in the morning after an overnight fast to the Cardiomet Clinical Investigation Center (Cardiomet CIC) of the Lausanne University Hospital. Their body weight and blood pressure were measured and their body composition was assessed by bioelectrical impedance analysis. Thereafter, they underwent a standard 75 g oral glucose tolerance test (OGTT) with measurement of plasma glucose and insulin at time 0 and 120 min. Fasting plasma triglycerides, total cholesterol, HDL cholesterol, urea, creatinine, ASAT, ALAT and urinary urea and creatinine concentrations were assessed using a bench-top clinical chemistry analyzer (RX Monza, Randox Laboratories Ltd, Crumlin, UK). Plasma insulin and glucagon were measured by radio-immuno assays using kits from Millipore, St Charles, Missouri, USA). A 24 h urine collection was obtained for determination of urea and creatinine excretion. Total nitrogen excretion was calculated assuming that urea accounted for 85% of total urinary nitrogen and that extra-renal nitrogen losses were 2 g/day. Total energy expenditure and net substrate oxidation rates were measured during 45 min before and over the 120 min after oral glucose ingestion by indirect calorimetry (Deltatrack II, Datex Instruments, Helsinki, Finland).

On the following day, intrahepatocellular lipids (IHCL), visceral fat volume, and total liver volume were measured by clinical Magnetic Resonance (MR) methods at the Department of Clinical Research of University Bern.

IHCL content was determined by ¹H MR spectroscopy (MRS) on a clinical 3 T MR system (TIM Trio, Siemens Medical, Germany) using the whole body coil for excitation. A volume of interest ($2.5 \times 2.5 \times 3$ cm³) was localized in the liver using the body array surface coils for signal detection and a double echo localization sequence combined with Siemens' 2D "prospective acquisition correction".

(PACE) scheme,⁶ based on a 2D gradient echo image to monitor the position of the diaphragm for triggering in expiration (MRS echo time TE 30 ms, TR according to the breathing cycle between 2.5 and 6 s, 4000 Hz spectral width, 2048 data points). MRS was preceded by fast spin echo MRI (HASTE [Half Fourier Acquisition Single Shot Turbo Spin Echo], echo time 89 ms, repetition time 1030 ms, flip angle 150°, nominal resolution $1.7 \times 1.3 \times 5$ mm³) in three planes using the same PACE triggering to visualize the liver and to reliably reproduce the placement of the ROI in follow-up examinations. The ROI was placed evading large vessels and proximity to extrahepatic fat. The magnetic field distribution over the ROI was optimized in

breath-hold using the manufacturers automated gradient shim routine. For choice of proper flip angle, a B₁ mapping scan was recorded in expiration prior to MRS. MR spectra were recorded with water presaturation to determine the lipid and metabolite spectra (32 acquisitions, 60 Hz suppression bandwidth, center frequency at 3 ppm) and without water suppression to acquire the water signal as internal standard (16 scans, center frequency at 4.7 ppm). Automatic fitting of the MR spectra was performed with the home-written software FiTAID allowing for the use of Voigt lines and implementation of prior knowledge restraints.⁷ The lipid spectrum was modeled using 9 Voigt lines to describe all spectral components and initial model optimizations based on an average spectrum from several subjects, further 5 lines were used to cover the metabolites and residual water. Absolute quantification was performed in analogy to Bortolotti et al⁵ and was based on the peak areas of the methylene protons that are not neighbors of an allylic or carboxylic carbon, basic assumptions on lipid composition, the water peak area from non-water-suppressed scans, an assumed liver water content and relaxation corrections based on literature values.⁸ Results were expressed as volume percentage of lipid.

Volumes of the liver and visceral adipose tissue (VAT) were determined using T₁-weighted images of the abdomen, recorded in breath-hold (multi-spin-echo technique, echo train length 7, echo spacing 7.6 ms, repetition time 452 ms, echo time 38 ms, flip angle 130°, 30 axial slices in 6 slabs covering the pelvis at the lower end and the diaphragm at the upper end, slice thickness of 10 mm, gap between slices 10 mm, 5 slices per breath-hold sequence, acquisition matrix 256 × 147 with a resolution of 2 mm/pixel, body coil was used for excitation and signal acquisition). Volumetry was performed using a semi-automatic implementation of the point counting method, which represents a sparse sampling scheme whereby an operator accepts or rejects points from a regular grid that covers the targeted anatomic structure in a random orientation.⁹ Visceral fat was counted on images between pelvis and the upper end of the diaphragm.

After these initial measurements, WPS was provided as bags containing 20 g of commercialized whey protein (WheyProtein94[®], Sponser, Wollerau, Switzerland), with instructions to consume the content of one bag diluted into 300 ml water 30 min before breakfast, lunch and dinner. Total WPS supplementation amounted to 60 g/day. Their food and drink intake was otherwise left *ad libitum*. The study was performed as an open label, unblinded, uncontrolled study.

1, 2 and 3 weeks after the beginning of WPS, volunteers returned to the cardiomet CIC and fasting blood sample was obtained for the measurement of plasma triglycerides, total cholesterol, HDL cholesterol, urea, creatinine, ASAT, ALAT and glycemia. 24-h urine collections were also obtained to measure urea and creatinine excretion. Compliance to WPS was assessed by collecting the empty supplementation bags.

After 4-weeks WPS, all measurements performed at inclusion, OGTT and MR determination of IHCL, visceral fat volume, and liver volume were repeated.

2.3. Analytic procedures

After collection, blood and urine samples were sent to the Central Laboratory of CHUV for measurements of fasting plasma total- triglycerides, total cholesterol, HDL cholesterol, urea, creatinine, ASAT, ALAT and 24 h urea and creatinine excretion. For the other blood parameters, blood was centrifuged at 4 °C for 10 min, at 3600 rpm, and plasma were stored at -20 °C/-80 °C until further analysis. Glucose concentrations were measured by the glucose oxidase method with a Beckman Glucose Analyzer II (Beckmann Glucose Analyzer II, Beckmann Instruments, Fullerton, CA). Plasma

Table 1
Characteristics of subjects before and after one month of WPS.

	BASELINE	WPS	P-value
<i>Anthropometric variables</i>			
Body weight (kg)	99.7 ± 5.3	100.2 ± 5.4	NS
BMI (kg/m ²)	37.6 ± 1.8	37.8 ± 1.8	NS
Fat mass (kg)	44.8 ± 3.4	43.5 ± 3.2	0.009
<i>Blood parameters</i>			
Glucose (mmol/L)	5.2 ± 0.2	5.2 ± 0.3	NS
Insulin (μU/mL)	16.8 ± 2.1	17.2 ± 2.9	NS
HOMA IS	4.0 ± 0.6	4.3 ± 1.0	NS
2h-Glucose (mmol/L)	7.6 ± 0.9	7.4 ± 0.8	NS
2h- Insulin (μU/mL)	111.1 ± 20.6	97.1 ± 19.1	NS
Glucagon (ng/L)	37 ± 2	40 ± 4	NS
NEFA (μmol/L)	615 ± 57	616 ± 60	NS
BOHB (μmol/L)	58 ± 25	41 ± 9	NS
Triglycerides (mmol/L)	1.65 ± 0.22	1.34 ± 0.17	0.020
Cholesterol (mmol/L)	5.65 ± 0.32	5.25 ± 0.35	0.024
HDL Cholesterol (mmol/L)	1.13 ± 0.07	1.13 ± 0.05	NS
ASAT (U/L)	21 ± 1	21 ± 1	NS
<i>Substrate oxidation</i>			
Energy Expenditure (kcal/FFM/min)	0.019 ± 0.001	0.018 ± 0.001	NS
Carbohydrate oxidation (kcal/FFM/min)	1.39 ± 0.31	1.33 ± 0.35	NS
Lipid oxidation (kcal/FFM/min)	0.85 ± 0.12	0.63 ± 0.20	NS
<i>MR</i>			
IHCL (vol%)	7.8 ± 2.2	6.3 ± 2.1	0.017
Liver volume (cm ³)	1761 ± 138	1756 ± 169	NS
Visceral mass (cm ³)	3213 ± 245	3184 ± 229	NS

All values are expressed as mean ± SEMs.

Differences between pre and post whey protein supplementation (WPS) were assessed by the paired parametric *t*-test. *p*-value <0.05 was considered significant NS, not significantly different.

insulin (RIA kit from LincoMillipore, St CharlesBillerica, MissouriMO, USA) and glucagon (RIA kit from LincoMillipore, St CharlesBillerica, MissouriMO, USA) concentrations were measured by radio-immunoassays, plasma non esterified fatty acids (NEFA kit from Boehringer MannheimWako Chemical GmbH, MannheimNeuss, Germany), and plasma beta-hydroxybutyrate (BOHB) concentrations (kit from Boehringer Mannheim, Mannheim, Germany) were measured enzymatically.

2.4. Statistical analysis

All data were expressed as mean ± SEMs. Parameters measured every week throughout the WPS were analyzed by a one way

ANOVA for repeated time. An average value (WPS mean) was calculated for the whole WPS period, when time effect was not significant. Values were compared between pre and post WPS by paired *t*-tests. The distribution of IHCL concentrations was markedly skewed, and data were log-transformed for statistical analysis. Correlations between IHCL and other parameters were assessed by the Spearman's rank correlation coefficient test.

3. Results

Characteristics of subjects before and after WPS are shown in Table 1. Obese patients had a BMI ranging between 30.9 and 52.4 kg/m², and IHCL concentrations ranging between 1.9% and 20.5% of liver volume. 5 subjects had NAFLD using a cut-off values of IHCL of 5%.¹⁰ 3 subjects had 2 h plasma glucose concentrations >140 mg/dl (ca 7.8 mmol/l), indicating impaired glucose tolerance. Average HOMA index was >2.77 indicating that this group of obese women had significant insulin resistance.¹¹

Positive correlations were observed between IHCL and liver volume ($\rho = 0.63$, $p = 0.036$, Fig. 1), visceral fat volume ($\rho = 0.86$, $p = 0.001$, Fig. 1), ALAT ($\rho = 0.73$, $p = 0.010$), and HOMA IS index ($\rho = 0.62$, $p = 0.041$). No correlation was observed between IHCL and BMI or total fat mass.

WPS led to a sustained increase in calculated daily nitrogen excretion (Table 2). Plasma urea concentration also increased while plasma creatinine, daily urinary creatinine excretion and creatinine clearance did not change. Body weight remained unchanged over the 4-week supplementation while body fat mass was slightly reduced and fat free mass was slightly increased. Visceral fat volume and liver volume were not changed (Table 1).

After 4-week WPS, IHCL concentrations had decreased by 20.8 ± 7.7% ($p = 0.017$), fasting plasma triglyceride had decreased by 15.0 ± 6.9% ($p = 0.020$) and total plasma cholesterol concentration had decreased by 7.3 ± 2.7% ($p = 0.024$). Fasting and 2h plasma glucose and insulin concentrations were not changed (Table 1).

4. Discussion

Previous studies have shown that a high protein diet reduced hepatic lipid concentrations in high-fat or high-sucrose fed rodents or humans, suggesting that a high protein intake may, directly or indirectly, improve hepatic steatosis.^{3–5} We therefore assessed, in obese glucose intolerant young women, whether a 4-week

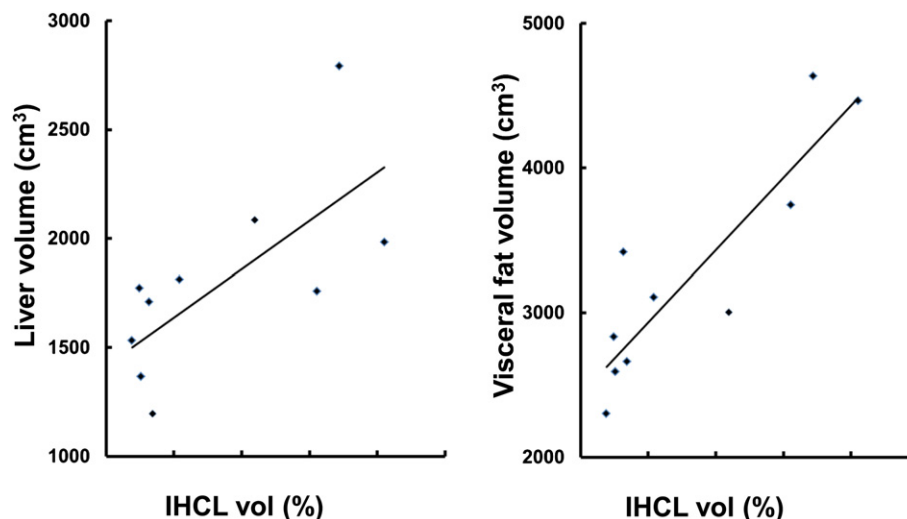


Fig. 1. Correlations between IHCL and liver volume ($\rho = 0.63$, $p = 0.036$), and between IHCL and visceral fat volume ($\rho = 0.86$, $p = 0.001$).

Table 2

Evolution of nitrogen and creatinine daily excretion, creatinine and urea plasmatic concentration and creatinine clearance during the month of supplementation.

	Week 0	Week 1	Week 2	Week 3	Week 4	WPS	P-value
<i>Urinary Collection</i>							
Nitrogen excretion [g/day]	15.6 ± 1.0	19.6 ± 1.4	20.0 ± 1.7	22.3 ± 1.2	20.7 ± 2.0	20.6 ± 0.8	0.000
Urinary Creatinine [mmol/day]	12.9 ± 0.9	12.3 ± 0.9	12.4 ± 1.0	13.6 ± 0.8	12.2 ± 1.1	12.6 ± 0.5	NS
<i>Plasma Collection</i>							
Urea [mmol/L]	4.9 ± 0.2	5.9 ± 0.4	5.5 ± 0.5	6.1 ± 0.4	5.7 ± 0.4	5.8 ± 0.2	0.002
Creatinine [μmol/L]	68 ± 4	68 ± 2	67 ± 2	67 ± 2	65 ± 2	67 ± 1	NS
Creatinine Clearance [ml/min]	137 ± 12	127 ± 9	131 ± 13	141 ± 9	131 ± 11	132 ± 5	NS

Values are expressed as mean ± SEMs. Effects of time during WPS supplementation was assessed by a one way ANOVA repeated for time among weeks 1–4. When effect of time during supplementation was not significant, an average value (WPS) was calculated.

Difference between week 0 and WPS supplementation was assessed by the paired parametric *t*-test. *p*-value <0.05 was considered significant NS, not significantly different.

supplementation with whey protein, with an otherwise spontaneous, uncontrolled food intake, would reduce hepatic steatosis and concomitantly improve hyperlipidemia and insulin sensitivity.

IHCL concentrations showed a large interindividual variability in obese subjects, ranging from 1.9% to 20.5%. IHCL concentrations were correlated with total liver volume and with visceral fat volume, but not with total body fat or BMI, corroborating several reports showing that hepatic fat deposition is tightly linked to visceral obesity.^{1,2,12} IHCL were correlated with HOMA IS, corroborating the well known association of NAFLD with insulin resistance.^{1,13} IHCL were also weakly correlated with ALAT levels, which are known to be a marker of hepatic fat.¹

After 4-week WPS, IHCL were significantly decreased by 21%, and fasting plasma triglycerides and cholesterol concentrations were decreased by 15% and 8% respectively. This reduction of IHCL concentrations was not related to changes in visceral fat volume or total liver volume, nor with important changes in body weight or body fat mass. This therefore indicates that the improved IHCL and plasma triglyceride profiles were to be attributed to an effect of protein rather than to changes in body composition.

We can only speculate about the possible mechanisms underlying the reduction in IHCL and plasma lipids induced by WPS. Although WPS provided ca 250 kcal/day, body weight did not change significantly while total body fat decreased significantly although to a very slight extent. This suggests that WPS led to a spontaneous decrease of food intake. This hypothesis appears corroborated by the evolution of daily urinary nitrogen excretion over time. Pre-WPS daily nitrogen excretion amounted to ca 15 g/day, which corresponds, assuming 16% nitrogen content in proteins, to an average ca 94 g/day protein intake. After WPS, daily nitrogen excretion increased significantly to ca 21 g/day, which corresponded to a total daily protein intake of 129 g/day. This means that, if subjects were hundred percent compliant and consumed the totality of the prescribed 60 g protein supplementation, WPS led to a reduction of spontaneous protein intake from other foods by 27%. This can be readily explained by the well known satietogenic effect of dietary protein.¹⁴ It is likely that the satiating effect of WPS decreased the intake not only of dietary proteins, but of dietary carbohydrate and fat as well. It is therefore possible that a decreased carbohydrate and lipid load was responsible for the decreased IHCL and plasma triglyceride concentrations observed after WPS. In support of this hypothesis, it has indeed been demonstrated, in overfed rats with hepatic steatosis, that increasing the dietary protein content of the diet reduced intrahepatic lipids through a decreased carbohydrate intake.³

Beside a reduction in spontaneous carbohydrate and fat intake, it is possible that a high protein intake also reduced hepatic fat through more direct effects. A high protein diet is known to enhance postprandial thermogenesis, an effect which is linked, at

least in part, to the high energy cost of urea synthesis and amino acid conversion into glucose.^{15,16} Since these two processes take place in the liver, one can expect that the increased energy requirement of the hepatocytes was met, at least in part, by an increased intrahepatic lipid oxidation. Although not documented in this study, where only fasting concentrations were monitored, feeding high protein meals is also known to increase postprandial glucagon concentrations.¹⁷ The ensuing high glucagon : insulin ratio may therefore have stimulated hepatic lipid oxidation and ketogenesis while inhibiting hepatic de novo lipogenesis¹⁸. Finally, other, direct effects of specific amino acids on intrahepatic lipid metabolism may be speculated.

Dietary protein metabolism also has complex interaction with glucose metabolism. On one hand, an amino-acid infusion enhances hepatic glucose production¹⁹ and decreases whole body insulin mediated glucose disposal.²⁰ On the other hand, co-ingestion of protein and glucose have been shown to decrease postprandial glycemia, an effect which can be attributed to a delayed gastric emptying^{21,22} WPS however failed to significantly alter fasting and 2 h plasma glucose and insulin concentrations. Insulin sensitivity was also not grossly altered, as indicated by HOMA IS index.

In summary, this study demonstrates that a 4-week supplementation with 3 times 20 g whey protein per day significantly reduced intrahepatic and fasting plasma triglyceride in obese subjects consuming an otherwise spontaneous diet. A satiating effect of the protein supplementation, leading to a lower carbohydrate or fat intake, an increased liver energy expenditure, and/or a higher glucagon:insulin ratio, may all be involved in these effects. This preliminary, uncontrolled study therefore suggests that a high protein diet may, in the long term, reduce the risk of non-alcoholic steatohepatitis and of cardio-vascular disease in obese patients. While a high protein diet may also have adverse effects, the present study did not hint at adverse renal effects. Further studies will however be needed to evaluate the optimal amount and sources of dietary proteins intake.

Statement of authorship

MB, KAL, CB and LT designed and developed the protocol; MB, EM, MC, EVD, GC and VG recruited subjects, carried out the clinical trial, and analyzed data, AB, DGQC, TB, RK and CB developed and performed MRS protocols, MB, LT and PhS drafted the manuscript, all reviewed and edited the manuscript.

Conflict of interest

LT has received research support from the Nestlé company, Vevey, Switzerland for other studies. Other authors have no conflict of interest to disclose.

Acknowledgments

We thank Uwe Boettcher and Jian Xu of Siemens, Healthcare, for providing and supporting the MRS sequence, and K. Zwygart for help with the data acquisition.

Support, Grants: This work was supported by research grant 310000-121995 from the Swiss National Foundation for Science to LT and from Cardiomet/CHUV to KAL

References

- Kotronen A, Westerbacka J, Bergholm R, Pietilainen KH, Yki-Jarvinen H. Liver fat in the metabolic syndrome. *J Clin Endocrinol Metab* 2007;**92**:3490–7.
- Kotronen A, Yki-Jarvinen H. Fatty liver: a novel component of the metabolic syndrome. *Arterioscler Thromb Vasc Biol* 2008;**28**:27–38.
- Pichon L, Huneau JF, Fromentin G, Tome D. A high-protein, high-fat, carbohydrate-free diet reduces energy intake, hepatic lipogenesis, and adiposity in rats. *J Nutr* 2006;**136**:1256–60.
- Gudbrandsen OA, Wergedahl H, Liaset B, Espe M, Mork S, Berge RK. Dietary single cell protein reduces fatty liver in obese Zucker rats. *Br J Nutr* 2008;**100**:776–85.
- Bortolotti M, Kreis R, Debarb C, Cariou B, Faeh D, Chetiveaux M, et al. High protein intake reduces intrahepatocellular lipid deposition in humans. *Am J Clin Nutr* 2009;**90**:1002–10.
- Thesen S, Heid O, Mueller E, Schad LR. Prospective acquisition correction for head motion with image-based tracking for real-time fMRI. *Magn Reson Med* 2000;**44**:457–65.
- Chong D, Slotboom J, Boesch C, Kreis R. Versatile fitting tool for simultaneous modeling of spectral arrays using prior knowledge restrictions in two dimensions. In: *Proceedings of the 17th Meeting of the International Society of Magnetic Resonance in Medicine Honolulu 2009*, p. 240; 2009.
- de Bazelaire CM, Duhamel GD, Rofsky NM, Alsop DC. MR imaging relaxation times of abdominal and pelvic tissues measured in vivo at 3.0 T: preliminary results. *Radiology* 2004;**230**:652–9.
- Buehler T, Ramseier N, Machann J, Schwenzler N, Boesch C. Determination of body compartments at 1.5 and 3 Tesla, combining three volume estimation methods. In: *Proceedings of the 18th Meeting of the International Society of Magnetic Resonance in Medicine Stockholm 2010*; 2010.
- Neuschwander-Tetri BA, Caldwell SH. Nonalcoholic steatohepatitis: summary of an AASLD single topic conference. *Hepatology* 2003;**37**:1202–19.
- Bonora E, Kiechl S, Willeit J, Oberhollenzer F, Egger G, Meigs JB, et al. Insulin resistance as estimated by homeostasis model assessment predicts incident symptomatic cardiovascular disease in caucasian subjects from the general population: the Bruneck study. *Diabetes Care* 2007;**30**:318–24.
- Bahl M, Qayyum A, Westphalen AC, Noworolski SM, Chu PW, Ferrell L, et al. Liver steatosis: investigation of opposed-phase T1-weighted liver MR signal intensity loss and visceral fat measurement as biomarkers. *Radiology* 2008;**249**:160–6.
- Korenblat KM, Fabbrini E, Mohammed BS, Klein S. Liver, muscle, and adipose tissue insulin action is directly related to intrahepatic triglyceride content in obese subjects. *Gastroenterology* 2008;**134**:1369–75.
- Westerterp-Plantenga MS, Nieuwenhuizen A, Tome D, Soenen S, Westerterp KR. Dietary protein, weight loss, and weight maintenance. *Annu Rev Nutr* 2009;**29**:21–41.
- Fukagawa NK, Bandini LG, Lim PH, Roingard F, Lee MA, Young JB. Protein-induced changes in energy expenditure in young and old individuals. *Am J Physiol* 1991;**260**:E345–52.
- Veldhorst MA, Westerterp-Plantenga MS, Westerterp KR. Gluconeogenesis and energy expenditure after a high-protein, carbohydrate-free diet. *Am J Clin Nutr* 2009;**90**:519–26.
- Gannon MC, Nuttall JA, Damberg G, Gupta V, Nuttall FQ. Effect of protein ingestion on the glucose appearance rate in people with type 2 diabetes. *J Clin Endocrinol Metab* 2001;**86**:1040–7.
- Girard J, Perdereau D, Fougelle F, Prip-Buus C, Ferre P. Regulation of lipogenic enzyme gene expression by nutrients and hormones. *Faseb J* 1994;**8**:36–42.
- Boden G, Tappy L. Effects of amino acids on glucose disposal. *Diabetes* 1990;**39**:1079–84.
- Krebs M, Krssak M, Bernroider E, Anderwald C, Brehm A, Meyerspeer M, et al. Mechanism of amino acid-induced skeletal muscle insulin resistance in humans. *Diabetes* 2002;**51**:599–605.
- Gannon MC, Nuttall JA, Nuttall FQ. Oral arginine does not stimulate an increase in insulin concentration but delays glucose disposal. *Am J Clin Nutr* 2002;**76**:1016–22.
- Ma J, Stevens JE, Cukier K, Maddox AF, Wishart JM, Jones KL, et al. Effects of a protein preload on gastric emptying, glycemia, and gut hormones after a carbohydrate meal in diet-controlled type 2 diabetes. *Diabetes Care* 2009;**32**:1600–2.